

THE IMPROVEMENT OF THE FULLY DENSE FREEFORM FABRICATION
(FDFF) PROCESS BY DESIGNING THE ANGULAR ADAPTIVE SLICING
ALGORITHM AND DESIGN OF EXPERIMENTS

THESIS

Presented to the Graduate Council of
Texas State University-San Marcos
in Partial Fulfillment of
the Requirements

for the Degree of

Master of SCIENCE

by

Mohammad Hayasi, B.S.

San Marcos, Texas
August 2012

THE IMPROVEMENT OF THE FULLY DENSE FREEFORM FABRICATION
(FDFE) PROCESS BY DESIGNING THE ANGULAR ADAPTIVE SLICING
ALGORITHM AND DESIGN OF EXPERIMENTS

Committee Members Approved:

Bahram Asiabanpour, Chair

Farhad Ameri

Vedaraman Sriraman

Approved:

J. Michael Willoughby
Dean of the Graduate College

COPYRIGHT

by

Mohammad Hayasi

2012

FAIR USE AND AUTHOR'S PERMISSION STATEMENT

Fair Use

This work is protected by the Copyright Laws of the United States (Public Law 94-553, section 107). Consistent with fair use as defined in the Copyright Laws, brief quotations from this material are allowed with proper acknowledgment. Use of this material for financial gain without the author's express written permission is not allowed.

Duplication Permission

As the copyright holder of this work I, Mohammad Hayasi, authorize duplication of this work, in whole or in part, for educational or scholarly purposes only.

To my wonderful wife, Maryam

ACKNOWLEDGEMENTS

Here I would like to take an opportunity to thank my great advisor, Dr. Bahram Asiabanpour, for his endless, timeless support and guidance throughout the course of project development. Undoubtedly, he is well informative and knowledgeable professor in the scope of Engineering, especially Rapid Prototyping (RP). He has been very approachable and friendly advisor and his knowledge transfer to me in the field of RP unquestionably helped me to achieve remarkable accomplishments in academia sector. This current form of research would not have ended up with some success, if I had not worked with him.

Additionally, I am highly grateful to my committee members, Dr. Farhad Ameri and Dr. Vedaraman Sriraman for their valuable and constructive technical comments on my research. Taking statistical courses with them truly gave me insight into the experimental design aspects of my project.

Lastly, I am sincerely grateful to my beloved and wonderful wife for timeless moral support and encouragements. Her kind, patient and accompany at the severe moments of my usual and especially academic life is heartily appreciated.

This manuscript was submitted on June 7, 2012.

TABLE OF CONTENTS

	Page
ACKNOWLEDGEMENTS	vi
LIST OF TABLES	x
LIST OF FIGURES	xi
ABSTRACT	xiv
CHAPTER	
I. INTRODUCTION	
Introduction	1
An Overview of RP Processes	2
Machine Path Generation for RP Systems	3
FDFF Process	4
Problem Statement	4
Project Objectives	5
Organization of Thesis	6
II. FUNDAMENTALS OF THE FDFF PROCESS	
The Concept of FDFF	8
The FDFF Stages	10
The FDFF Advantages	17
Functional Part Examples.....	19

III. RESEARCH METHODOLOGY	
Developmental Research.....	21
Experimental Research Designs	22
IV. ADAPTIVE-SLICING SYSTEM DEVELOPMENT	
An Overview of CAD Model Slicing	24
Direct Slicing Structure.....	25
Role of Feature Recognition in Slicing.....	27
Introduction to Adaptive Slicing System	28
Types of Part Geometry Distortion Errors.....	29
Interior and Exterior Contour Creation	33
New Adaptive Slicing Algorithm.....	38
System Implementation	44
Results and Discussion.....	45
V. CURVED-FORM ADAPTIVE SLICING	
Adaptive Slicing for Sloping Surface	53
Curved-form Adaptive Slicing Algorithm	60
Machine Path and CNC-codes Generation.....	67
System Implementation.....	69
System Results, Verification and Validation	71
VI. EXPERIMENTAL DESIGN FOR FDFP PROCESS IMPROVEMENT	
Design of Experiments (DOE) Approach	74
Factors Identification	74
Strength Measurement Standard.....	79

Design of Experiments	80
Result Analysis	83
VII. CONCLUSION AND FUTURE WORKS	
Conclusion	94
Future Works	95
APPENDIX A: DATA TABLES	97
APPENDIX B: SOFTWARE MANUAL	102
REFERENCES	107

LIST OF TABLES

Table	Page
4.1. A comparison between FDFP process time and cost for using uniform and adaptive slicing methods	52
6.1. Feasible materials selection and process parameters that resulted in acceptable bonding between layers	82
6.2. Factors' levels and the coded values for brazing process	83
6.3. Analysis of Variance for tensile strength.....	84
6.4. Analysis of Variance for tensile strength.....	89
6.5. The optimum settings for tensile strength in brazing process	92
6.6. Response prediction for two best operating points setting.....	93
6.7. Fabricated parts at optimum point setting	93

LIST OF FIGURES

Figure	Page
1.1. A general representation of RP process steps	3
1.2. General steps for the fully dense freeform fabrication (FDFE) method	4
2.1. Six degree of freedom and 12 movements Part accuracy analysis	12
2.2. Internal feature tooling	13
2.3. Boolean (derived) operation to creat a nest for a part.....	13
2.4. Selective slice nest tooling: Part and block (a). selected slice (b), final tool (c).....	14
2.5. Layer alignment system design and implementation.....	15
2.6. Sacrificed tab method	16
2.7. The visualization of the sequences of FDFE process	18
2.8. Demolition hammer assembly and test	19
2.9. Fully dense bike crank manufactured by the FDFE process and functional test.....	20
3.1. Research methodology	23
4.1. The illustration of Slicing approach, a) uniform slicing and b) adaptive slicing	25
4.2. Direct slicing and path generation system structure	27
4.3. Two identical slices on the bottom and top of the layer cut by maximum thickness approach	30
4.4. The staircase effect while two created contours are same size in inner area	32
4.5. A sample part for facet creation test in Inventor	34

4.6. The boundary path generation algorithm	36
4.7. Subroutine for vector creation	37
4.8. Subroutine for contour creation	37
4.9. Staircase effect detection a) a 3D solid model with its sliced CAD	39
4.10. A 3D solid model with its partially enlarged sliced model illustrating the change of curve direction on layers	41
4.11. Flow chart for the proposed adaptive slicing algorithm	43
4.12. The user interface form	45
4.13. Visualization of the original Inventor CAD model (a) the simulated 3D format in AutoCAD for the adaptively sliced sample part (b) front view of the sliced sample illustrating the variable thicknesses in different regions	47
4.14. Visualization of the original Inventor CAD model (a) the simulated. 3D sliced model in AutoCAD for the adaptively sliced sample part (b) the sliced front view of CAD model illustrating the variable thicknesses in different regions (c).....	49
4.15. Visualization of the original Inventor CAD model (a), adaptive 3D slices (b), front view of the sliced CAD model (c), the illustration of few layers grouped based on their similar thickness and spread on 2D plane (d).....	50
5.1. Illustration of the magnitude of geometry deviation error using simple adaptive slicing	54
5.2. Illustration of the magnitude of geometry deviation error using sloped-edge adaptive slicing	54
5.3. Illustration of outside (a) and inside slicing position.....	56
5.4. A view of ZIGER slice.....	57
5.5. Illustration of the magnitude of geometry deviation error using curved-form adaptive slicing	59
5.6. A view of sample layered model accompanying detail slicing information	61
5.7. Rotational (C) and cutting (A) angles	61
5.8. Visual representation of machine head angles (A,C) and cutting vector.....	62

5.9. Two different cutting strategies: (a) Multiple cuts to form a convex edge (b) single cut for a concave edge.....	63
5.10. Graphical representation of how a convex edge is identified	64
5.11. Illustration of single cutting stream for concave edge (a) and multiple cutting streams for convex edge (b) formed by a number of thin slices.....	66
5.12. Curved-form adaptive slicing algorithm	67
5.13. Top view of the arrangement of 7 distinct adaptive slices onto two available sheets with specified thicknesses	68
5.14. The explicit computation of h_f in the projected view of a sample adaptive slice	69
5.15. The user interface form	71
5.16. (a) 3D CAD model, (b) 3D view of curved-form adaptive	72
5.17. (a) 3D CAD model and (b-d) 3D and side view of curved-form adaptive slicing ...	73
6.1. Error calculation for layer k with dislocation and geometrical error.....	77
6.2. Galvanized (red hot) versus Stainless steel (unaffected) bolts in an induction heater	78
6.3. ASTM standard 2294-96 configuration	79
6.4. Acceptance and rejection region using P-value.....	85
6.5. Interaction plot for tensile strength.....	86
6.6. Optimization plot for tensile strength in soldering process	88
6.7. Interaction plot for tensile strength in brazing process.....	90
6.8. Optimization plot for tensile strength in brazing process	92
7.1. Curved-form adaptive slicing method inspired by the apple peeling function	96

ABSTRACT

THE IMPROVEMENT OF THE FULLY DENSE FREEFORM FABRICATION (FDFF) PROCESS BY DESIGNING THE ANGULAR ADAPTIVE SLICING ALGORITHM AND DESIGN OF EXPERIMENT

by

Mohammad Hayasi, B.S.

Texas State University-San Marcos

August 2012

SUPERVISING PROFESSOR: BAHRAM ASIABANPOUR

Fully dense freeform fabrication (FDFF) is a process based on thin line cutting processes, variable thickness layering, slicing in different orientations, and bulk layer attachment. The combination of these capabilities enables the production of good quality complex parts from practically any material at a very fast pace. To reduce the prototyping time and improve the quality of the fabricated functioning products, multiple design and operational factors affecting the response value (FDFF process performance) is required to be addressed and subsequently optimized in the favor of the enhancement of process

quality. In this research, firstly in order to decrease the process time the adaptive slicing technique with automatic spreading the generated two-dimensional (2D) slices on the predefined sheets in various thicknesses for the FDFP process are explained. Following the adaptive slicing, a curved-form adaptive slicing method is presented. In this method, multiple cuttings of the edge boundary of each adaptive layer with variable cutting vectors angles fairly form near to the CAD model curved surfaces. The proposed system is compatible with the 5-axis waterjet machines. Secondly, affecting factors (e.g., types of bonding materials, a range of heating temperatures, types of metal sheets, etc) on the quality of the fabricated prototypes are investigated using statistic designed experiment. In the improved FDFP process, three-dimensional (3D) solid CAD models with any kind of geometry complexity are designed and adaptively sliced in Autodesk Inventor. To cut angularly the profiles, CNC G-codes are automatically generated which are perfectly matched with 5-axis Waterjet machining requirements.

CHAPTER I

INTRODUCTION

Introduction

Since the introduction of the stereolithography (SLA) process as the first rapid prototyping (RP) process in 1988, several RP processes which use different mechanisms or materials have been introduced. Some of them such as SLA, laminated object manufacturing (LOM), selective laser sintering (SLS), fused deposition modeling (FDM), and 3D printing (3DP) have become commercially available. RP systems have been reviewed frequently from different perspectives (Asiabanpour & Khoshnevis, 2004; Chua et al., 1997a; Kamrani & Naser, 2006; Onuh & Yusuf, 1999; Yan & Gu, 1996). Although RP systems fabricate parts with unlimited geometrical complexity at shorter cycle time, the fabricated parts still suffer from poor surface quality, weak structure, and limited raw material and part dimension. Therefore, building fully dense metal or non-metal parts has always been of special interest to both researchers and the industry. Stacking up layers to build a 3D geometry has been practiced since at least the 18th century, using wax layers for topography and photo-sculpture (Abd Elghany, 2009). In recent years, the idea of building metallic prototypes from metal sheets or foil slices has been reported by different researchers. The application of such a process in rapid manufacturing is more of interest as it will both produce parts that meet closely the mechanical properties defined

in the design intent, as well as significantly lessen the build time compared to previous known RP systems.

An Overview of RP Processes

Additive manufacturing (AM), also known as additive fabrication, additive processes, additive techniques, additive layer manufacturing, layer manufacturing, and freeform fabrication, is the “process of joining materials to make objects from 3D model data, usually in a layer upon layer, as opposed to subtractive manufacturing methodologies” (ASTM International F 2792-09, 2010). Many AM processes are commercially available, such as direct metal laser sintering (DMLS), FDM, SLS, SLA, and 3D printing. From the part prototyping sequence point of view, RP processes can be categorized into two groups. In the first group (layer-based processes), the entire layer is built at once by applying binder or heat to the base material (e.g., speed part or to some extent 3DP). In the second group (point-by-point-based processes), the machine’s build head is moving point by point in one layer to extrude, glue, fuse, or cut the material. In spite of the fact that the second method is slower, some of the most popular RP processes such as STL, SLS, and FDM are in this group.

Obviously, for the point-by-point RP processes, a machine path is needed to control the movement of the machine’s build head. Because of the differences in the RP processes in this group, there is no standard machine path code for them. For each RP process, based on its characteristics and requirements, the required data is extracted from the computer-aided design (CAD) model and converted into proper format for the RP machine. Part external wall formation, filling method, and part separation from the surrounding material determine the machine path pattern. This machine path pattern

could be a robotic movement in the XY-plane for FDM or contour crafting machines, a laser pattern for material solidification and sintering in the STL and SLS machines, or a laser cutter pattern for the LOM machines (Asiabanpour & Khoshnevis, 2004). The general steps for layer-by-layer fabrication are as follows:

1. Creating 3D CAD model and generating an exchange file (e.g., STL, IGES, etc.)
2. Slicing the CAD file represented in output formatting according to the desired RP process expectation
3. Generating machine path and CNC-codes compatible with the desired RP process
4. Cleaning and post processing the fabricated prototypes to improve part quality

Figure 1.1 demonstrates the general steps of RP process.

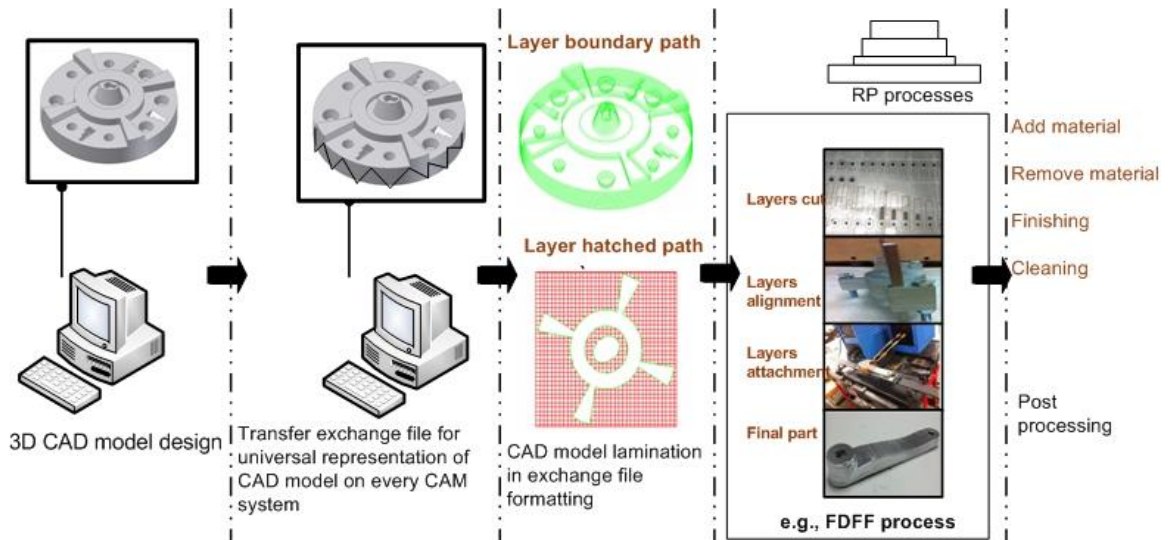


Figure 1.1. A general representation of RP process steps.

Machine Path Generation for RP Systems

Every RP system has its own specifications. The part boundary form, part filling method, and part separation from the surrounding material determine the machine path pattern for every layer. These processes require different machine path pattern generation strategies. Therefore, unlike CNC standard tool path files (e.g., APT and G-Code), there

is no standard tool path file for RP systems. Similarly, because of the need for more complex parts, conventional manual tool path code writing will not be effective for many machining processes such as CNC mill, lathe, drill, and laser cutting. Therefore, geometrical data in CAD systems must be extracted and translated into a usable format for a specific manufacturing process.

FDFP Process

FDFP is a freeform fabrication process based on thin line cutting processes (e.g., abrasive waterjet cutting or laser cutting), variable thickness layering, slicing in different orientations, and bulk layer attachment (Glen et al., 2011). The combination of these capabilities enables the production of good quality complex parts from practically any material-including metals, plastic, wood, wax, ceramic, and even glass-at a very fast pace. Using this method, a CAD model is sliced into computer layers; the material sheet is then cut from the computer layers. After adding the bonding materials between layers, the layers are aligned into a work-holding system. Using pressure and/or heat, layers are attached to form a 3D prototype from a fully dense material (see Figure 1.2).

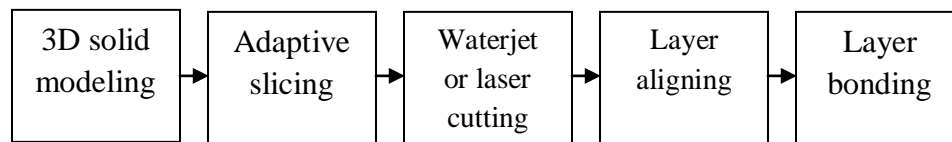


Figure 1.2. General steps for the fully dense freeform fabrication (FDFP) method.

Problem Statement

In the FDFP process, despite the fact that the utilization of fully dense metallic sheets with uniform thickness contributes to the reduction of build time, the appropriate slicing approach could also help decrease the number of slices thereby significantly decreasing build time. This problem can be properly addressed by an adaptive slicing

method that generates non-uniform layers using different available sheet thicknesses on shop floors. In terms of FDFP process time reduction, quickly attach the layers together will also help improve the processing time in addition to slicing approach. Thus, an appropriate attachment of the layers not only would expedite the FDFP process but it would maintain the entire part geometry at optimal level.

While reducing the FDFP processing time, enhancing the quality of functional parts fabricated by FDFP is an imperative step. As adaptive slicing decreases the number of layers, the fabricated part with the attachment of such layers, however, suffers from a remarkable staircase effect error (a common geometry distortion error in any slicing system). To address such a problem, generating curved-form adaptive slices seems to be a feasible solution. Furthermore, the quality of FDFP parts heavily relies on the strong joining of the layers together. A bad bonding for metallic parts undermines the application of the FDFP process. To realize an acceptable high quality using proper metallic bonding, it is required to investigate essential factors affecting the tensile strength of the bonded layers and to subsequently control the degree of their impact.

Project Objectives

The main objectives of the research are to reduce the build time and to improve the quality of the fabricated functioning products for the FDFP process. To achieve the first aim, CAD files go through the adaptive slicing whereby the number of layers needed to build a FDFP prototype significantly decreases, thereby reducing the total build time. To meet the second aim, the generated adaptive slices are investigated for the generation of curved-form layers that perfectly fit with the geometry of CAD model and hence increase the quality of the part. In addition, the multiple design and operational factors

affecting the response value (FDFF process performance) requires addressing and subsequently optimizing the enhancement of process quality by the application of design of experiment (DOE) and regression analysis.

Organization of Thesis

The rest of the thesis is organized as follows. Chapter II, “Fundamentals of the FDFF process,” gives a general idea of the fabricating fully dense metallic parts. It provides insight into how the metallic cut slices are aligned then attached together. This is the main advantage of using the FDFF process over other RP processes.

Chapter III, “Research Methodology,” explains certain techniques and approaches have taken to develop a new slicing system implementable on a 5-axis abrasive waterjet (AWJ). As for the analytical and experimental research, techniques and methods are proposed.

Chapter IV, “New Adaptive-slicing System Development,” deals with the development of new improved adaptive slicing for CAD models designed by Autodesk Inventor. This section of the research is aimed at reducing the build time of the parts fabricated by FDFF.

Chapter V, “Curved-form Adaptive Slicing,” is, in fact, the continuation of the previous chapter with the distinction that it takes the generated adaptive slices into consideration for the purpose of creating curved-form sloping layer surfaces to get the layered part very close to its original CAD model. This part of the research is primarily dedicated to the enhancement of part quality.

Chapter VI, “Quality Enhancement of FDFF parts,” scrutinizes the identification of any material-related or machine-setting-related factors affecting the improvement of

part quality. Careful study of the steps of the FDFP process contributes to this factor identification. The parts that go through two different layer attachment approaches (i.e., soldering a heat-based and induction-heat-based attachment) are fabricated, then DOE and regression analysis followed by model validation is employed to set the optimum criteria for the production of ideal FDFP products.

Chapter VII, "Conclusions and Future Works," presents the conclusions of the research and suggests a new direction for future research.

CHAPTER II

FUNDAMENTALS OF THE FDFP PROCESS

The Concept of FDFP

Stacking up layers to build a 3D geometry by using wax layers for topography and photo-sculpture has been practiced since at least the eighteen-century, (Abd Elghany, 2009). In recent years, the idea of building metallic prototypes from metal sheets or foil slices has been reported by different researchers. Nakagawa and Kunieda (1984) first conducted research in the area of layer-by-layer or laminated tooling fabrication was reported by. Their work was focused on manufacturing blanking dies for sheet metal components. Then Vouzelaud et al. (1992) conducted research into tools making by stacking horizontally layers of sheet steel and then joining them together was also reported by. In order to more easily clamp the sheet metal slices together, particularly for cavities, the works of Glozer and Bervick (1992) as well as Walczyk and Hardt (1996) concentrated on stacking the sheets vertically. To investigate robust methods of joining metal sheets for the manufacture of tools, Bryden et al. (2001) reported on the Lastform project, a three year EPSRC (IMI) program, in which industry partners and three universities collaboratively tested different suitable adhesive and braze joining methods in several distinct process conditions. Following the Lastform project, a group of researchers (Gibbons et al., 2003) with collaboration of industry partners conducted

comprehensive research on the laminate manufacturing of the die-cast tooling. In their project, suitable material for die-casting industry was carefully selected and then analyzed for cutting condition, thermal fatigue, and heat treatment of the bonded laminate structure; the selection of perfect joining material bearable at extreme high temperature; the optimal way of cutting direction; and the design of suitable cooling channels. Finally, the finishing of the prototype by Computer Numerical Control (CNC) machine followed. Other researchers have also proposed the application of CNC material removal processes in building functional prototypes (Frank et al., 2004; Schmitz et al., 2001).

In other recent research, Himmer et al. (2003) employed a multiple laser process for cutting the sheets, then joined them using laser welding and finally improved the surface quality by CNC machining in a fully automated manner. To prototype injection moulds for plastic parts, Mognol et al. (2006) proposed hybrid rapid tooling, i.e., high speed machining, electro discharging machining and direct metal laser sintering for the purpose of achieving the manufacture of each component of the mould and a greater reaction to diverse group of products. Additional rapid tooling research presented by Perchtl et al. (2005) addressed the potential challenge of low self-stiffness of the metallic foil is used in the manufacture of, for example, moulds for gravity casting, die casting or injection molding. To overcome this problem, he developed a two sub-process technique. In the first sub process, each layer is stacked and accurately positioned over the previous slice by laser beam spot welding. To enhance the mechanical properties of the part, a second sub-process followed. It involved diffusion welding in a furnace with inert gas or vacuum. Ultrasonic bonding of thin foils has also been introduced to rapid prototyping of sophisticated layered parts. In this process, the selected patterns of the new thin foil slice

are ultrasonically welded to the previous laid layers (Devine, 1984; Gao and Doumanidis, 2002; Kirzanowski, 1989;).

The use of CNC machining—in both conventional and layered fashions—is usually accompanied by some limitations, such as the impossibility of making complex internal features due to the tool radius and machining cost. Additionally, the use of processes such as ultrasonic additive manufacturing is very slow because of the thin layers of foil that need to be used. These processes are also limited to certain types of materials mainly metals.

FDFP is an ideal metallic lamination process that falls in the category of fabricating metallic bulk layers. It focuses mainly on the untouched part of such process, that is, the integrated layer aligning and compression method for FDFP that can accurately align and position layers together in a short period of time and cost effective fashion. Admittedly, the joint force of cutting any metal sheet with thickness of up to 8 in. by AWJ cutter machine, the fabrication of curved-form adaptive layers together with accurate layers alignment and cutting-edge attachment technology has made the application of FDFP process in building functional parts from small to bulk size a feasible alternative over the current commercial RP systems.

The FDFP Stages

Using the FDFP system, a CAD model is firstly layered into computer slabs then the generated slabs are carefully checked for any missing data in terms of design expectation followed by error-free machine path and CNC-codes generation. After adding the bonding materials between layers, the layers are aligned into a work-holding

system. Using pressure and/or heat, layers are attached to form a 3D prototype from a fully dense material. The following paragraphs describe the subsystems of this process.

Solid modeling-In this process, a 3D part is designed in Inventor Autodesk solid modeler software. Solid models designed in other software can be imported and used in this software as well.

FDFE slicing software- As its name implies, the basis of the FDFE slicing system is to slice from a design-by-feature solid model. Autodesk Inventor solid modeler, as a design-by-feature solid modeler, is used for 3D solid modeling. The proposed system needs to be implemented using Visual Basic codes inside Inventor. This system would generate varied slice thickness based on the part's complexity in each cut level.

Furthermore, the software would be capable of slicing in three directions, along the X, Y, and Z axes. In addition, parts can be rotated in space before slicing, meaning they can be sliced in different orientations and directions. Practically, slice (thickness) sizes would be based on predefined commercially available sheets.

Cutting layers- This software outputs two AutoCAD script files that draw the slices in both 2D and 3D formats, which can then be saved in DWG and DXF files, making them compatible with almost all AWJ cutter, laser cutter, and CNC machines. The AutoCAD 2D drawing is then imported into automated cutter process (e.g., abrasive waterjet or laser cutter) software in DWG or DXF format, and the slices are cut. Sheet materials of different thicknesses can be laid out next to one another in the cutter machine and all materials can be cut in a single machine setup

Layer alignment- The tooling necessary for the construction of a FDFP part must satisfy two requirements: First, the tooling must be able to maintain alignment of the slices relative to each other. Second, the tooling must maintain pressure on the part in order to get a proper bond. Generally, the 3D parts in the space have six degrees of freedom and twelve movements (moving along and rotating around X, Y, Z axes and their opposite directions) (Figure 2.1). For the stacked slices in the FDFP process, some of the movements are needed to be limited by the upper and lower layers. Based on the 3-2-1 rule (Nee et al., 2010), all remaining movements should be limited.

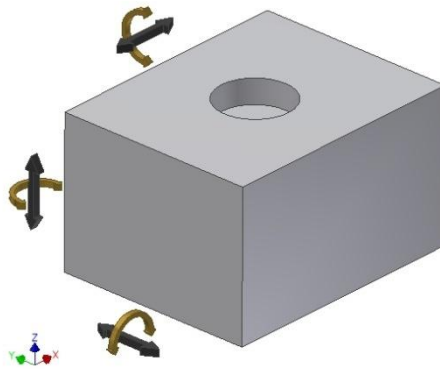


Figure 2.1. Six degree of freedom and 12 movements Part accuracy analysis.

Five different alignment methods have been tested and the most appropriate alignment mechanism that performed flawless in measuring part accuracy has been selected (Glen et al., 2011).

a) Internal features

The simplest alignment method is internal feature tooling in which the part's internal features (e.g., holes) are used as the reference point. Alternatively, additional holes or precisely machined edges may be used as alignment and reinforcement tools (Williams et al., 2007) (Figure 2.2).

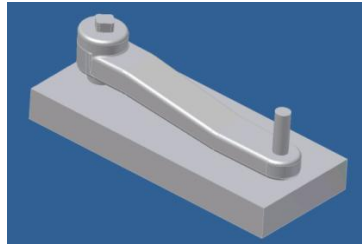


Figure 2.2. Internal feature tooling.

b) Full nest

Fully nested tooling is a very basic derived clamp that provides alignment and pressure at all points of an FDFP part. Its CAD model construction from the part is very simple, involving only a Boolean remove of the desired part from a predefined block; followed by CNC machining operation or layered manufacturing of the nest to create the physical nest (Figure 2.3).

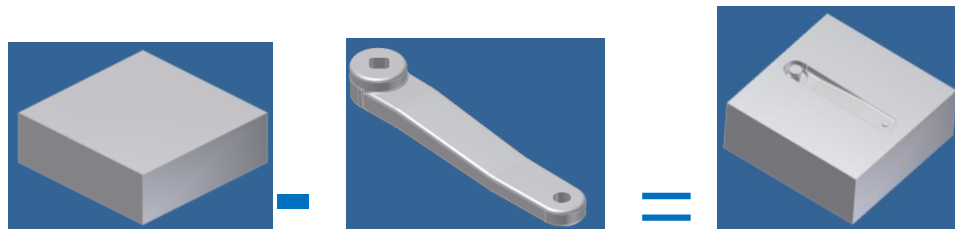


Figure 2.3. Boolean (derived) operation to create a nest for a part.

c) Selective slice nest

This method facilitates the opportunity to limit all twelve movements for all layers while directing the required force for bonding between layers. Unlike the full nest method, it takes only selected slices in the X and Y directions, rather than having to mill out an entire accurate negative of a part. This method uses the Derive function to subtract

the part from block geometry. Then, by evaluating the part complexity, a few slices in critical locations are generated as datum curves (Figure 2.4).

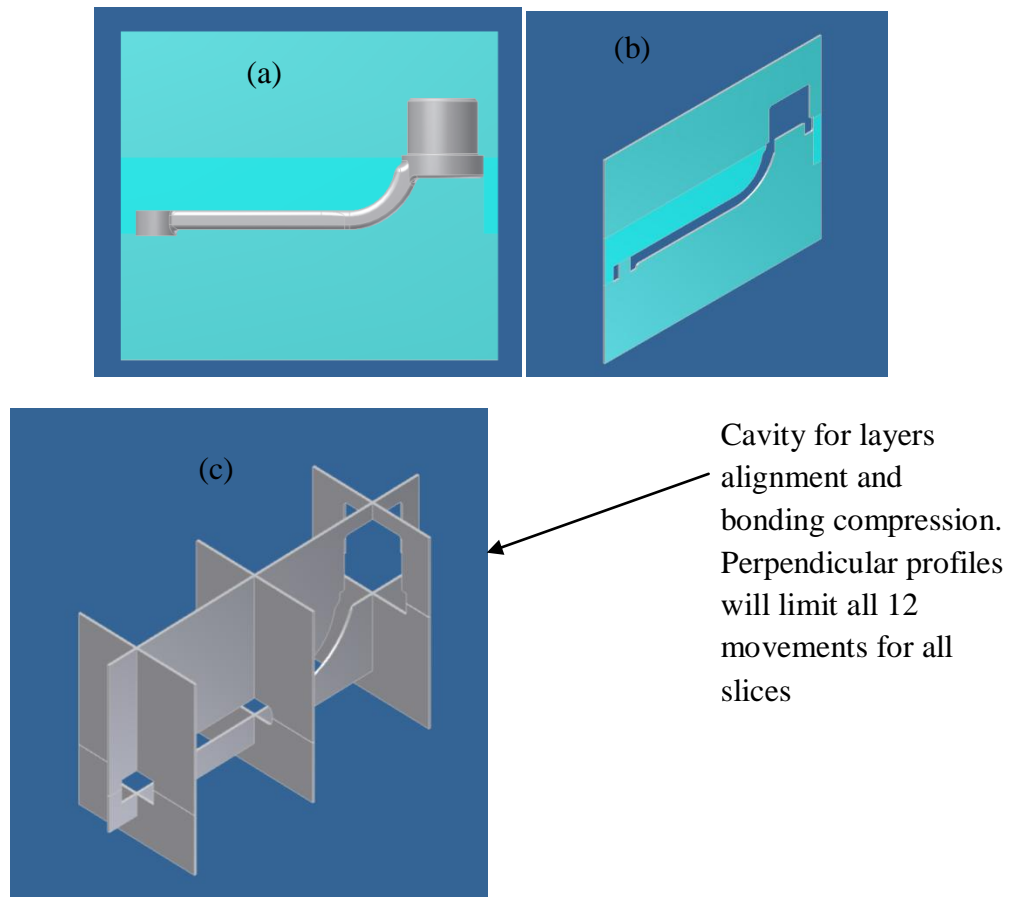


Figure 2.4. Selective slice nest tooling: Part and block (a). selected slice (b), final tool (c).

d) Pin-based

The alignment mechanism uses a list of variables corresponding to the extreme points of the outline of each layer generated in the FDFE adaptive slicing software. A system of linear actuators move pins horizontally to each of the points, providing a stencil for the location of the layer to be placed. The sliced layer and bonding material is then placed into the four-point stencil. Another actuator lowers the work table to proceed to the next layer, and the process is repeated (Figure 2.5).

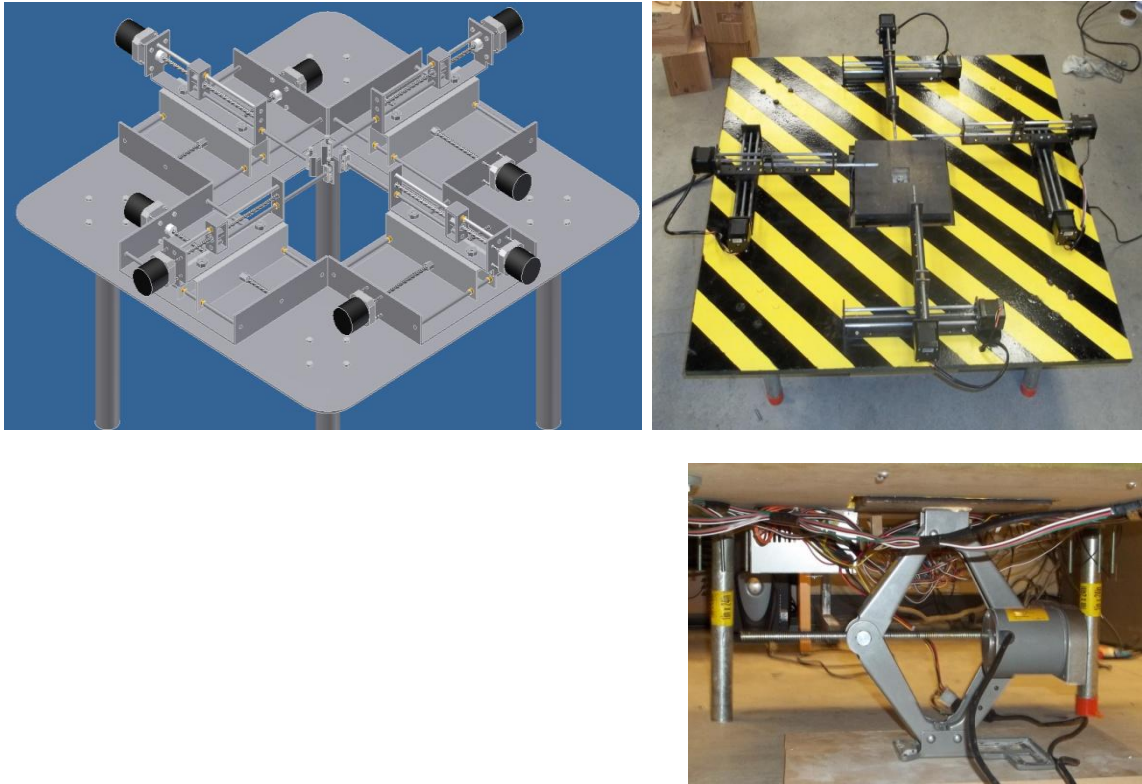


Figure 2.5. Layer alignment system design and implementation.

e) Sacrificed tab

In this method, a few external tabs with internal cut are added to the part CAD file. These tabs are cut during layer slicing. Sacrificed tabs and the combination of a square rod and threaded fasteners are used to align layers precisely and provide the required compression force needed in the layer bonding stage. This means the elimination of any alignment and compression tooling, which would require major tool custom design and restricting the use of induction heating method (Figure 2.6).



Figure 2.6. Sacrificed tab method.

To compare the effectiveness of the five methods for the representative part, different criteria were simulated and tested. Consequently, method e (Sacrificed tab) was chosen as it clearly eliminates any need for alignment and compression tooling (it uses small tabs connected to the part that later they will be cut).

Layer bonding- Depending on the material(s) of the slices, no bonding material (e.g., diffusion welding), glue, plastic, metal, or composite materials—similar to or different from sliced sheets—can be used. The added layer thickness from the use of bonding material can be compensated for by using the FDFD variable slicing software. The needed energy bond can be a room temperature and evaporative (in the case of glue, for example), heat based (e.g., direct flame, oven, furnace), or sources such as electromagnetic pulses, ultrasonic waves, microwaves, or induction heater. When applying heat energy, the use of pressure from a clamp, press, or locking system improves the attachment quality. To firmly attach the layers, a compression mechanism is required to hold layers together during the layer bonding stage (heat-based bonding). After all layers are aligned and temporarily bonded, they are placed in the laminating mechanism consisting of the compression and heat components. The main requirement for this mechanism is to provide secure clamping on oddly shaped surface, provide sufficient clamping force, provide constant force while heat is applied, and allow for even

and thorough application of heat (see Figure 2.7 for the visual representation of FDFE process).

The FDFE Advantages

The advantages of the FDFE system over other processes are: fast cutting processes, capability of generating slices of variable thicknesses from a predefined standard sheet, and ability to produce parts from any material; an AWJ cutter can cut any solid material up to 8 inches thick. The latest generation of AWJ cutters is capable of micro machining. Therefore, this process can be used for fully dense micro scale components. The FDFE system can also take advantage of cutting the curved-form sheet layers using 5-axis AWJ machine whose machine path is created by the development of conformed-to-CAD design sloped-edge adaptive slicing system.

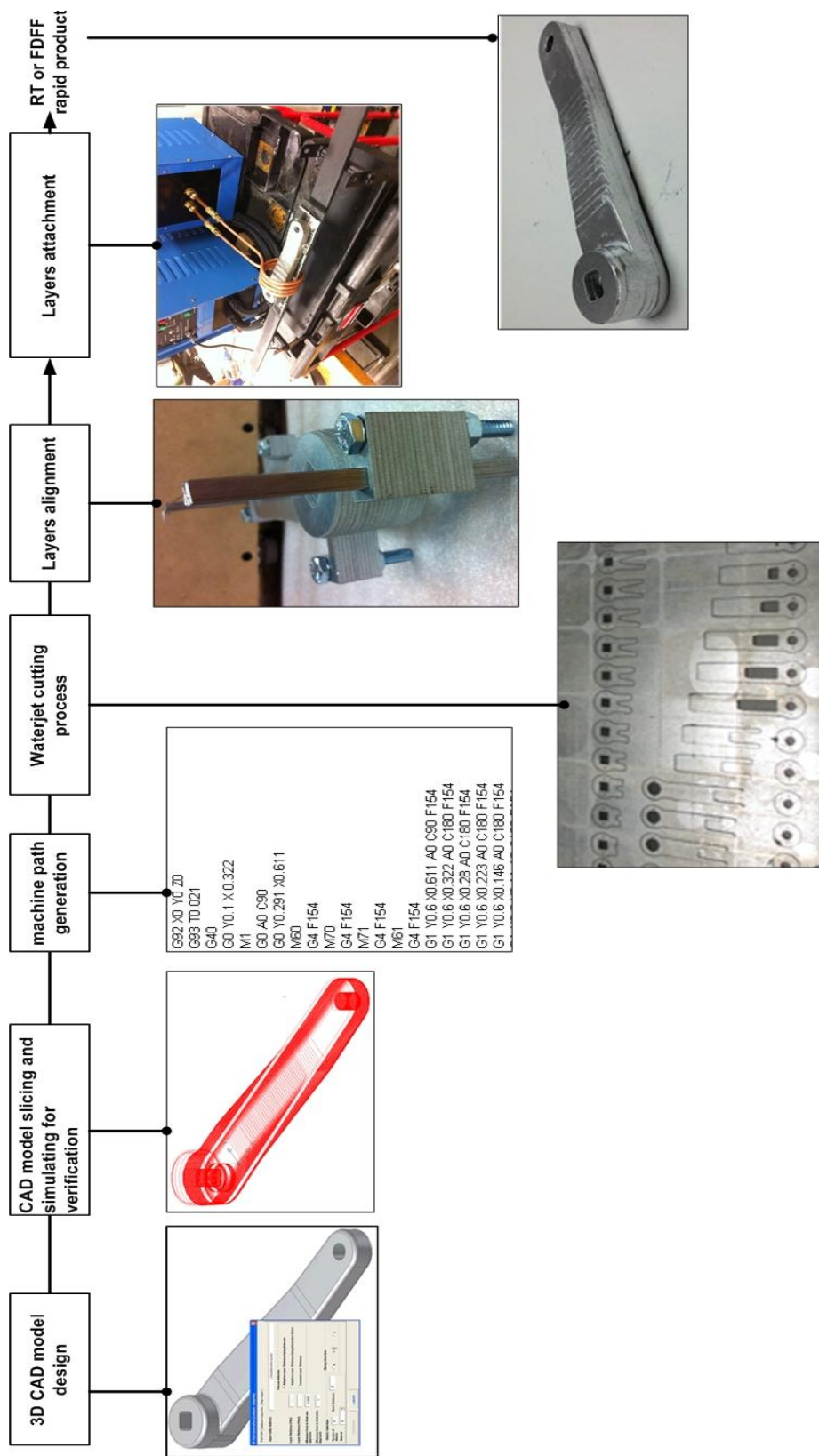


Figure 2.7. The visualization of the sequences of FDFFF process.

Functional Part Examples

To illustrate the flexibility of the FDFP process in producing a variety of functional parts, in this section several functioning parts including a demolition hammer head and a bike crank are presented.

Prototype 1: Demolition hammer head. The main expected mechanical property for a hammer is its high impact strength. For this hammer, a 0.25-inch stainless steel and a 0.03-inch stainless steel sheet were inserted as the available sheets into the FDFP software. In this example, both thick and thin hammer head layers were cut using the laser cutter. To attach the layers, a 60%–40% tin-bismuth powder mix wetted by J.W. Harris Stay-Clean® paste flux was used. After alignment, the layers were clamped and the part was heated in an oven at 550° F. Figure 2.3 illustrates the hammer head prototyping and test. More videos illustrating the hammer head functionality tests are posted in the following links: <http://www.youtube.com/watch?v=aF1o1L3TYvU> and <http://www.youtube.com/watch?v=GerJOYjc57M>.

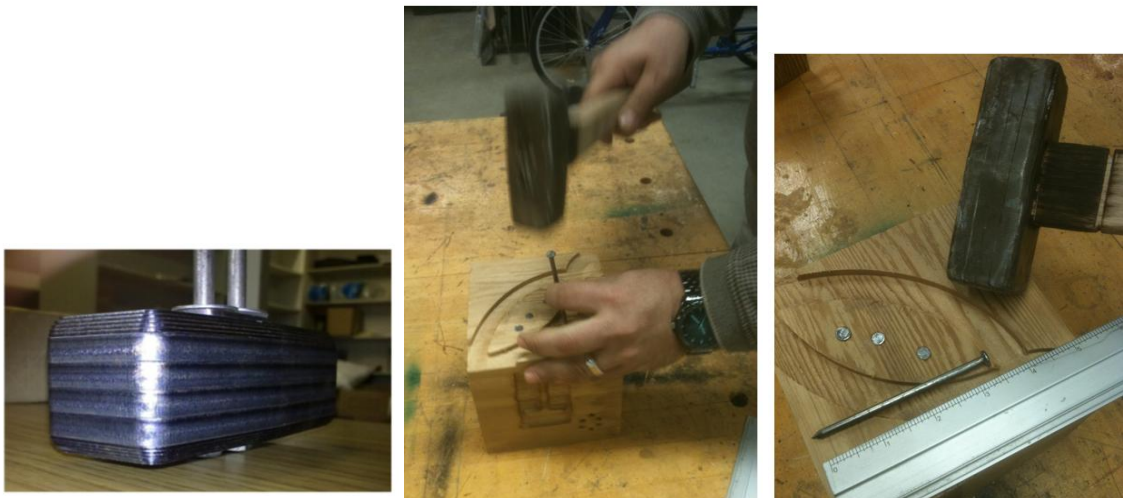


Figure 2.8. Demolition hammer assembly and test.

Prototype 2: Bike crank. The second prototype is a bike crank. This sample is made of 0.25 in. and .025 in. stainless steel sheets and bonded with .003 in tin foil. The internal feature tooling method was used to align the layers. A propane torch was used to heat the crank for three minutes (Figure 2.9). This part later was tapped and installed on a bike and used as a functional part. A video illustrating the bike crank functionality test is posted on YouTube in the following link:

<http://www.youtube.com/watch?v=Jjn9fCpwpvA>



Figure 2.9. Fully dense bike crank manufactured by the FDFE process and functional test.

CHAPTER III

RESEARCH METHODOLOGY

Developmental Research

Even though the idea of fabricating bulk metallic laminate from various sheet thicknesses has been of research interest for almost two decades or so, the studies on the several aspects of such a process, for example, layers alignment and attachment and the making use of effective adaptive slicing have not been given scrutiny. To respond to the foregoing demands, the FDFP process has been under development at RPD lab at Texas State since 2008. Since then, there has been remarkable effort and progress on the development of the FDFP process. While attempting to invent acceptable optimum layers alignment and attachment, the need for experimental research designs as well as development research on meeting the mechanical properties and geometry requirements of FDFP parts are imperative.

In the developmental research, firstly, in order to enable the fabrication of thick layers for the aim of reducing the build time, the machine path (i.e., internal or external contours for each layer) will be generated. The proposed algorithm will be implemented within the Autodesk Inventor programming environment using API functions for Inventor. Afterward, the created adaptive layers will be taken into the second part of

software development in which a specific custom machine path for curved-form adaptive slices, enabling a 5-axis waterjet machine to cut the curve-form edges, will be generated.

Experimental Research Designs

Experimental research designs are used for the controlled testing of causal processes. The general procedure is to manipulate several independent variables to determine their effect on a dependent variable. To identify and then classify the influential independent factors, analytical research on the sub-processes of FDFE will be conducted. The identification of the affecting factors would help take proper steps in addressing issues related to the causes of defect or failure. The analytical study will help to investigate major problems of the fabricated parts such as, dislocation of layers, weak attachment between layers, and staircase effect errors on the boundary of the layered edges. Additionally, factors classification will help us to conduct the DOE according to the classified factors affecting on the response value. Following the identification of factors of concern, experimental tests are needed to be carried out for finding an acceptable range of each factor that will then help assign the number of levels in the designed experiment.

To get an optimum response value leading to the part quality, full factorial design and regression analysis in the controlled equal experimental conditions should be followed.

Figure 3.1 shows graphically the role of both experimental research designs and developmental research towards the fulfillment of the desired goals.

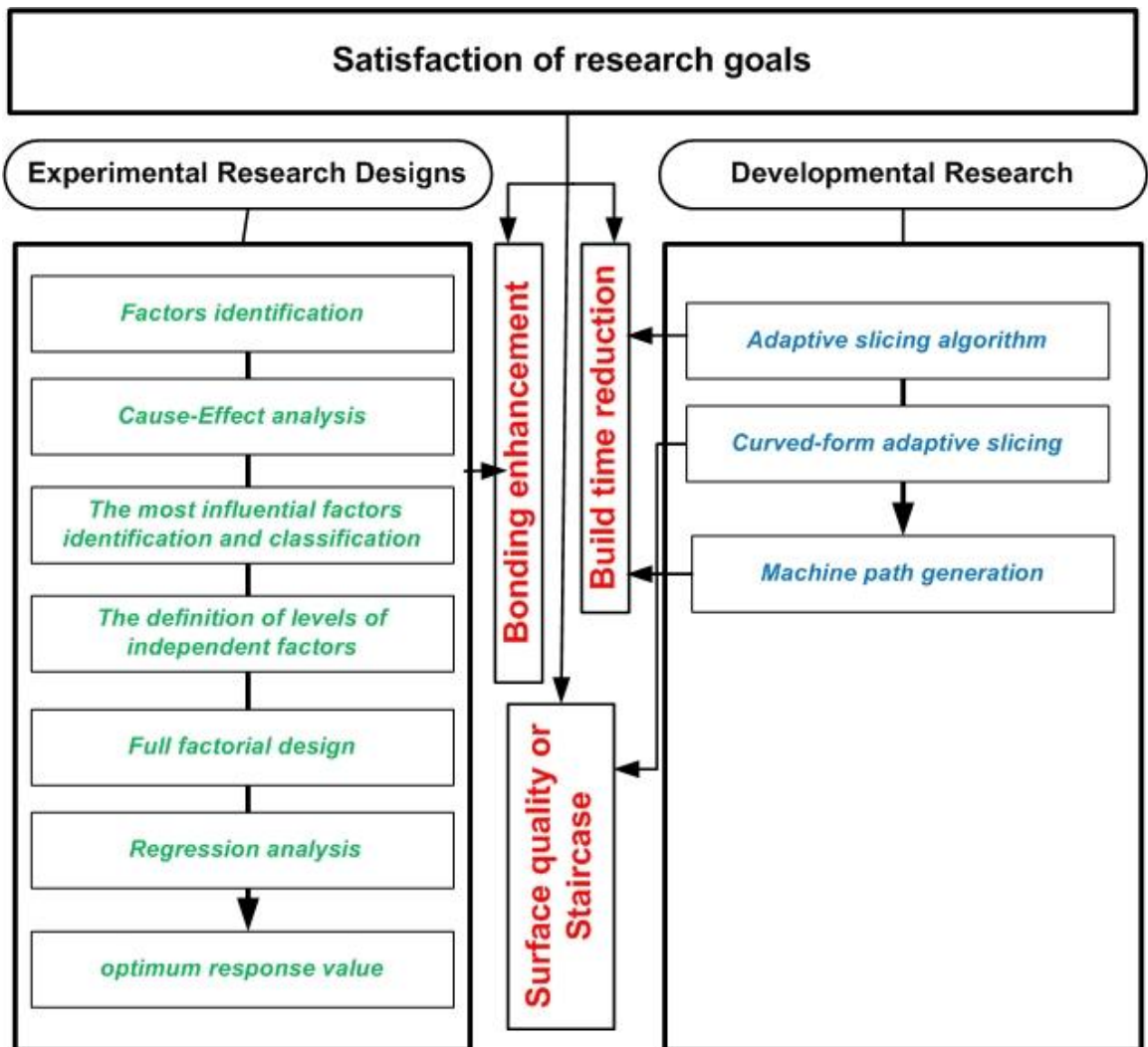


Figure 3.1. Research methodology.

CHAPTER IV

ADAPTIVE-SLICING SYSTEM DEVELOPMENT

An Overview of CAD Model Slicing

Slicing a CAD model through intersecting the model with the XY-plane at each Z increment is a well-known method of path generation. Slicing a CAD model is carried out through different methods such as stereolithography (STL) file slicing, neutral format (e.g., IGES, HP/GL and STEP) (Chua et al., 1997b) or direct model slicing. Among the available RP processes, the STL format is the most widely accepted file format in the RP industry. The reasons for this popularity are the simplicity of the format and ease of file generation without requiring very sophisticated CAD software (Jurrens, 1999; Koc, 2000). Different methods for slicing an STL file have been proposed (Asiabanpour and Khoshnevis, 2004; Choi and Kwok, 1999; Leong et al., 1996; Vuyyuru et al., 1994).

All popular RP processes make parts in a uniform layer thickness fashion. Consequently, most of the path generation efforts have focused on that area. In the uniform layer thickness method, all layers have equal thickness. Some theoretical and software works have also been proposed in adaptive layer thickness prototyping. In the adaptive slicing technique, the slicing thickness varies according to the part geometry complexity. It is theoretically proven that this method can produce parts with higher

accuracy, less deviation from the CAD model, and shorter fabrication time (Dolenc and Mäkelä, 1994; Kulkarni et al., 2000; Vouzelaud and Bagchi, 1995) (Figure 4.1).

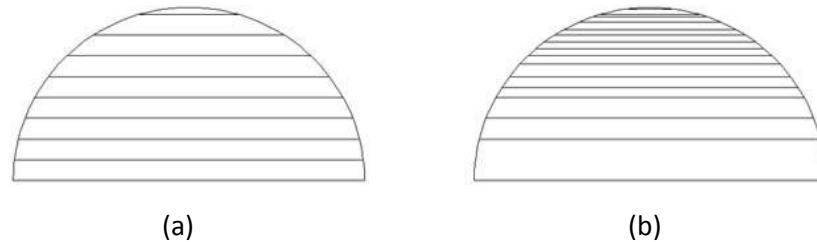


Figure 4.1. The illustration of Slicing approach, a) uniform slicing and b) adaptive slicing.

Direct Slicing Structure

Development of slicing approaches (uniform or adaptive) can be categorized into two main groups of direct and indirect slicing. Slicing a CAD model through intersecting the model with the XY-plane at each Z increment is a well-known method of path generation. Slicing a CAD model is carried out through different methods such as STL file slicing, neutral format (e.g., IGES, HP/GL, and STEP) (Chua et al., 1997b) or direct model slicing. Among the available RP processes, the STL format is the most widely accepted file format in the RP industry. The reasons for this popularity are the simplicity of the format and ease of file generation without requiring very sophisticated CAD software (Jurrens, 1999; Koc et al., 2000). Different methods for slicing an STL file have been proposed (Asiabanpour and Khoshnevis, 2004; Choi and Kwok, 1999; Leong et al., 1996; Vuyyuru et al., 1994). Another slicing approach uses exact CAD models. Some direct slicing works by Chang (2004), Jamieson and Hacker (1995), and Chen et al. (2001) have been reported. In these works, researchers have used a CAD software package (e.g., PowerSHARE, Parasolid) to model and then to generate the boundary path. The boundary path (contour) in these three cases is generated by use of macros

which are provided by the underlying software. The work by Chang slices a 3D model designed in PowerSHARE into N sections with the aid of a special macro. The resulting section at each Z level consists of curves such as lines, conic arcs, and Bezier spans. Then, these entities that form a contour are coded and saved into a custom predefined file for generating G-code by using a computer-aided manufacturing software presented by the same company (PowerSHARE). Chen's method creates a PIC file containing boundary loops as a special format that can be employed to picture a layer on screen using another software package.

Because their approach applies macros to entire 3D object thoroughly, the elapsed time for creating contours would be long. In another attempt made by Jamieson and Hacker, B-rep of a solid model designed in Parasolid is used for the purpose of direct slicing. In this approach, they applied macro(s) to faces of B-rep model in order to generate a boundary path. As reported in their paper, a simple part comprising cylindrical and rectangular faces is taken at least 90 min to generate the contours for all layers.

As for direct slicing in the present research, first the protrusion and subtractive features that form a model are recognized and extracted. Then, the faces of these features that are intersecting the XY plane at a certain Z level are listed for slicing. Then, for each face the intersections of facets, which are generated by Inventor Application Programming Interface (API) functions (e.g., `GetExistingFacets`, `CalculateFacets`), with the XY plane are exploited. Facet generation API function is applied only to the faces of the selected feature that intersects with XY plane at each Z increment. Therefore unlike most of the previous works (Asiabanpour and Khoshnevis, 2004; Choi and Kwok, 2002; Dolenc and Mäkelä, 1994) that the system searches the entire STL file to find an

intersecting facet, this system is searching from very limited list of facets resulting from the intersecting features with XY plane at each certain Z level. Hence, the total run time for machine path generation compared with methods that search the entire STL file will be significantly shorter. Finally, intersecting lines are sorted to form closed loop contours. While computing a contour, hatching data at X and Y directions are also computed to produce custom designed machine path for different RP processes. The above stages are schematically shown in Figure 4.2.

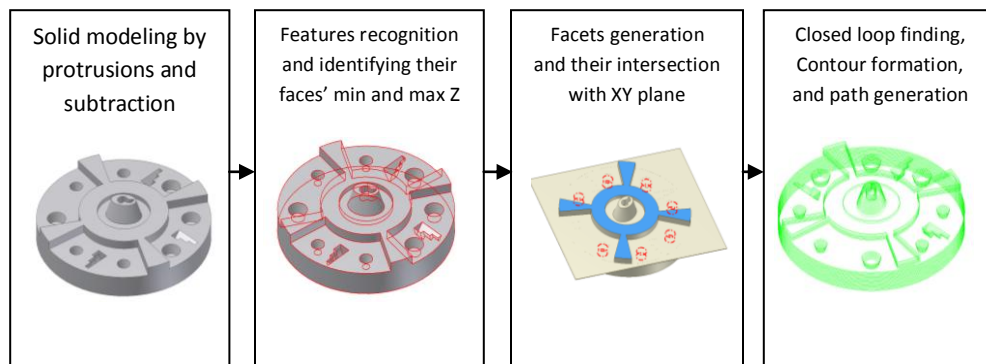


Figure 4.2. Direct slicing and path generation system structure.

Role of Feature Recognition in Slicing

Autodesk Inventor as a solid modeller uses various design features to form a solid model. The approach used for CAD models in this research is called design-by-feature solid modelling. All design features that form a solid model are classified into two groups. The first group includes the features that decrease a volume of a part; these are subtractive features. The second group includes the features which increase a part volume; these are protrusion features. Each design feature in Inventor is defined as an object whose all properties (e.g., Type of Feature, Faces, Edges, RangeBox...) would be accessed by Visual Basic codes. Some design features (e.g., Extrude, Revolve, Loft, Coil,

and Sweep) in Inventor have a special property, called “Operation”, by which the type of features is easily recognized. In contrast, some features (e.g., Shell, Hole, Chamfer, and Fillet), based on their design essence, are recognized as subtractive. In addition to subtractive or protrusion features recognition, other important data for the model slicing such as the maximum and minimum Z points of a feature and the faces of a feature with their maximum and minimum Z points are extracted.

By having the maximum and minimum Z points of the features, those of features which intersect with XY plane at certain Z level are initially selected. Then, a shortlist of the faces of the selected features that are certainly intersecting with XY plane in that Z level is selected by using the maximum and minimum Z points of faces. Therefore, the system only works with very limited number of faces compared to all faces available in the model. Consequently, the system’s run time is significantly decreased. The type of recognized features will also contribute to the proposed system in generating an internal/external hatch for the custom designed machine path for different RP processes.

Introduction to Adaptive Slicing System

In any type of adaptive slicing system, the investigation of the curvature of part geometry will be a key in determining a suitable thickness value being defined by the user. It has been theoretically proven that this method can produce parts with higher accuracy, less part geometry deviation, and shorter build time. Presented in this research is a new adaptive slicing approach for CAD models created by Inventor. The kernel of the proposed approach is to project all pairs of corresponding slices at the top and bottom of the considered layer on XY, XZ, and YZ horizontal surface to detect any possible part geometry distortion. A special error for layer thickness determination matched with user-

defined sheet thicknesses is then computed. One of the unique features of this new system is its ability to process very large and intricate models with difficult-to-recognize internal and external features. In addition, it is capable of producing machine paths that are compatible with waterjet and laser cutting processes that apply a variety of metal/non-metal sheet thicknesses. Despite previous works that cut the entire part from bottommost to topmost position at maximum available thickness, the proposed system starts cutting at minimum available thickness then allows the current layer becomes thicker or thinner as the comparison of the obtained error with threshold error. This part of the proposed system avoids any large geometry deviation error caused by sharply concave or convex corners. The factors in the form of error computation that help determine the thickness of a layer at Z increment position are discussed in the following sub-section.

Types of Part Geometry Distortion Errors

Quantifying the geometry distortion error is the main factor in determining the right value for layer thickness in both uniform and adaptive slicing. Dolenc and Mäkelä (1994) introduced one of the widely used errors: cusp height. In fact, the relationship between the maximum allowable cusp height and normal vector at any point on the tessellated model is applied to find the thickness of each layer. Many other researchers Cormier et al. (2000), Jung and Ahluwalia (2005), Pande and Kumar (2008), Xu et al. (1997) use this factor as an error measurement in their own algorithms. Investigation of all points on the top or bottom slice of a layer allows for calculation of the values of the maximum allowable cusp height, would lead to the division of the current thickness into small slices or keeping it at maximum thickness. Any sharp concave or convex vertexes might appear whether we apply maximum or minimum thickness (see Figure 4.3), but it

might lead to a significant part geometry deviation if maximum thickness is finally applied by knowing that no geometry distortion at top and bottom slices detected using the desired cusp height. In an attempt to solve this problem, Singhal et al. (2008) presented a comprehensive accurate direct slicing procedure in which the sharp concave/convex vertices are first recognized and then named as a block point where no slicing occurs. If such vertexes fall within top and bottom slices of the layer, the slicing position is moved either over or below the identified vertexes. The obtained thickness is then sliced at the smallest available thicknesses.

There are two problems with their work. First, any concave or convex region may be represented by continuous curved surface not only through two or more adjacent slanting surfaces whereby we could easily detect the mentioned vertexes. Second, in the case of subdivision of the obtained layer into smaller ones, it might not be the integer number of available minimum thicknesses that would cause the failure of the slicing process.

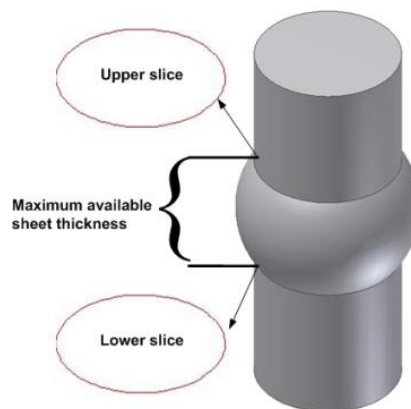


Figure 4.3. Two identical slices on the bottom and top of the layer cut by maximum thickness approach.

The second error measurement as a surface roughness, Ra, is used to determine the thickness of the layer. The major advantage of applying Ra amount over cusp height is its suitability for integrated design and manufacturing. Pandey et al. (2003) utilized Ra value on physical edge profile of fused deposition modelling (FDM) to fit the best thickness for under investigated layer. Singhal et al.(2008) implemented DOE to attain the optimal response value (Ra) for SLS prototypes which is used along with build direction at any point on a pair of slices of the layer in a specific non-linear formula for the purpose of determining an optimal thickness between user-defined minimum and maximum acceptable thicknesses. It seems that the use of this approach in a layer-by-layer fully dense fabrication process may not make sense as there is no realistic correlation between the surface roughnesses of a single metal/non-metal layer with layer thickness.

Using intermediary STL file format which consists of facets information such as vertexes and normal vectors, previous research attempted to intersect horizontal surfaces at a Z increment with the short list of facets at the Z level in order to obtain connected line segments by which a collection of interior and exterior contours is formed. The vertexes of line segments are used to calculate cusp height as discussed above. This process, however, is very time consuming as it requires investigation of all vertexes for finding optimum cusp height. To solve this problem, Zhao and Laperriere (2000) introduced a new tolerance (area deviation) so as to adaptively slice a CAD model. Despite widely used tessellated CAD models, they worked on direct CAD model inside CAD package software to create contours. Then the interior area of the created top and bottom contours of the layer encompassing entities like lines, circles, and ellipses are

computed for the purpose of comparing the measured area deviation with allowable tolerance to see whether the layer becomes thicker or thinner. In Figure 4.4, a staircase effect appears on the layer while two created contours have an equal area which leads the above mentioned solution to failure.

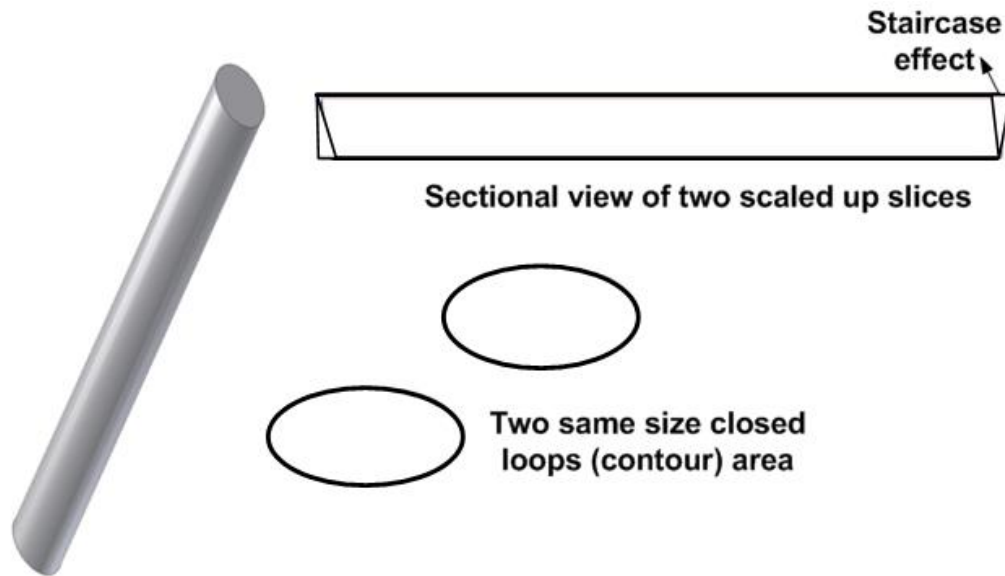


Figure 4.4. The staircase effect while two created contours are same size in inner area.

All of these tolerances are regarded as 2D measurements in which the degree of layer curvature is measured at different points. This 2D measurement is assumed to become a weaker decision factor in layer thickness selection when the complexity of the geometry of a CAD model is greatly increased. In response to this issue, Kumar and Choudhury (2005) presented a type of 3D tolerance named as volume deviation in direct slicing for achieving higher accuracy in adaptive slicing process. The volume deviation between a CAD model and built-up part in 5-axis laminated object manufacturing is calculated so that the deviation between the actual model and the built-up part is significantly reduced. This technique is, in fact, a promising solution for slicing CAD models with remarkable higher precision, but since it works directly with surfaces of the

part to mathematically compute the related volumes the complexity in the geometry of the surfaces would need some complicated mathematical computation that may jeopardize the validity of such system.

Generally speaking, it can be concluded that the higher accuracy of adaptive slicing requires a comprehensive approach by which the geometric complexity of a part is taken into consideration at different dimensions. In the following, the technique in measuring the geometry curvature of the complicated parts towards adaptive slicing is explained.

Interior and Exterior Contour Creation

After features recognition, the shortlist of faces intersecting XY plane at a $Z=z$ are sent to the Inventor's API function for the purpose of facet creation. At each increment of Z , a set of points resulted from intersection of XY plane with the created facets is generated. The next step would be the connection of the points to each other to form the interior and exterior loop(s) or contour(s). Therefore, facet creation is basically the initial step towards the loops creation.

Facet creation: As shown in Figure 4.5, a model may encompass numerous design features. With the assumption that a cross-section XY plane is passed through $Z=z$, the features F1, F2... F13 are selected due to crossing the XY plane at $Z=z$. Some faces of the selected features that intersect with XY plane, are then selected and sent to the Inventor's facet creation function (GetExistingFacets). The intersection between XY plane and the created facets results in a group of vectors (lines). A data structure, in fact for programming purpose, containing the following fields has been provided that would be exploited for saving the properties of each obtained vector.

- SP (indicating the start point of a vector)
- EP (indicating the end point of a vector)
- CreatedByFeature (Determining the type of a feature that would contribute in identifying external and internal hatch. For Example, when the value of CreatedByFeature is True, internal hatch should be generated)
- Flag (Boolean value that would prevent from double computation. The value of “True” for Flag means that a vector cannot be employed again in the next computations)

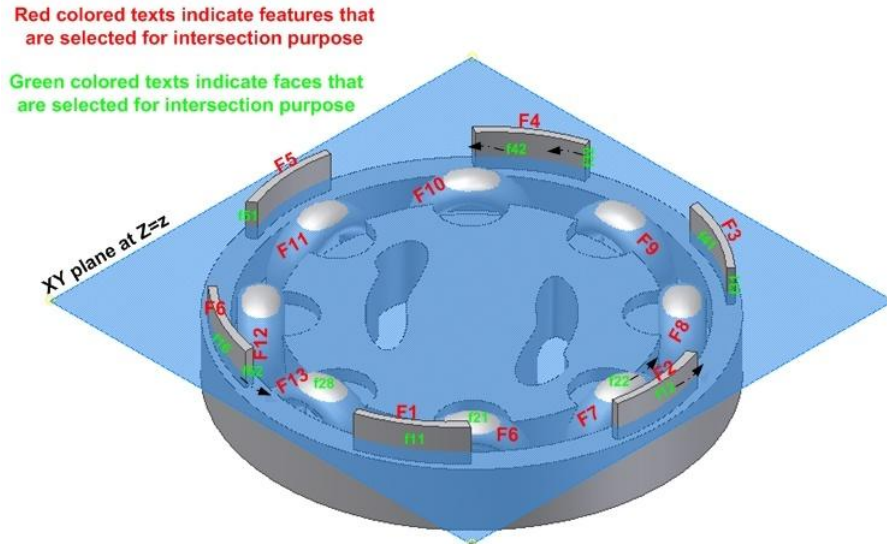


Figure 4.5. A sample part for facet creation test in Inventor.

Contour (loop) creation: After creating the intersecting vectors in each Z increment, they should be ordered and connected to form a continuous path (see Figure 4.7). In order to sort the vectors, algorithm starts from one vector and tries to find the next connected vector to this vector in a machine path generation process. Then, it continues the same approach until it reaches initial point of the first vector (a closed loop). While forming a vector loop using the required vectors from within the data

structure, the field (Flag) of each selected vector is set to be “True” by which the vector is prevented from double computation for the next loops. The connected vectors, which formed a loop, are saved in an array representing the loop’s properties. This approach is repeated until there is no vector whose Boolean field possesses the value of “False” (see Figure 4.8). Using the vectors data saved in the array, a boundary path for a RP machine based on the syntax of machine path code can be generated. While contour (boundary paths) creation encompassing the connected vectors, estimated process time (EPT) for the generated contour is calculated by the equation as follows:

$$EPT_1 = \sum_{j=1}^{count_vectors} (length(vector_j) * MachineFeedRate)$$

All the required stages that were explained above, the vector creation and boundary are repeated in different Z levels (see Figure 4.6).

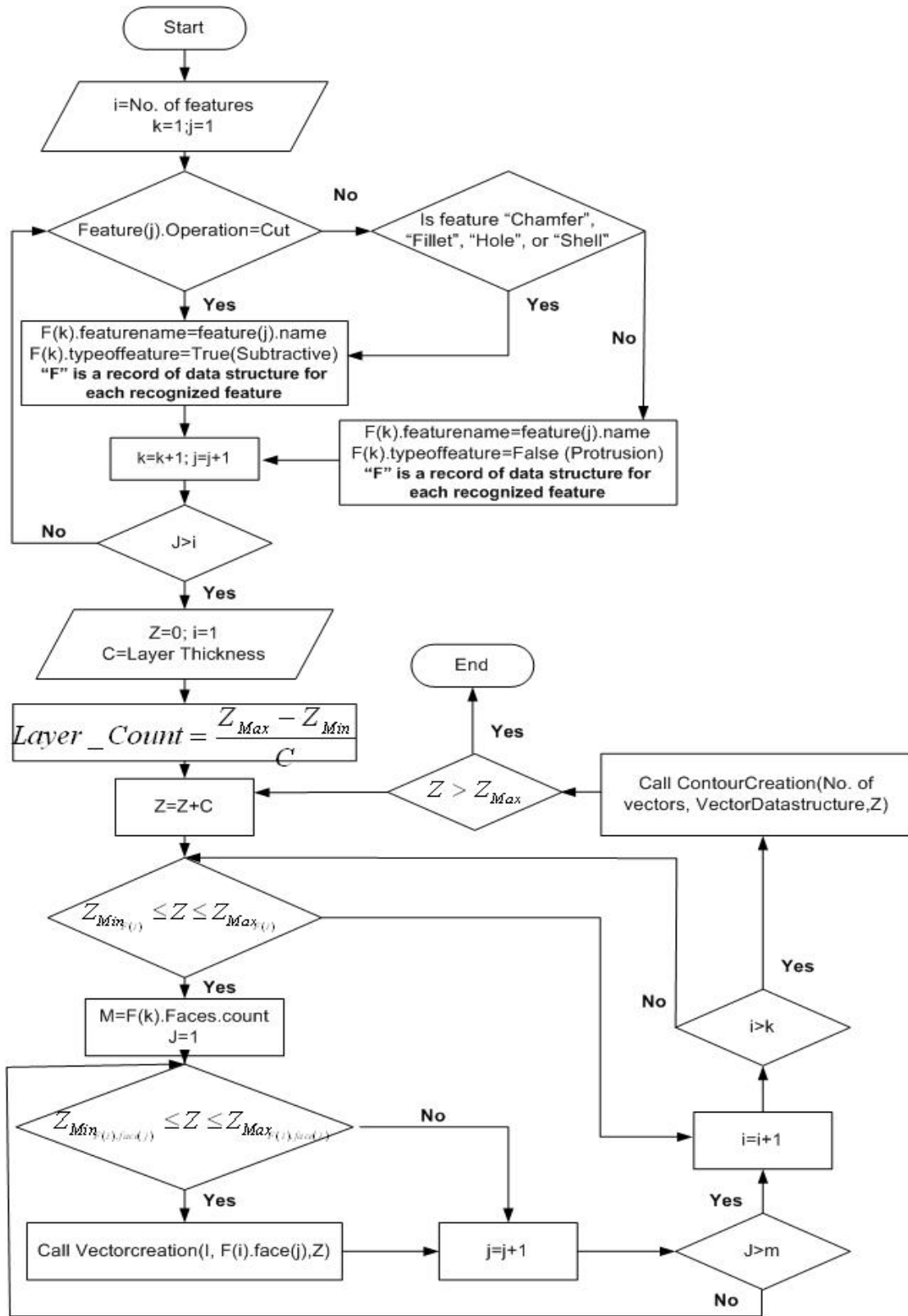


Figure 4.6. The boundary path generation algorithm.

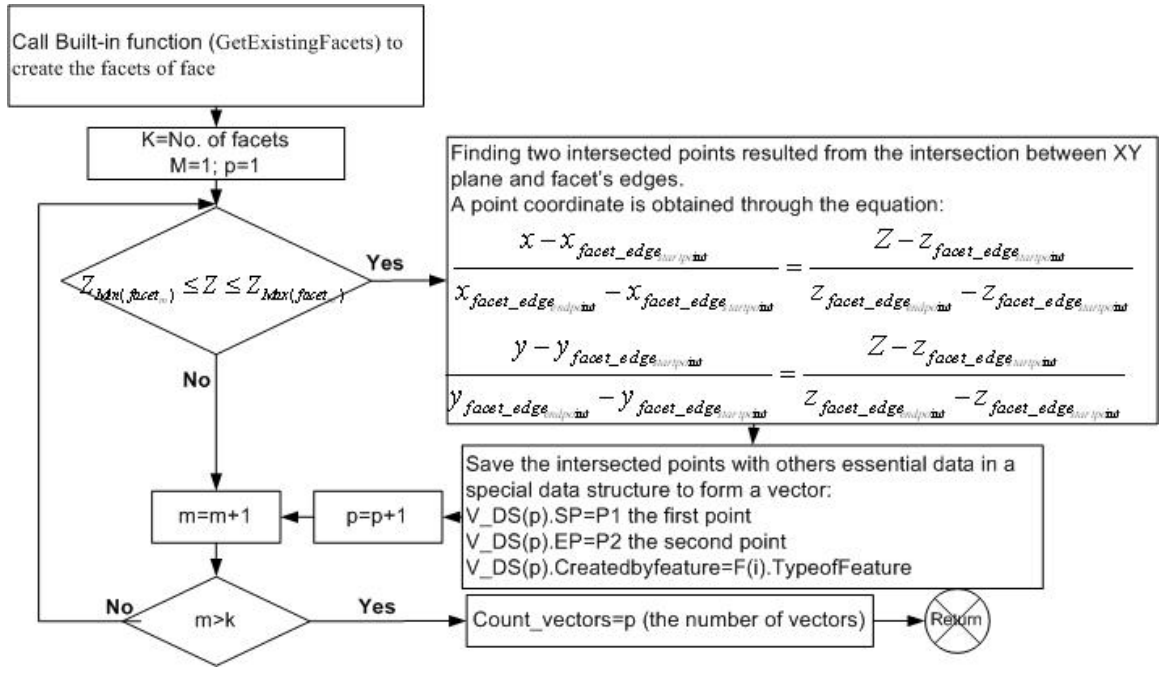


Figure 4.7. Subroutine for vector creation.

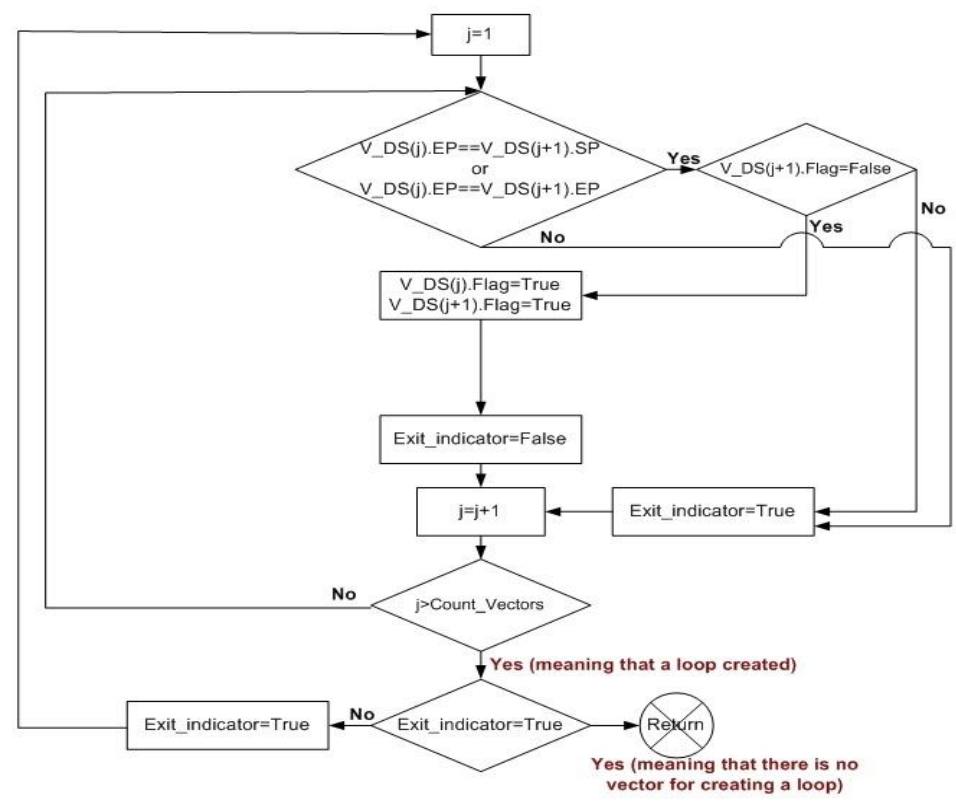


Figure 4.8. Subroutine for contour creation.

New Adaptive Slicing Algorithm

The previous works, while very significant in this field, have a few limitations. They commonly slice the direct CAD model or the tessellated version of the CAD model first at maximum available thickness, then apply some specific tolerances to break down the thicker slab into thinner ones or not to do so. The presence of any concave or convex area may yield a significant geometry deviation error when no staircase effect is identified at either slice of the layer. The area deviation could not be solely the accurate estimation for the degree of geometry deviation. Furthermore, the adaptive direct slicing which results in the intricate loops (contours) geometry has not been widely accepted as it needs the parametric equation of the enclosures. In addition, the use of the predefined available thicknesses for slicing purpose both for direct and indirect adaptive slicing has not been reported.

To overcome such limitations, a new direct slicing path algorithm is developed. It starts with the creation of all contours explained in Section 4 at a specific X, Y, or Z level depending on which cutting direction is chosen by the user (for simply explanation Z direction is assumed for slicing). Then, the bottommost slice resulted from the intersection of horizontal surface with the selected faces within Z boundary area (the area between z and $z + LT_{\min}$) is created. Note that the bottommost slice at $z=0$ cannot be obtained as all facets on bottom surfaces are parallel to the XY-plane. Thereafter the position of the second slice at Z direction upward on CAD model is obtained by moving XY-plane parallel to the first slice at the minimum distance (minimum available thickness) in order to avoid significant part geometry deviation when no obvious staircase

effect found at either slice. It is interesting to say that even though the presence of concave and convex area between two slices at minimum thickness would be inevitable, the geometry distortion at this point is small enough compared with that of thicker layer. The interior and exterior loops (contours) are then projected onto XZ-plane for the purpose of calculating the maximum and minimum points (x_{\min} , x_{\max}) of each pair of projected contours. The triangle areas known as the staircase region at the right and left corners of all projected contours are computed, respectively. If the value of one of the right or left triangle areas of all investigated pair contours is less than the user-defined allowable error, then the second layer is removed from memory (see Figure 4.9). Unless the imposed condition (allowable error) is not satisfied, the removal of the layers is continued.

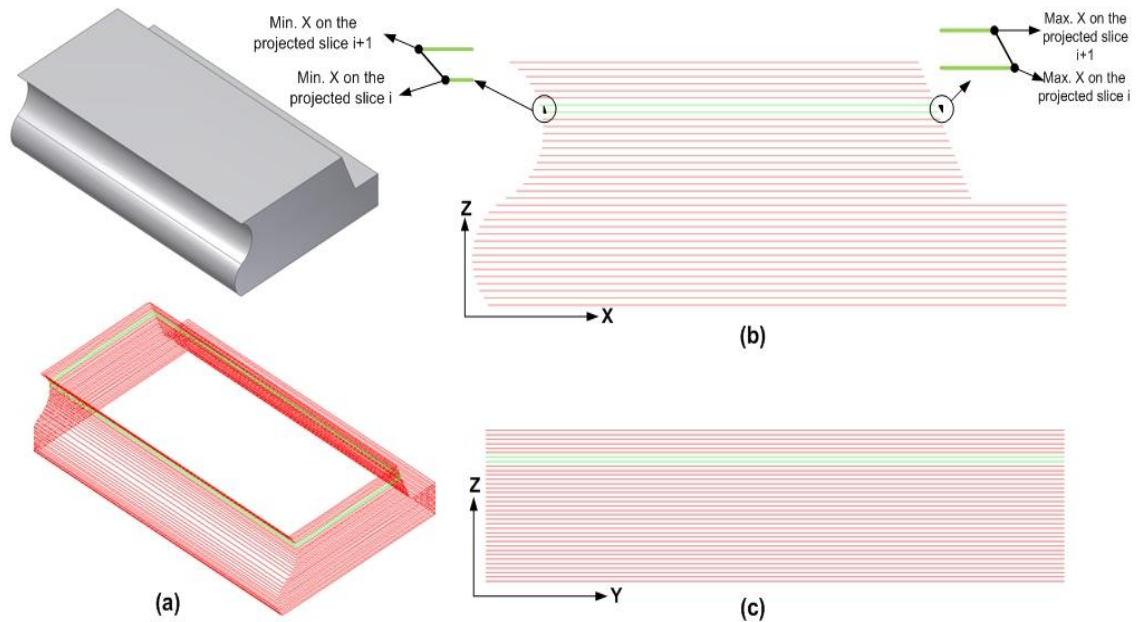


Figure 4.9. Staircase effect detection a) a 3D solid model with its sliced CAD model b) the identification of staircase effect in either side of the slices projected on ZX-plane c) lack of staircase effect on the right and left side of the slices projected on ZY-plane.

In addition to triangle areas investigation, sudden changes in the curved area on part geometry must be taken into account by comparing the cross product of vectors created by the connection of either maximum or minimum points of upper or lower slices and Z normal vector. It is commenced by figuring out the cross product of the vector (\vec{V}_{L_i}) and Z normal vector ($\vec{A} = \vec{V}_{L_i} \times \vec{N}_z$) in the preceding layer (L_i) then comparing it with that of the succeeding layer ($\vec{B} = \vec{V}_{L_{i+1}} \times \vec{N}_z$). If the sign of second cross product value is distinct from its corresponding in preceding layer, then eliminating the upper slice is stopped and the appropriate layer thickness is set at the desired amount. Figure 4.10 shows that how the sudden change might be taken place while it is being tried to execute the slice elimination algorithm. Following the discarding the upper slice, if the current vertical distance between the removed slice and the initial slice is matched with the user defined thicknesses then the adaptive thickness is established, otherwise the current distance is manipulated to fall within available user-defined thicknesses. After reaching a position at Z level where the calculated tolerance exceeds the threshold amount, the new position at $z + LT$ (fitted thickness) is set as the fresh initial Z level. The same approach for slicing the CAD model at the new Z level is iterated.

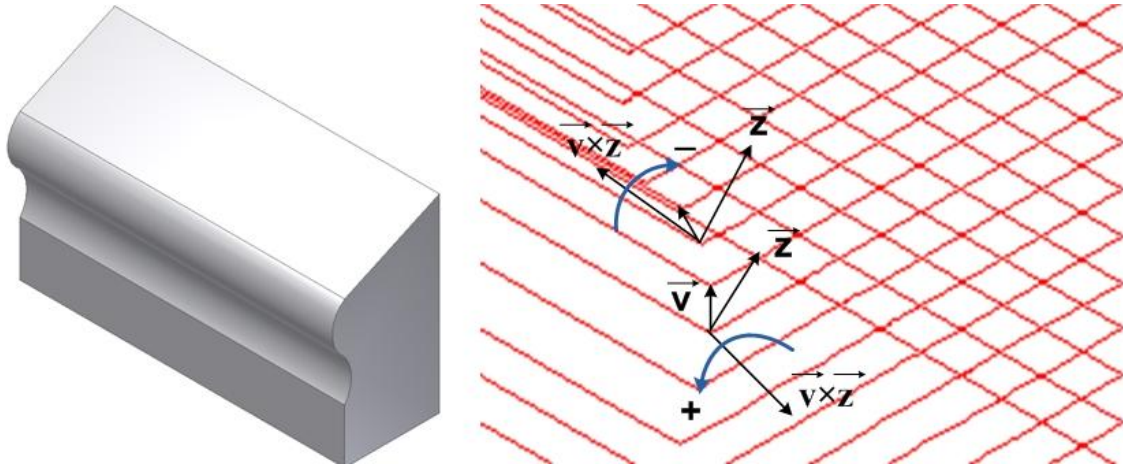


Figure 4.10. A 3D solid model with its partially enlarged sliced model illustrating the change of curve direction on layers.

Additionally, it is possible that no computed triangle areas as the representative of error threshold would surpass the tolerance when sliced in Z direction. So it is likely that the obtained adaptive slices would disregard the geometry distortion in different views. As a result, in order to identify staircase effects in other directions, a similar approach explained for the slices mapped on XZ -plane is implemented for all pairs of the projected contours on the YZ -plane as well.

Surprisingly, it may not be able to detect all curved area on part while implementing the algorithm on both YZ and XZ planes. Therefore, it might be existed any curvature on part geometry which was not revealed by the projection of the contours on either sides. To tackle such problem, it is required to check the area deviation for all pairs of contours generated in lower and upper slices of the layer to see whether or not the area deviation is exceeding the defined tolerance. Because all contours generated in this system were created by the connection of the continuous vectors in clockwise fashion, the inner area of each closed loop boundary (contour) is easily computed by the following equation in contrast with the previous direct slicing approaches that used

complex mathematical calculation for each entity (e.g., spline, ellipse, circle, etc) of closed loops.

$$\text{Inner Area} = \frac{(x_1y_2 - x_2y_1) + (x_2y_3 - x_3y_2) + \dots + (x_ny_1 - x_1y_n)}{2}$$

Where x_i, y_i are the coordinates of the initial and ending points of the line segments (vectors). The process of adaptive slicing is continued to reach the topmost of the CAD model (see algorithm flowchart in Figure 4.11 for more details). To maximize the benefits of adaptive slicing, the proposed system enables users to cut the CAD model in two other orientations (Y, Z) as well. Because there is only two available machines (waterjet and laser cut) by which any metal or non-metal part can be cut into various thickness without need for a proper machine setup, the proposed direct adaptive slicing system was tested on FDFP process which is based on the parts cut by water jet and laser cutter machines.

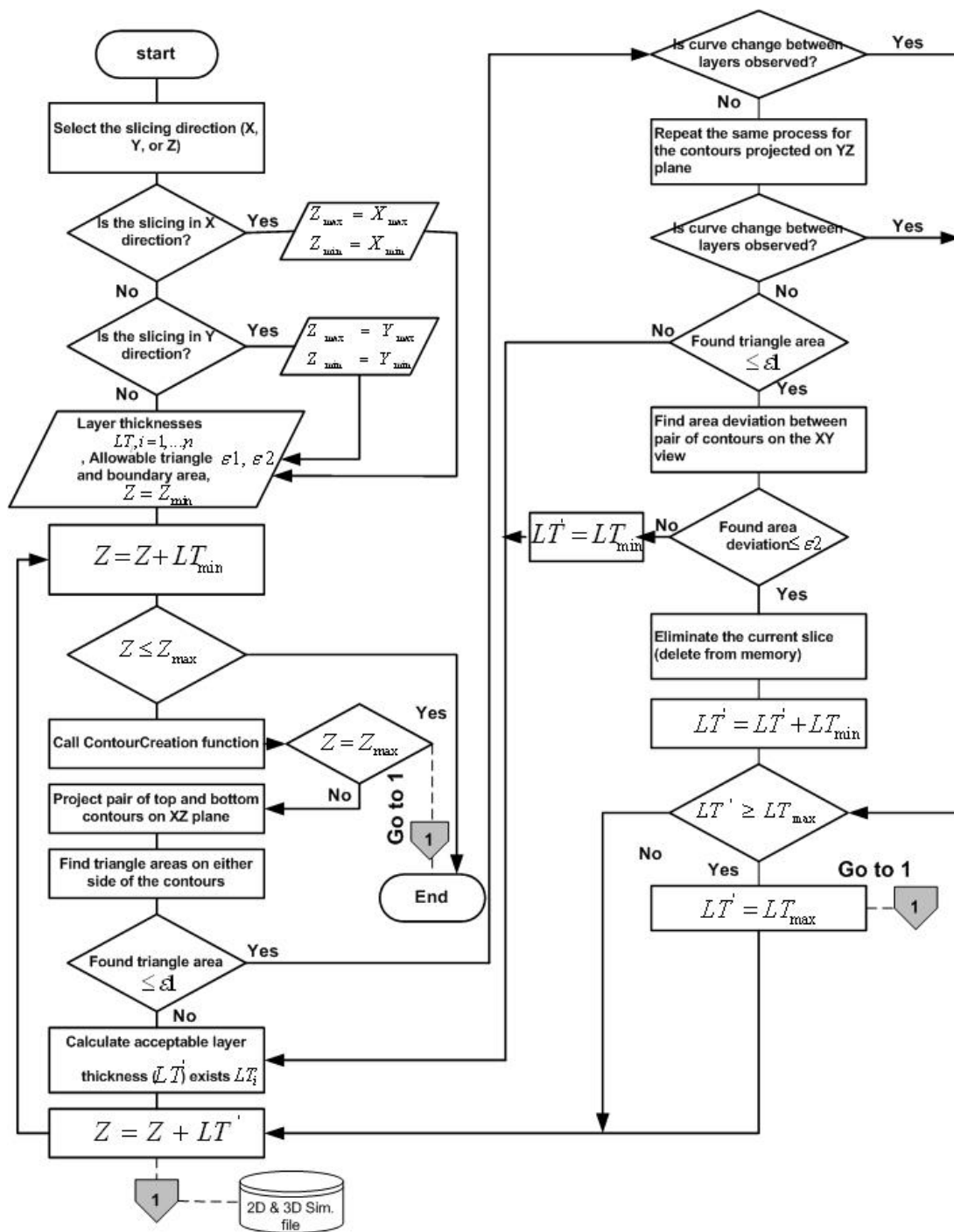


Figure 4.11. Flow chart for the proposed adaptive slicing algorithm.

System Implementation

These algorithms were implemented using the Visual Basic for Application (VBA) and Autodesk Inventor mechanical design software. The Autodesk Inventor API functions were used to gain access to specific objects of a part model (e.g., Feature, Type of Feature, Face, Facets, Edge). The Inventor's VBA provided an easy way of accessing the design features and generating the facets for all faces of the features. A user interface form facilitates data entries (i.e., slice direction in either X, Y, or Z directions, various sheet thicknesses, allowable errors for boundary area deviation and triangle area). Figure 4.12 illustrates user interface form for direct adaptive slicing system. The user can select the file name and directory to save the generated codes. Even though the generated machine codes (i.e., contour data) are saved in one text file, the software output can be demonstrated layer by layer in the 2D and 3D versions. In the 2D version, the generated layers are spread on the XY-plane and grouped in different columns according to their sheet thickness realized by the proposed system. In contrast, in 3D version all layers in their own thickness are stacked together in build direction to form an approximate real 3D solid model for better visualization of the final physical part being fabricated by FDFD process. This format of demonstration makes it easier to check the accuracy of the generated code (see Appendix B for detail on how to run software).

Figure 4.12. The user interface form.

Results and Discussion

Results: This software was successfully tested for many complex models with a variety of features. For better evaluation of the system, 2D and 3D AutoCAD script files generation were added to the system's output. Such files are easily run in AutoCAD to illustrate the boundary for different layers. The following three examples illustrate system output in AutoCAD environments. In the first two examples, the following required inputs essential to launch the program are entered by the user: three available sheets with thickness of 0.025, 0.1, and 0.2 in., the slicing orientation of Z, Y, and X for examples 1, 2, and 3 respectively. Allowable triangle area tolerance (0.0045) and allowable boundary area distortion (4%) are provided to control the thickness of the layers based on the part geometry characterization. In the third example, available thicknesses are assumed to be 0.01, 0.03, 0.05, and 0.1 in. and the CAD model is sliced in Z orientation with allowable tolerances as 0.0035 and 3%, respectively.

Example 1: Adaptive slicing with the lack of staircase effect on XZ and YZ views: Figure 4.13(a) shows the solid CAD model drawn in Inventor. This model is chosen to verify the methodology dedicated to the slicing of a part while the staircase effect is lacking. System starts slicing the CAD model from the bottommost at $z=0$ featured in region 1 (Figure 4.13(b)). It continues moving upward at Z-direction by adding minimum thickness of 0.025 in. Because there is no staircase effect in the region 1, the system stop eliminating the thinner layers until it reaches slice #2 where the maximum thickness of 0.2 in. is applied. The same way is followed for the second layer at stop point positioned in slice #3. Then it continues the slicing in region 1 until getting to slice #7. The obtained layer between slices #3 and #7 accounts for the thickness of 1.075 in. which is not in the list of available sheet thickness. To fit the acceptable thickness, the system defines the nearest thickness of 1.0 in. to the current value of 1.075 in. Since the thickness (0.075 in.) of the layer from slices #4 to #7 cannot be fitted with any available thicknesses, it is divided into three small slabs each 0.025 in. height. The region 2 is the interesting area where no sign of staircase effects is found while projecting the created contours on either ZX or ZY plane. In this situation, the present system relies on boundary area deviation of the slices projected on XY plane. The computed area deviation for all pair of the slices from #7 to #24 never satisfies the allowable boundary area tolerance meaning that equal thickness of 0.025 in. is applied for all slabs in region 2 (Figure 4.13(c)).

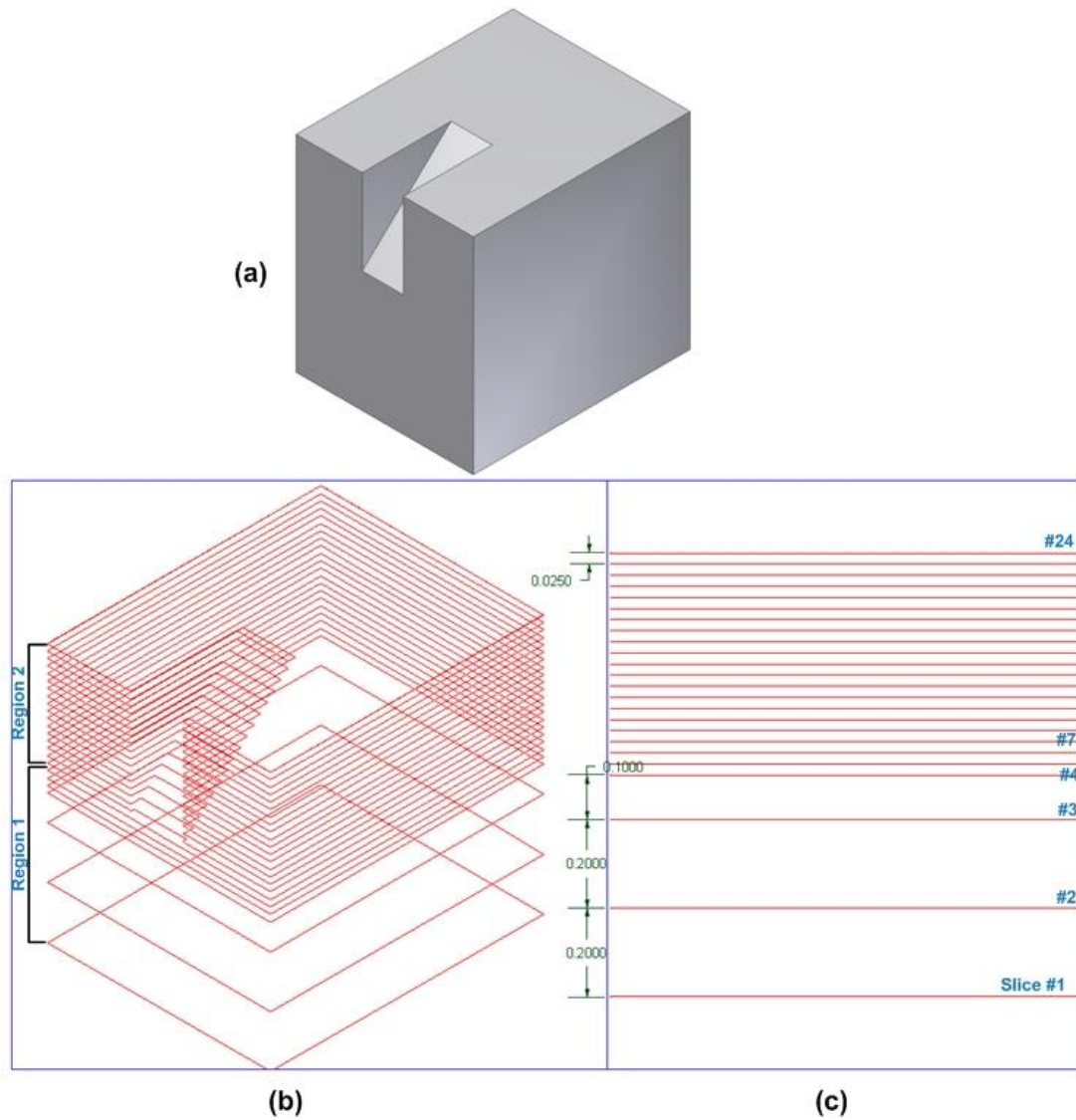


Figure 4.13. Visualization of the original Inventor CAD model (a) the simulated 3D format in AutoCAD for the adaptively sliced sample part (b) front view of the sliced sample illustrating the variable thicknesses in different regions.

Example 2: adaptive slicing the CAD model with the existence of concave and convex regions: The system commences the slicing from the bottommost of the part at $x=0$. Initially knowing the staircase effect on the right side of the projected contours (see Figure 14(c)), the triangle area formed by the staircase is calculated from slice #1 to above slice #4 in which obtained error does not exceed the defined tolerance (0.0035).

Even though the satisfaction of the allowable error makes the position of the cutting slice to reach the above convex vertex, but the implementation of cross product of vectors resulting from the connection of corner points prevents the part at position 1.05 in. upward being sliced. Thereafter the current achieved thickness (1.05 in.) in region 1 (Figure 4.14(b)) is divided into three layers (first at the thickness of 0.1 in. and the next two at 0.025 in.), starting from slice #1 ending slice #4. Region 2 consists of the curved geometry in which the computation of the triangle area is carried out to assign an acceptable thickness for the layers in this region. The comparison of the calculated area with the predefined tolerance results in two layers each at the thickness of 0.1 in. Region 3, in fact, is firstly layered from slice #6 to slice #8 with the minimum thickness of 0.025 in. due to having the simple geometry. Secondly, owing to the curved area (internal feature) in the boundary of the respective region, it continues forming 8 layers from slice #8 to #16 with the thickness of 0.025 in. each. Region 4 from slice #17 to #19 consists of simple rectangular area which is cut at the acceptable thickness of 0.1 in. For region 5, the triangle areas on the left side of the projected contours dose not surpass the defined error (0.0035) and virtually a layer with the thickness of 0.025 in. is shaped. Since the height of the formed layer could not match with any available sheet thickness, it is sliced in two layers each at 0.025 in.

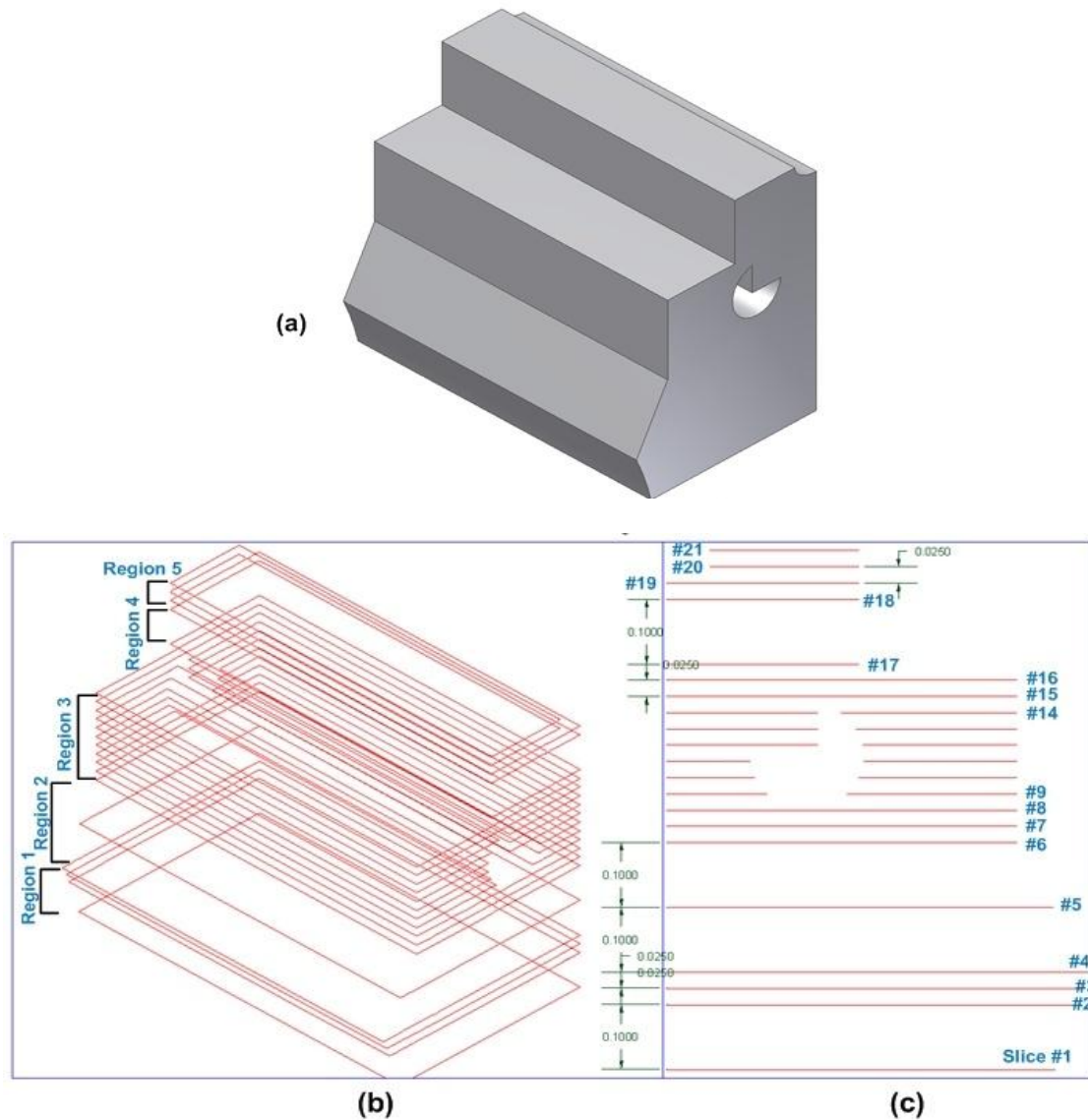


Figure 4.14. Visualization of the original Inventor CAD model (a) the simulated, 3D sliced model in AutoCAD for the adaptively sliced sample part (b) the sliced front view of CAD model illustrating the variable thicknesses in different regions (c)

Example 3: Figure 4.15(a) depicts a front axle drawn in Inventor. This complex geometry model is chosen to demonstrate the ability of the system in adaptively slicing any sophisticated CAD model with various sheet thicknesses. The system generates 3D simulated file in AutoCAD to display the accuracy of the slicing (Figure 4.15(b)). In front view of the sliced CAD model (Figure 4.15(c)), the different thicknesses conformed to

the available sheet thicknesses are applied throughout the part according to its geometry. In addition to 3D sliced file, a 2D file encompassing all layers spread on XY plane is generated. The generated layers are grouped based on their equal value of thickness in different columns parallel to each other to distinguish the layers required to be cut at single setup on waterjet cutting machine (see Figure 4.15(d)). It has to be noted that very few slices (at most one or two) shown in Figure 4.15(d) as red color might be left at the topmost of the part with the unmatched thickness while slicing the CAD model due to having thickness less than the available minimum one.

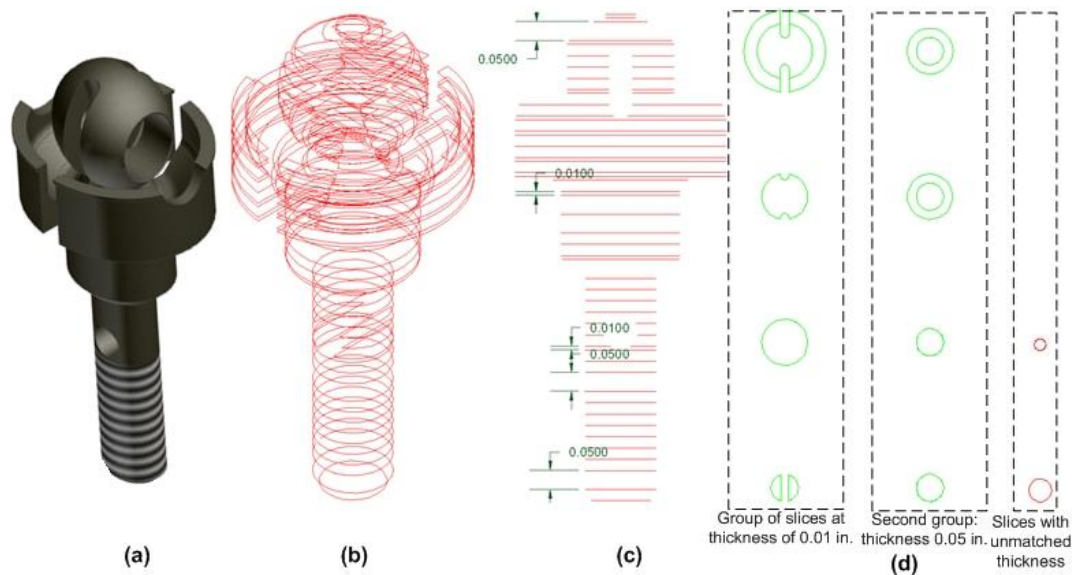


Figure 4.15. Visualization of the original Inventor CAD model (a), adaptive 3D slices (b), front view of the sliced CAD model (c), the illustration of few layers grouped based on their similar thickness and spread on 2D plane (d).

Discussion: The benefits of the proposed system and its contribution to the body of knowledge can be categorized in the areas of error free feature recognition, linkage to other systems, software computing time reduction, and manufacturing processing time and material cost reduction and mechanical properties improvement:

The proposed system is using a design-by-feature solid modeller and is implemented by Visual Basic codes inside Inventor using API functions to access both geometry and topology information of the design-by-feature solid model. The access to geometry and topology information facilitates fast and error free access to significant manufacturing data through the string of the connected objects in object model, the possibility of recognizing the complicated volumetric (manufacturing) features aiming to generate a feasible tool path as oppose to the systems that use neutral CAD files as the source for feature recognition which are often accompanied with erroneous data.

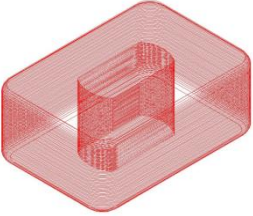
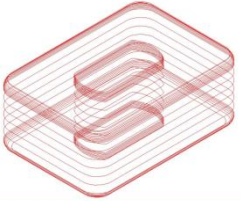
The ability of coding the obtained manufacturing data, facilitates linkage with the application/programming platforms such C++, VB, MS Access, MS Excel, and SQL Server for data exchange in facilitating the integration between CAD,CAM, and even supply chain systems (Ameri, et al., 2011).

The proposed system is using an algorithm that reduces the software computing time significantly. System proposed by Jamieson and Hacker (1995) finishes the contouring of the entire part in 90 minutes and system proposed by (Asiabanpour and Khoshnevis, 2003) makes each slice in 40 seconds. While these numbers may vary from computer to computer and part to part, the results is not comparable with the proposed system that can make contours for the entire model of a complex part generally in less than a minute.

As shown in Table 4.1, the usage of the proposed system with the capability of generating slices of variable thicknesses from a predefined standard sheet and cutting different thicknesses at the same setup can save significant process time, bonding materials, and cost compared to other processes with uniform thin layers. Another benefit

of using thicker layers compared to thinner layers is the significant improvement of mechanical properties of the manufactured parts (uniform materials vs. bonded layers), while the manufactured part error stays the same.

Table 4.1. A comparison between FDFE process time and cost for using uniform and adaptive slicing methods.

Slicing\performance	Process (cut) time (Min.)	No. of layers (i.e., bonding material cost)
Uniform layers 	54.50	67
Adaptive layers 	29	23
Saving (%)	46%	65%

CHAPTER V

CURVED-FORM ADAPTIVE SLICING

Adaptive Slicing for Sloping Surface

The rapid fabrication of a CAD model independent of any tooling is appealing as it would significantly reduce time, effort and cost - all crucial factors to the success of any business. To build a rapid 3D prototype that geometrically matches its 3D CAD model, current commercial RP systems often apply very thin layers of metal foil, fine metal/ non-metal powder, or liquid resin laminating from the bottom to top of the CAD model such that steps appearing on the edges of the layered model become less significant. This, however, increases build time and thus fabrication cost. Thick-layer lamination with sloping surfaces offers a possible solution to overcome this problem by reducing the number of layers. Mechanical limitations of the commonly used RP systems make thick-layer building impossible. This is due to the fact that fusing, sintering, soldering, ultrasonic welding, and printing (typical RP building processes) of the dense collection of particles and molecules in any selected bulk region of a variable thick layer is unachievable using present technology. Methods of building functional metallic parts and tooling by means of AWJ and laser cutting of fully dense metal sheets in various thicknesses followed by alignment and attachment of layers have recently been

developed (Nakagawa and Kunieda, 1984; Vouzelaud et al., 1992; Glozer and Bervick, 1992; Walczyk and Hardt, 1996; Bryden et al., 2001; Glen et al., 2011).

The ability to rapidly cut various sheet metal thicknesses from small to large dimensions using AWJ or laser cutter machines helped to significantly reduce build time compared to RP approaches that employed very thin layers of material. Fully dense rapid prototypes that are built up from non-uniform (adaptive) layers suffer from staircase errors appearing on the boundary edges of the layered CAD model. (Figure 5.1).

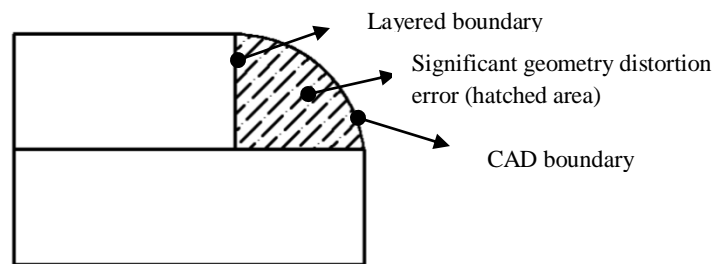


Figure 5.1. Illustration of the magnitude of geometry deviation error using simple adaptive slicing.

The sloped-edge adaptive slicing approach could improve the part quality to some extent but it still results in a geometry distortion error (staircase) even on sloping edges (Figure 5.2).

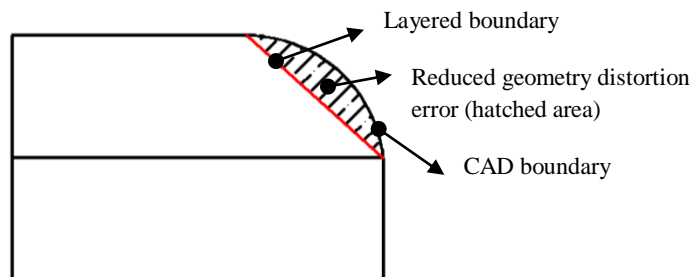


Figure 5.2. Illustration of the magnitude of geometry deviation error using sloped-edge adaptive slicing.

However, adaptive slicing for sloping surfaces takes advantage of applying the thicker layers effectively on the complex geometrical shapes containing the geometrical

characteristics of general 3D models such as convex and concave shapes, a sudden change of geometry, a ruled surface, and sharp edges, thus reducing the quantity of the slabs and the reduction of geometry distortion. To successfully implement this approach more axes of control are required, and the sloping surface path has to be obtained.

Generally speaking, the sloped-edge adaptive slicing goes through the two major steps, namely the determination of the adaptive slice thickness that is done by the calculation of various geometry deviation errors and the connection of the corresponding upper and lower contours points of a layer in order to form the cutting trajectory. In an attempt to build the parts with the sloping surfaces in RP, Hope et al. (1997b) presented the TruSurf system. It first takes the geometry and topology information of a sample CAD model from a file with IGES format. Accessing to the B-spline surfaces of the CAD model exist in the file and come with parametric data, the presented system tries to obtain the top and bottom contours resulted from the intersection of XY plane with B-spline surface at the defined Z level. Following the determination of the numbers of contour points defined by the user, the top and bottom contour points using parametric equation are computed by which the continuous connection of points through lines to approximate the actual CAD slices is facilitated. Using the presented algorithm and simple vector equations, the system succeeded in joining the corresponding top and bottom contour points to create a cutting vectors and trajectory. The linear movement of 5-axis machine head from start to end points of the connected contour lines and rotational movement of the machine head at two angles in cylindrical coordinates (cutting angle and polar angle) helped to build the layers with slanting surface and variable thickness.

Hope et al. (1997a) extended the application of the TruSurf system to the concise determination of variable layer thickness according to the surface geometry complexity. Also, they generated the layer sloping surface either inside the CAD boundary, outside, or a combination of both to meet the finishing requirements of the final prototype by comparing inside and outside tolerances with the computed cusp height. For example, if finishing procedures are to remove material from the prototype surface, the tolerance would fall outside the CAD boundary (cusps of extra materials) resulting in outside inclined ruled surfaces (Figure 5.3(a)). Conversely if filling material needs to be applied to the surface of the prototype, then the tolerance would fall inside (cusps of missing material) and end up with inside sloped surfaces (Figure 5.3(b)). Either way requires material deposition or removal post-processing to make the prototype identical to its original CAD model.

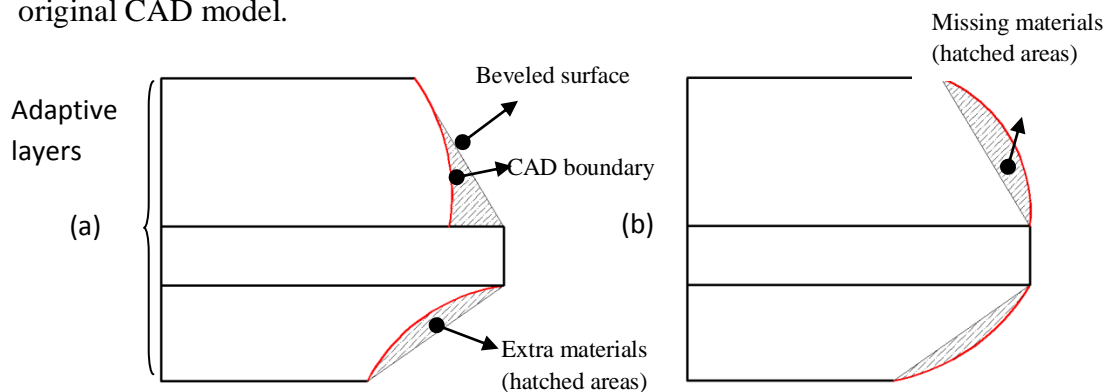


Figure 5.3. Illustration of outside (a) and inside slicing position (b).

Chamberlain et al. (1998) presented the zero integrated error ruled edge slice (ZIGER slice) algorithm in which cross sections of the sample 3D model are represented in STL format at one degree angle increments giving a total of 359 sections. Sections are first obtained by averaging sample points of facet vertices. The connection of such sample points approximates the slice slope. Then, two important measures of error,

average absolute error and maximum absolute error, contribute to the determination of adaptive thickness slicing. In fact, the above errors were the negative and positive areas emerging between the CAD surface and approximate slope surface (See Figure 5.4).

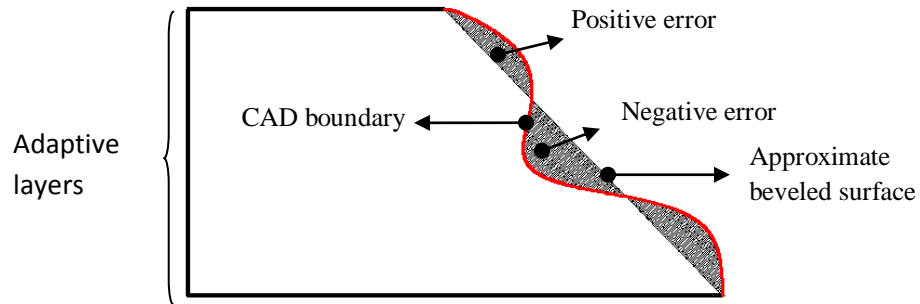


Figure 5.4. A view of ZIGER slice.

Utilizing STL file format, the work of Taylor et al. (2001) computed the intersection of a CAD model represented in STL format with the Z plane at a specified Z value to create a chain of line segments forming the closed-loop or contour. The start and end points of these line segments are swept half the layer thickness above and below the cutting plane to form rectangles in the vertical or slanting depending on the angle of the cutting vector. These rectangles based on the start and end points of a line segment on the created contour and the cutting angle correspond to discrete cutter locations during machining of that contour. In conjunction with adaptive ruled layers, Koc and Lee (2002) took into account the generation of ruled surfaces obtained by joining the corresponding top and bottom contour points of an adaptive layer. They concentrated on developing accurate connections of those points such that any twisted surfaces, surface approximation errors, and incorrect contour point joins would be avoided. The algorithm worked well for the connection of top and bottom contour points that were different in number and lent itself to the creation of ruled lines and surfaces, hence easing the generation of machine cutting paths suitable for 5-axis RP.

In another attempt to form ruled surfaces between the contours of an adaptive slice, Gupta et al. (2004) proposed an algorithm to stitch together unequal optimized numbers of top and bottom contour points to obtain acceptable ruled lines, thereby generating well-shaped sloping surfaces and conforming closely to the part surface boundary. Besides computing the optimum number of contour points and developing an adaptive slicing approach, they also provided a solution to the problem of cutting triangle patches that emerged from the multiple connection of one contour point with different points in its corresponding top or bottom contour. Yoo and Walczyk (2005) developed an advanced cutting trajectory algorithm for the profiled edge laminate (PEL) rapid tooling (RT) process (the process of the fabrication of large-scale dies and molds). Instead of slicing a CAD model represented by STL format, they directly performed the slicing process through SolidWorks API. A method for discretization of continuous profiles (i.e. the combination of arcs, splines, parabolas, and ellipsoids) of the CAD model has been developed. To stitch the obtained contour points appearing in front and back profiles for the purpose of accurate PEL surface reconstruction and the creation of optimized cutting vectors, an adaptive surface reconstruction algorithm consisting of Delaunay triangulation and a new complementary stitching algorithm were successfully implemented. The PEL technique is believed to be suitable for thick-layer rapid tooling that is suitable for 5-axis AWJ cutting machines leading to high quality prototypes.

In a nutshell, despite the fact that many endeavors have been carried out in the scope of beveled-edge slicing, no research has been reported to address curved-form lamination for intricate beveled surfaces. Therefore, the possibility of generating accurate machine path enabling curved-form sloped-edge lamination compatible with 5-axis AWJ

cutters will enable fabrication of functional parts from fully dense sheets with geometrical characteristics very near to their original CAD models.

To improve conformity to CAD model geometry, curved-form adaptive slicing on the sloped edges is presented. Multiple cuts of the edge boundary of each adaptive layer at variable cutting angles improve conformity to the CAD model curved surfaces (Figure 5.5).

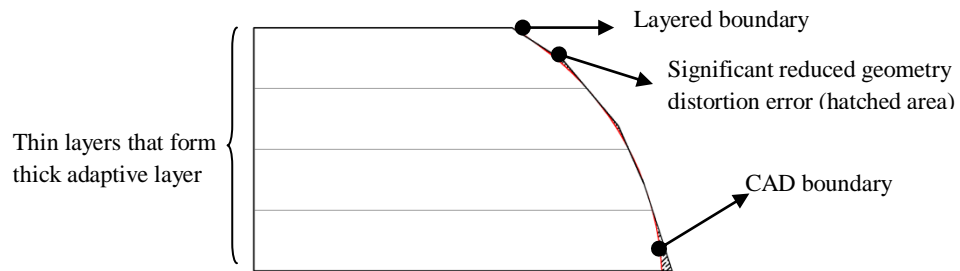


Figure 5.5. Illustration of the magnitude of geometry deviation error using curved-form adaptive slicing.

The aim of the present chapter is to generate sloping surfaces on the edge of an adaptive layer. The resulting surface has much less geometry deviation error and closely fits its CAD model boundary. The proposed system works in the following order: It takes in topology and geometry information from previously generated adaptive layers presented in Chapter 4. Then, the thickness of an adaptive layer and the bottom and top contours of adjacent layers are fed into the proposed algorithm in the form of the continuous connection of vectors and their cutting vector with the facet normal for the creation of curved-form sloping surfaces. Following curved-form adaptive slicing, a customized machine path and CNC code compatible with 5-axis AWJ cutters will be generated for any user-defined sheet thicknesses.

Curved-form Adaptive Slicing Algorithm

The successful implementation of the curved-form lamination is greatly dependent on the way a CAD file either original or STL model is adaptively sliced. The input to curved-form adaptive slicing algorithms is an adaptive slice which carries a limited number of thin layers in order to be assigned an available thick layer. In adaptive slicing the CAD model is initially sliced at the maximum available thickness. Adaptive slicing then applies some specific tolerances to decide whether or not to break the thicker slab down into thinner ones. From this some basic information of a typical adaptive slice such as layer thickness and contour points of the top and the bottom slices of the associated layer are generated. The present system requires topology and geometry information of all thin layers that shape an adaptive slice with the desired thickness (Hayasi and Asiabanpour, 2011).

For each layer whether thin (consisting of a bottom and top slice) or thick (encompassing more than two slices), an array of a specific data structure containing the required information for the slices (e.g. the internal and external closed-loop of each slice, the co-planar vectors of each contour, a surface identity assigned to each contour vector, and facet normal vector belonging to each contour vector) will be created. The contours are obtained by the continued connection of vectors or line segments resulting from the intersection of the XY-plane with selected facets at the defined Z level in counter clock-wise (CCW) fashion. Since a contour vector or line segment is the result of connecting two points laid upon the edges of a facet, the identity of a surface extracted from a facet will be readily obtainable by Autodesk Inventor API functions. Furthermore,

a facet normal vector is added as an attribute into the data structure of each contour vector as a result of placing start and end points of a line segment on the edges of that facet. Each contour vector is a principle element in the determination of cutting angle and trajectory (Figure 5.6).

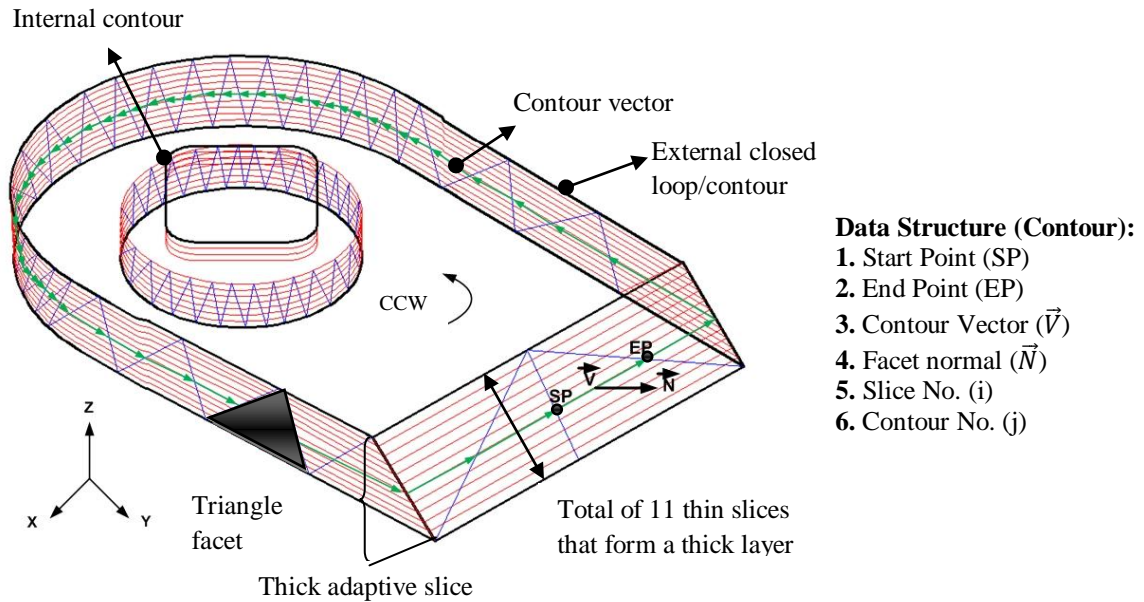


Figure 5.6. A view of a sample layered model accompanying detail slicing information.

Using a contour vector belonging to a specific contour at a sub-slice of the adaptive layer, the system will provide a 5-axis AWJ machine vector movement from vector start to end points, rotational angle (C) around Z axis, and cutting vector angle (A) (Figure 5.7).

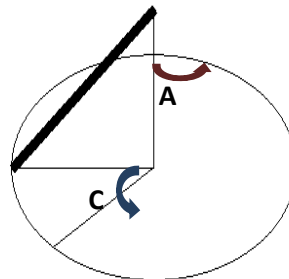


Figure 5.7. Rotational (C) and cutting (A) angles.

The contour vector (\vec{C}_{ij}) is simply obtained by subtracting the end point coordinates from the start point (i, j are the slice number within a thick adaptive slice and internal/ external contour number within that slice, respectively). Consequently, a cutting vector (\vec{V}_{ij}) can be computed by taking the cross product of the obtained contour vector and a facet normal (\vec{N}_{ij}) that had been added into the vector record in the defined data structure. Because all contour vectors are ordered in CCW manner, for internal closed-loops (contours) the cross product of vectors must be given by $\vec{V}_{ij} = \vec{C}_{ij} \times \vec{N}_{ij}$ and by the opposite ($\vec{V}_{ij} = \vec{N}_{ij} \times \vec{C}_{ij}$) for external contours in order to lead the pick of the cutting vector in the direction of the cutting stream. Following calculation of the above vectors, the two rotational and cutting angles are obtained as follows:

$$\text{Cutting Vector angle: } A = 180 - \cos^{-1} \frac{\vec{z} \cdot \vec{V}_{ij}}{\|\vec{z}\| \|\vec{V}_{ij}\|} \quad (1)$$

$$\text{Rotational angle: } C = \cos^{-1} \frac{\vec{x} \cdot \vec{V}_{ij}}{\|\vec{x}\| \|\vec{V}_{ij}\|}$$

Figure 5.8 is a graphic view of the vector computation on the simple adaptive slice including a few thin slices with multiple loops within a thin slice.

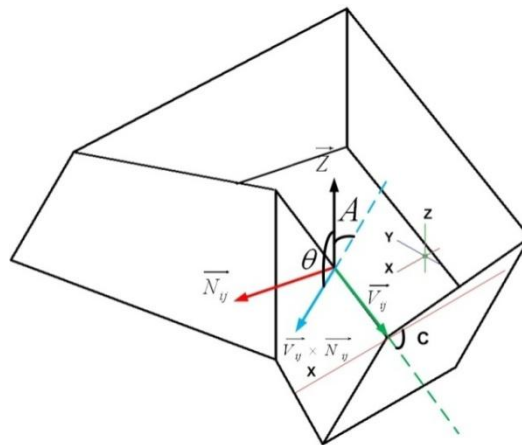


Figure 5.8. Visual representation of machine head angles (A,C) and cutting vector.

For cutting curve edges, the proposed system should be capable of recognizing concave or convex curves throughout the surface of the layered model while tracing all contour vectors in a CCW direction. This is an important part of the system as it will help to determine the appropriate action to cut the curved regions. For convex edges, the system will provide a custom machine path along which the multiple cuts required for that edge will be possible. The use of multiple cutting vectors for a single convex edge results in a curved-form edge closer to its original CAD edge with minimal geometric deviation (Figure 5.9 (a)). For a concave edge, it is impossible to apply multiple cuts in this fashion, as doing so results in removal of excessive material in the first single cut (Figure. 5.9(b))

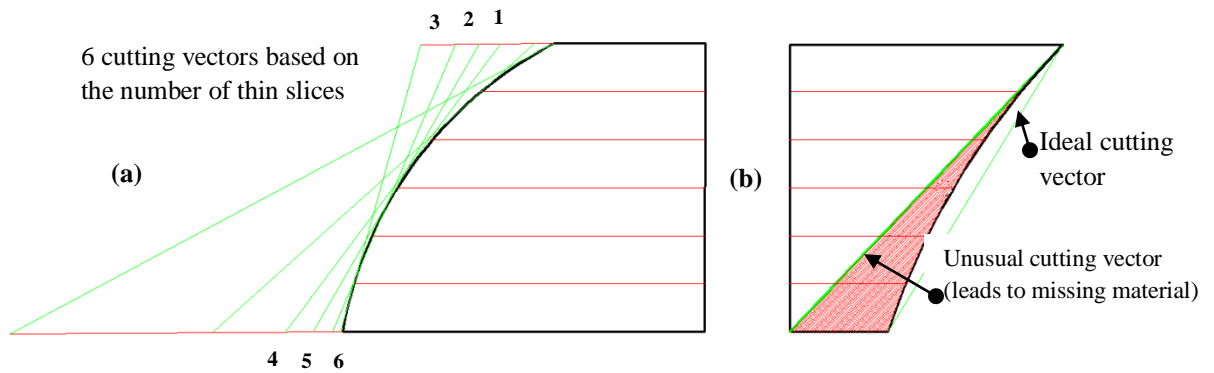


Figure 5.9. Two different cutting strategies: (a) Multiple cuts to form a convex edge (b) single cut for a concave edge.

As a result, the top and bottom points of the concave curve and subsequently the connection of these points need to be identified in order to create a single cutting vector, as a guide for the AWJ cutting stream.

In conjunction with the identification of convex and concave edges, a contour vector at a particular slice number, for example, k , is first picked and its start and end points (SP_{kj}, EP_{kj}) and its cutting vector (\vec{V}_{kj}) is extracted from the data structure. Then,

the midpoint (MP_{kj}) of SP_{kj}, EP_{kj} is found and mapped onto a plane parallel to the XY-plane and passing through slice no.1. To find a second point that lies on either the concave or convex curve and located on one of the contour vectors of the bottommost slice, a vector ($\overrightarrow{TV_{kj}}$) tangent to the surface at point EP_{kj} is projected on the same plane as the midpoint and a line parallel to that projected vector ($\overrightarrow{PV_{kj}}$) and passing through the projected midpoint (MP_{1j}) is obtained. The points resulting from the intersection of the line (L) with a short list of line segments (lines that surely intersect with the line L) located on the first slice are obtained. Among the points there is a point (IP_{1j}) placed on a contour vector whose surface identity equals that of $\overrightarrow{V_{kj}}$ and also lies on a vector (forming by the candidate point and point MP_{1j}) co-directional with $\overrightarrow{PV_{1j}}$. Once the desired point is obtained, a vector passing through that point and tangent to the part surface is created and its angle (θ) with \vec{Z} is computed. Again at point MP_{kj} , a vector tangent to the part surface is created and subsequently an angle (β) between this vector and \vec{Z} is found. A curve edge is regarded as convex if θ is greater than β , otherwise the edge is concave (Figure 5.10).

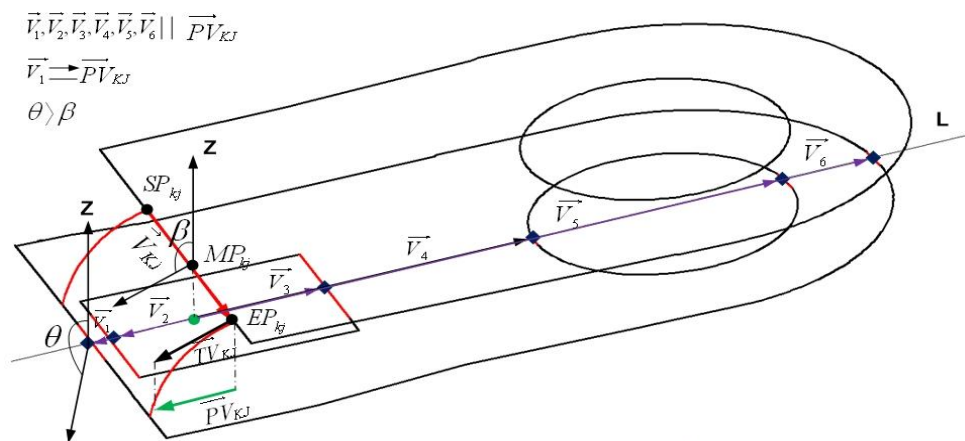


Figure 5.10. Graphical representation of how a convex edge is identified.

Once the adaptive slicing from the bottom to top of the CAD model is accurately accomplished, an external contour for each adaptive layer containing a number of thin slices is selected from among contours in the top slice of the layer. The initial vector in the chain of the vectors is obtained from the data structure of the contour vectors belonging to the selected contour and the possibility of being convex or concave at this point is evaluated using the method explained above. With regard to concave curves a straight sloping surface is formed by mapping the start and end points of the selected vector onto a plane parallel to the XY-plane and accommodating the contours of the bottom slice. Then two lines passing through the mapped points and parallel with the projected cutting vector of the top contour vector are drawn. The intersection of the lines with the corresponding line segments (contour vectors) on the bottom slice results in two additional points. Eventually, the desired beveled surface, which is created by the connection of those four points, would be a useful tool for both visual simulation of the curved-form cutting and as a source to generate 5-axis AWJ cutter machine trajectories (Figure 5.11(a)).

Unlike for concave curves the system is required to provide multiple slanting surfaces such that its output conforms to the curvature of convex region. With the assumption that the curvature of the part surface at the initial selected contour vector is found to be convex using the method explained, two lines passing through the start and end point of that vector and parallel to the cutting vector at this location are created. The two lines then intersect with a plane parallel to the XY-plane at a Z-level where the bottom slice is located (Figure 5.11(b)). The points resulting from the line-plane intersection are simply obtained by the following equation 2.

Line equation: $\frac{X-X_0}{a} = \frac{Y-Y_0}{b} = \frac{Z-Z_0}{c}$, $Z = Z_{slice(k)}$, $Z_0 = Z_{slice(top)}$
 X_0, Y_0 are the coordinates of vector's start or end points
 $V(a, b, c)$ cutting vector
 By setting $t = \frac{Z_{slice(k)} - Z_{slice(top)}}{c}$ then $X = X_0 + a \times t$ and $Y = Y_0 + b \times t$ (2)

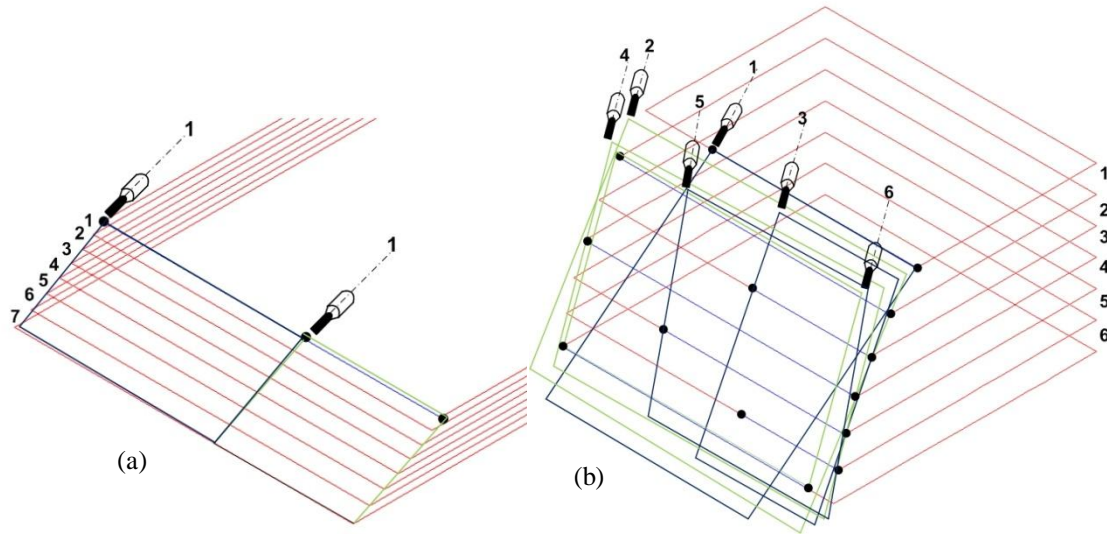


Figure 5.11. Illustration of a single cutting stream for concave edge (a) and multiple cutting streams for convex edge (b) formed by a number of thin slices.

The first slanting surface formed by the connection of the four points is retained in computer memory for further use in machine path generation. To complete beveled surface formation on the top slice, the system seeks to trace all the vectors within either external or internal loops of the slice and apply the above described algorithm. For the remainder of the thin slices, if the curvature of a part surface at a certain vector is found to be concave, the surface formation must be neglected based on the rule defined for such concave curves (i.e. single sloped cutting surface on concave edges). An overview of the developed algorithm presented as a flowchart is shown in Figure 5.12.

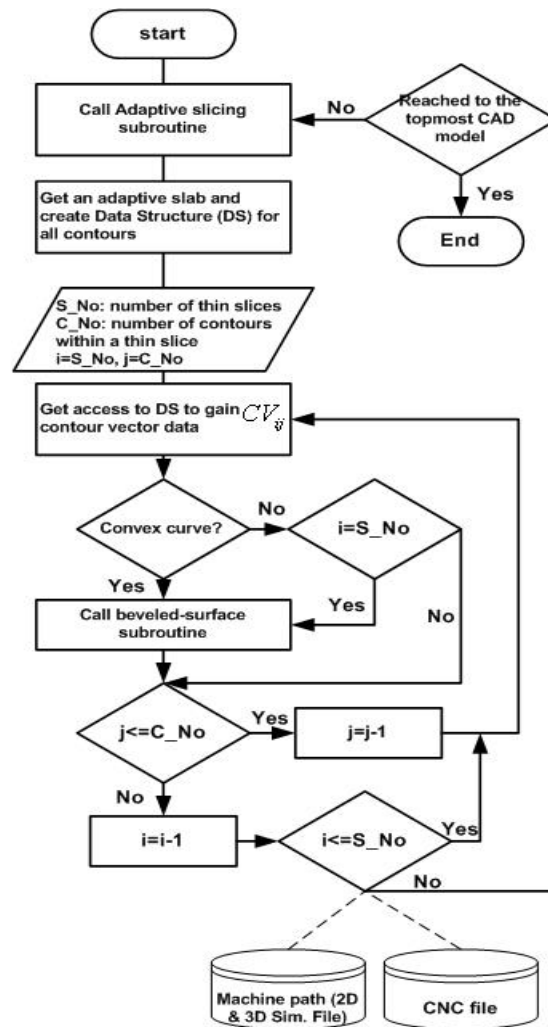


Figure 5.12. Curved-form adaptive slicing algorithm.

Machine Path and CNC-codes Generation

Currently available CAD/CAM and Computer-aided Manufacturing (CAM) systems are not capable of generating code for curved-form 5-axis AWJ cutting paths. Thus some custom modification of G-codes compatible with 5-axis AWJ machines would enable the production of objects very nearly resembling their CAD designs. Since a CAD model is mainly layered in adaptive manner by the use of available sheets on the shop-floor, the size of such sheets must be an input to fit different adaptive slices in their associated sheets according to the sheet thickness. Following CAD model lamination, a

group of slices whose thickness falls in the predefined sheet thickness are put together in matrix fashion on the sheet. In order to cut the layers in sequence, the position of each layer on its corresponding sheet is appropriately numbered. The CNC codes are written in such a way that an AWJ machine head would start cutting the layers from the thin through the thick sheet (Figure 5.13).

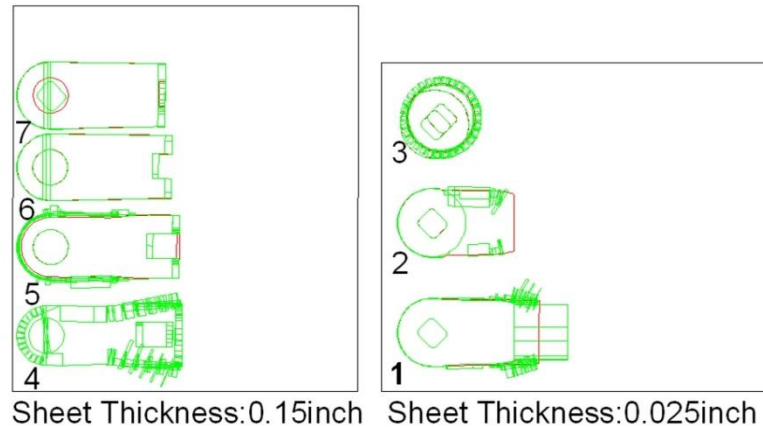


Figure 5.13. Top view of the arrangement of 7 distinct adaptive slices onto two available sheets with specified thicknesses.

In G-code generation, there are four basic parameters required for the purpose of 5-axis cutting, namely, linear movement of the machine head from start to end point of each contour vector, rotational and cutting angle of the machine head, and machine feed rate. The first four input data (SP, EP, θ , β) were simply obtained while generating the adaptive slices and applying the foregoing algorithm to each thick layer. There have been a few research efforts to determine how to use machine parameters and cutting depth to assign feed rate to get a good surface roughness quality. As a result, this part of the problem is not in the domain of our research and we mainly refer to previous work that arrived at a comprehensive feed rate formula. The following formula is then adopted from the research work of Limbachiya and Patel (2011).

$$v_f = \frac{\pi}{4} d_0^2 R \left(\frac{1}{1+R} \right)^2 \frac{p^{\frac{3}{2}}}{\mu_{job} d_i h_t} \sqrt{\frac{2}{\rho_w}} \quad (3)$$

Where,

d_0 = orifice diameter, d_i = insert diameter, R = ratio of mass flow rate of abrasive to flow rate of water, ρ_w = density of water, μ_{job} = specific energy of material, p = pressure in bar, and h_f =cut depth.

Parameters ($d_0, d_i, R, \rho_w, \mu_{job}$, and p) are easily obtained, but to calculate h_f we must measure the depth of either vertical or slanting surfaces at every contour vector position on the adaptive layer. The calculation of h_f is graphically depicted in Figure 5.14.

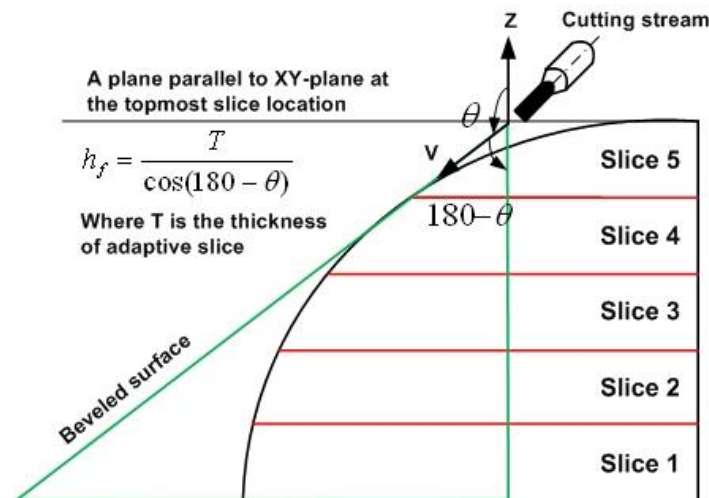


Figure 5.14. The explicit computation of h_f in the projected view of a sample adaptive slice.

System Implementation

The algorithm was implemented using VBA and Autodesk Inventor mechanical design software. Autodesk Inventor API functions were used to gain direct access to topology and geometry information of any complex CAD model. A user interface form facilitates data entries (i.e., slice direction in either X, Y, or Z directions, various sheet

thicknesses, allowable errors for boundary area deviation, triangle area, number of available sheets, sheets thickness, and the width and length of the sheets). Figure 5.15 illustrates the user interface form for triple slicing approaches that was developed in response to a user request. A user may select uniform slicing that best fits with the expected output. We have chosen to use the 5-axis angular slicing approach. The user can select the file name and directory to save the generated codes. Even though the generated 5-axis AWJ machine codes are saved in one text file, the software output can be obtained layer by layer in the 2D and 3D versions. In the 2D version, the generated layers containing line segments and sloping surfaces are grouped according to their sheet thickness and spread on the sheet rectangle surfaces in matrix form followed by numbering each adaptive slice. The 2D version is employed for simulating the cutting sequence of work pieces illustrated as 5-axis adaptive layers. In contrast, in the 3D version all layers along with their cutting surfaces in their own thickness are stacked together in the build direction to form an approximate real 3D solid model for better visualization of the final physical part being fabricated by the FDFP process. This format of demonstration makes it easier to check the accuracy of the generated code.

Figure 5.15. The user interface form.

System results, Verification, and Validation

The implemented system was successfully tested for slicing a variety of models with diverse types of surfaces (i.e., flat, convex, and concave), different slicing direction, and different number of sheets with different thicknesses. Two examples along with different stages of the curved form adaptive slicing are presented below:

Example 1: The entries for model 1 were: sheet thicknesses and sizes T1: 0.025 in, L1: 20 in, W1: 15 in, T2: 0.1in, L2: 15 in, W2: 30 in, and Cut direction: Y (Figure 5.16).

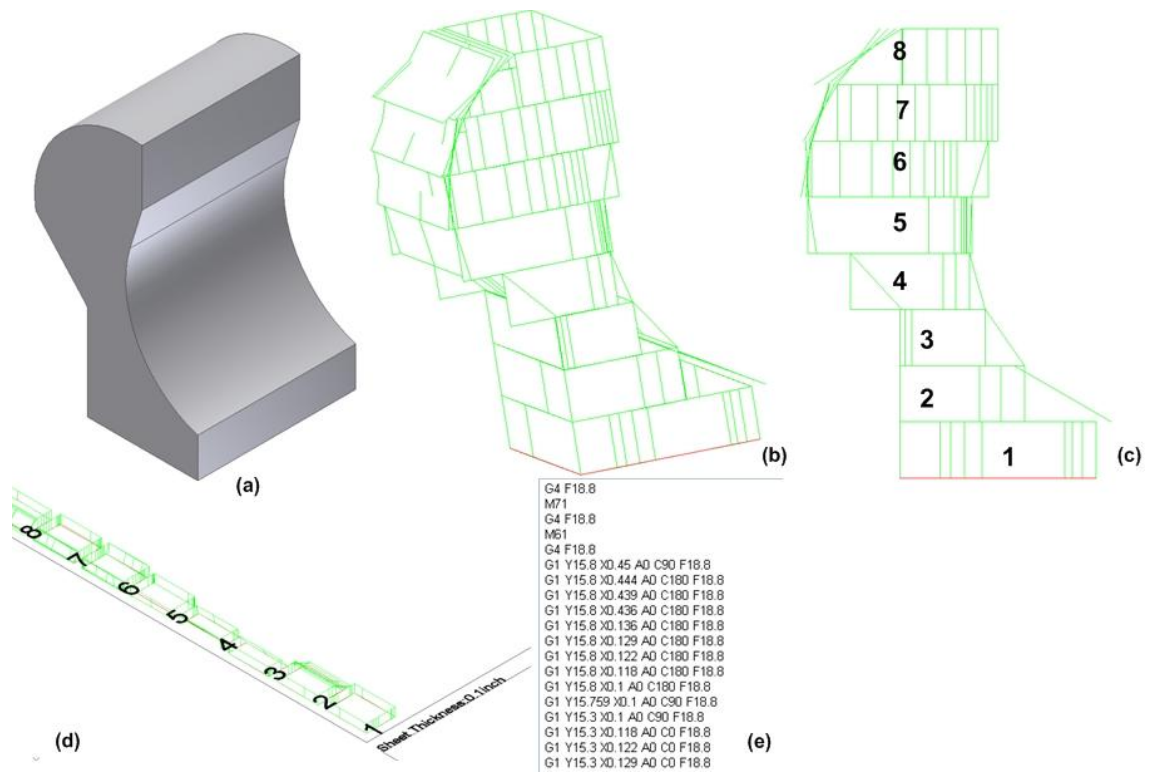


Figure 5.16. (a) 3D CAD model, (b) 3D view of curved-form adaptive slicing, (c) 2D front view of slicing, (d) 3D view of the adaptive slices spread on sheet, (e) The partial view of the generated G-codes

Example 2: The entries for model 2 were: sheet thicknesses and sizes T1: 0.1 in, L1: 20 in, W1: 15 in, T2: 0.25 in, L2: 15 in, W2: 30 in, and Cut direction: Z (Figure 5.17).

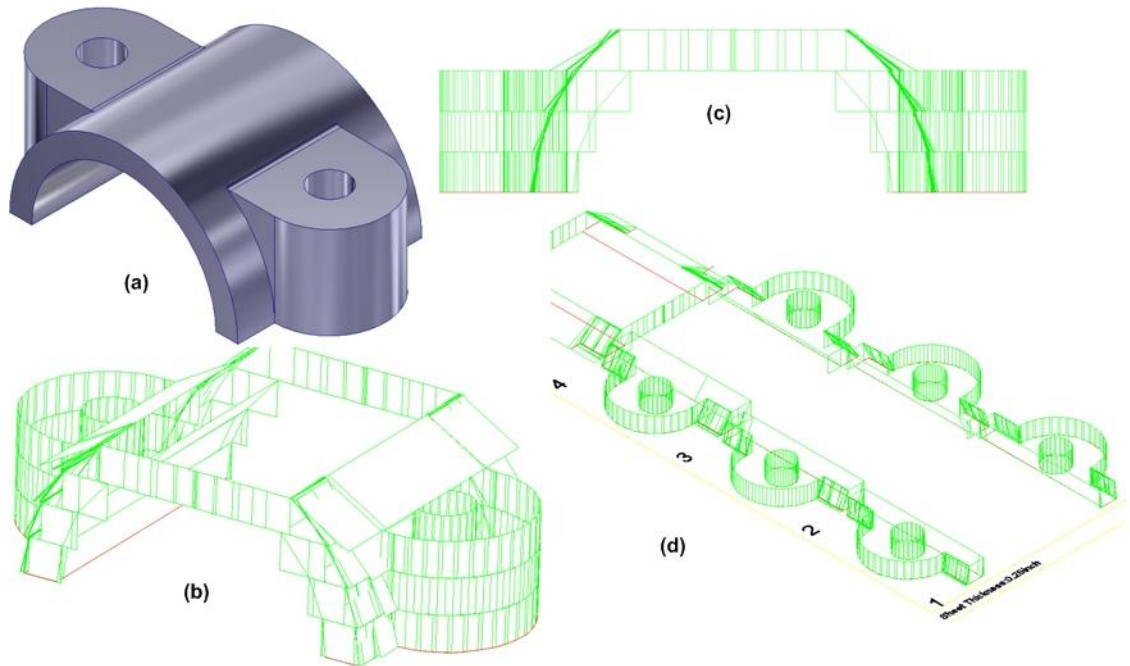


Figure 5.17. (a) 3D CAD model and (b-d) 3D and side view of curved-form adaptive slicing.

Concluding Remarks: In this chapter a new curved-form adaptive slicing method is presented. In this method, multiple cuts of the edge boundary of each adaptive layer with variable cutting vectors angles conform well to the CAD model curved surfaces. The proposed system is compatible with 5-axis AWJ machines. This system has been successfully tested on several models.

CHAPTER VI

EXPERIMENTAL DESIGN FOR FDFP PROCESS IMPROVEMENT

Design of Experiments (DOE) Approach

According to Myers and Montgomery (2002), DOE is a structured, organized method for determining the relationship between factors (Xs) affecting a process and the output of that process (Y). Hefin and Jiju (2003) stated that DOE is a special technique to study the effect of several independent variables that are affecting the response. To minimize the number of the experimental runs and complexity of the DOE, a good fit between the model and the process is necessary (Pfaff et al., 2006).

Full factorial design is a part of DOE approach in which all possible combinations of the factor levels are involved in the experiment. The results realized from the full factorial experiments would be more reliable, but conducting the full factorial experiments is costly and sometimes prohibitive. We mainly choose this method as the number of the identified affecting factors is not numerous to add cost more cost to experiment.

Factors Identification

In principle, the main aim of the research was to improve the FDFP process in order to produce parts with a high degree of quality. To achieve this end, the reduction of build time and the enhancement of the parts' quality synchronously would be the utmost

target. The identification of the affecting factors would help take proper steps in addressing issues related to the causes of defect or failure. An appropriate way that we chose to recognize the factors was by the deep study of each sub-process of FDFP explained in chapter II. Conforming to the build time reduction, the exhaustive adaptive slicing approach and automatic machine path and CNC-code generation were dealt with in chapter IV. Then, we took a further step in the development of curved-form adaptive slicing by which the layered surfaces geometrically very near to original CAD surfaces were resulted, thereby leading to the fabrication of high quality parts in terms of the high degree of geometry conformity.

Additionally, factors in the sub-process of the waterjet cutting machine, layers alignment, and layers attachment affecting the surface roughness, layer dislocation, and part strength, respectively, must be carefully investigated. In the following, multiple responses whose optimum values help improve the quality of FDFP parts and in total amending the FDFP process will be listed. Then, factors affecting the associated responses will be identified.

Surface roughness: AWJ machining technology is one of the popular non-traditional methods used in the industry for material processing with the distinct advantages of no thermal distortion, high machining versatility, high flexibility and small cutting forces. As the AWJ is used in industry extensively, optimization of the process parameters that determine efficiency, economy and quality of the process is becoming more and more important for its successful application. However, being a complicated cutting system, an AWJ is characterized by a large number of process parameters, which include water pressure, orifice diameter, traverse rate, standoff distance, impact angle,

focusing tube diameter, abrasive feed rate, etc. Among the factors, feed rate has a direct impact on the quality of the cut part. The determination of a proper feed rate would lead to the better surface finish on the cut area. Independent variables, such as water pressure, orifice diameter, standoff distance, sheet material, and sheet thickness whose optimal combinations impact the feed rate can be obtained using DOE. In this regard, many studies have been carried out for this aim, and the optimal model in which the effective federate that has a direct impact on the surface roughness has been academically published. For example, in our attempt to generate G-codes, we employed a formula developed successfully by Limbachiya and Patel (2011) and put all relevant independent variables existing in our system into that equation so as to attain the appropriate feed rate.

Part accuracy: Accuracy of the final physical part depends on the geometrical accuracy and the dislocation (deviation from position and orientation) of the actual layer compared to the CAD model of each layer. Figure 6.1 illustrates the error of the positioning of the layer. The surface that is formed between the boundary of the actual layer and CAD model is the error for the layer.

The optimum point will be minimization of the following equation:

$$\sum_{i=1}^m \sum_{j=1}^{n_i} \|S_{ij} - D_{ij}\|$$

Where:

m : Number of layers

n_i : Number of features in layer i

S_{ij} : Actual position of feature j layer i

D_{ij} : CAD model position of feature j layer i

Laser scanning and comparison with CAD files will be used to evaluate the overall quality of the part including dimensional accuracy and surface quality.

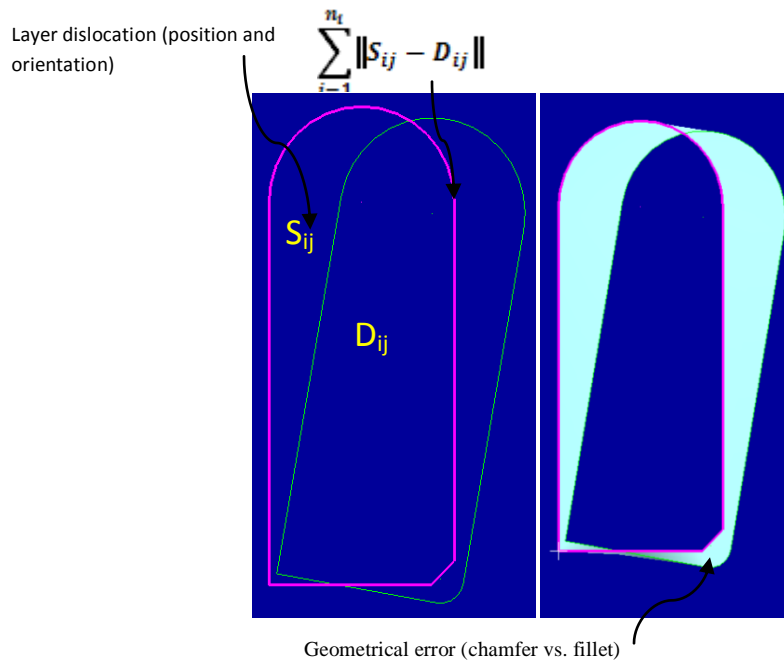


Figure 6.1. Error calculation for layer k with dislocation and geometrical error.

Laser scanning and comparison to CAD files will be used to evaluate the overall quality of the part, that is, dimensional accuracy.

Part tensile strength: The aligned layers need to be bonded in such a way that acceptable part strength can be realized. Good layers attachment would result in an FDFP part that is close to the mechanical properties of the desired part. Filler or bonding material is added between the layers, and a heating source is needed to firmly attach the layers together. Different heating sources were tested to bond metallic layers together. Preliminary results concluded that the three heating sources of furnace, direct flame, and induction heater are feasible methods for bonding layers together. However, they are all accompanied with some limitations. Heating with a furnace has benefits such as controlled atmosphere to limit the oxidation and uniform heating. However, it is very slow (i.e., 3 to 4 hours for a small part). Therefore, it was eliminated from the list. Direct flame (e.g., propane gas) is usable for diverse types of metals and it is very fast, usually

taking less than a minute. However, it reaches to the temperature only desirable for soldering – a process in which the filler metal used has a liquidus below 840°F (450°C) and below the solidus of the base metals- and not for the brazing-a process that produces coalescence of materials by heating them to the brazing temperature and by using a filler metal (solder) having a liquidus above 840°F (450°C) and below the solidus of the base metals.

Induction heating heats part to brazing temperature in less than 1 minute. However its usability is limited to certain (magnetic) materials (Figure 6.2). Both soldering and brazing methods use flux to shield the process from oxidation and to improve the bonding between layers.



Figure 6.2. Galvanized (red hot) versus Stainless steel (unaffected) bolts in an induction heater.

By conducting experimental tests for the two above bonding approaches (brazing, soldering), the type of filler materials compatible with the associated attachment method

and the types of sheet metals that work best for the heating source purpose were suggested in order to achieve an acceptable layer attachment. The quality of the attached layers, however, relies on independent factors, such as heating time, the quantity of filler material, and the sheet thickness. In the following paragraphs, standard mechanical test to measure tensile strength and the experimental design for parts fabricated through soldering and brazing methods will be discussed, and a heating process leading to the higher tensile strength will be chosen in an analytical manner.

Strength Measurement Standard

ASTM Standard D 2294-96, the standard testing method for creep properties of adhesives in shear by tension loading for metal-to-metal contact, was used for building and testing samples. In this test, maximum tension that leads to the bond fracture was used as the criterion for evaluating the bonding strength (Figure 6.3).

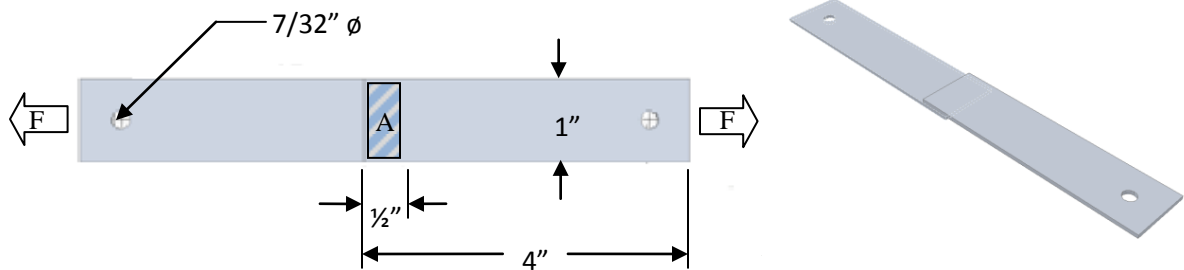


Figure 6.3. ASTM standard 2294-96 configuration.

Samples were pulled apart using a Tinius Olsen Electro Mechanical Tester, with 600kN capacity. The software determined the pull rate and measured the ultimate psi required to pull the joints apart.

Design of Experiment

As the two layer attachment processes (i.e., soldering and brazing) suggested, we designed two separate experiments corresponding to the processes and commenced the analysis of affecting factors within the process and obtained optimal parameters whose optimum values resulted in an acceptable optimized response value (tensile strength) when putting them into a specific formula achieved by regression analysis. Lastly, the two optimal values of the two processes will be compared to come up with the most effective layer attachment process.

DOE for tensile strength in soldering process: Tin Bismuth powder is usually used in thick film solder coatings. We also utilized this material for the stainless steel and galvanized sheet metals bonding. The six different mixtures of Tin & Bismuth percentage (Tin-bismuth: 100-0, 90-10, 80-20, 70-30, 60-40, 50-50) as bonding material weighted at three distinct levels of 0.1, 0.2, and 0.3 grams were defined for testing purposes. Sheet thickness based on experiments has been found to be an ineffective independent factor on the response value. In terms of heating time, as more time is needed to heat the sheet pieces, no more significant impact can be seen on the tensile strength of sample parts. Therefore, types of sheet metal and the percentage of bonding material in a set of experiments were found to be effective.

The number of runs for the measurement of the output or response value depends on the number of factors and their type numbers plus the replications in each treatment. Factorial designs as the specific techniques in the designed experiments approach are well-known for determining the exact factors influencing the process performance. Of

theses a full factorial design with N factors, each at M levels, is employed. To run the design of experiment, two sample replicas for each of the defined combinations (Tin-Bismuth) were taken for soldering two standard (ASTM Standard D 2294-96) metal sheets (either stainless steel or galvanized). A total of 36 runs for each metal sheet were equally carried out in room temperature condition. We also coded metal sheet stainless steel and galvanized as numbers 1 and 0 accordingly in order to simplify the statistical analysis in Minitab software. A dataset including 72 rows in which each row contains Tin-Bismuth percentage, filler material weight, sheet code, and tensile strength (obtained from pull test) were created and put into the worksheet of Minitab software (see Tables A.1).

DOE for tensile strength in the brazing process: To bond the metal sheets together through the brazing process at a shorter time, we need a source of heat by which the temperature of metal sheet reaches to the brazing point very fast without the deformation of a sheet. As a result, induction heating as an effective approach to the metal sheet bonding is employed. It is, in fact, the process of heating an electrically conducting object (usually a metal) by electromagnetic induction. An induction heater (for any process) consists of an electromagnet, through which a high-frequency alternating current (AC) is passed.

Before conducting the experimental design tests on the sample parts fabricated by induction heating, we went through comprehensive experiments by diverse selection of materials and machine settings in a systematic approach to identify a feasible combination that could produce good quality bonding for a FDFP part from steel-based

materials. Table 6.1 illustrates the materials selection and process parameters that successfully tested for brazing bonding using an induction heater for the FDFP process.

Table 6.1. Feasible materials selection and process parameters that resulted in acceptable bonding between layers.

Sheet Type	Galvanized steel or medium carbon steel
Filler Material	Silver Alloy Braze 560
Flux	Sure Flo flux
Software	FDFP Adaptive Slicing software
Alignment	Sacrificial tabs
Compression	Sacrificial tabs with Stainless Bolts
Heating Method	Induction
Induction Setting	700 Amps (Max)
Coil Type	Water cooled 4 turn 4 cm diameter

The fabrication of several medium sized parts experimentally under utilization of the accepted parameters illustrated in Table 6.1 led to the identification of three variables or factors, namely heating time, filler weight, and sheet thickness each at level of 3, 2, and 2, respectively. For factor “heating time”, a sample part started to reach at brazing point in 30 seconds proved by multiple tests on galvanized steel with different thicknesses. To see the role of heating time on part quality, two additional heating times 35 and 40 seconds included in the level of related factor. As for factor “filler weight”, Silver Alloy Braze layer measured at ½in. width by 1in. length (the size of area where two metal sheets join/contact) is regarded as having a low weight level. By doubling the

filler material in the same dimensions, the second level (high weight) of the associated factor is assigned. In conjunction with the impact of sheet thickness, two levels of concern, namely thin and thick thickness, were involved in the experiment as they play an effective role in part quality, too. The galvanized steel sheet with thickness of 0.065 in. is set for low level and second sheet with 0.25 in. thickness is considered as high level. Following the definition of the factors' levels, the associated codes that simplify DOE analysis in Minitab are presented in the table below:

Table 6.2. Factors' levels and the coded values for brazing process.

Factors	Levels	Coded values
Heating Time (second)	30	-1
	35	0
	40	1
Filler Weight	Low	-1
	High	1
Sheet thickness (inch)	0.065	-1
	0.25	1

Result Analysis

To run full factorial design for the soldering process, three factors including tin percentage, filler material weight, and sheet code at levels of 6, 3, and 2, respectively, were put as the entries into the statistical feature of Minitab (i.e., Full Factorial Design). Minitab software version 15.0 a well-known computerized statistical tool is used for precise analyzing and making decision on the selection of most suitable factor(s) which has the great impact on the response variable. The following Table 6.3 shows ANOVA analysis obtained by Minitab.

Table 6.3. Analysis of Variance for tensile strength.

Source	DF	Seq SS	Adj SS	Adj MS	F	P
A	5	3604610	3604610	720922	11.08	0.000
B	2	266696	266696	133348	2.05	0.143
C	1	18191758	18191758	18191758	279.67	0.000
A*B	10	1115202	1115202	111520	1.71	0.115
A*C	5	2342676	2342676	468535	7.20	0.000
B*C	2	20556	20556	10278	0.16	0.854
A*B*C	10	1020887	1020887	102089	1.57	0.156
Error	36	2341721	2341721	65048		
Total	71	28904106				

S = 255.045 R-Sq = 91.90% R-Sq(adj) = 84.02%

A, B, and C denote tin percentage, filler material weight, and coded sheet, respectively.

P-value and *F* ratio are the important parameters whereby we could judge as to

the selection of the best fitted factor(s) affecting on the process quality. In terms of *P*-value, whenever obtained *P*-value is relatively large and is greater than the base common controllable value ($\alpha=0.05$) (see Figure 6.4), we can strongly accept the null hypothesis which reveals that a factor has no any impact on response variable. Therefore from the results shown in Table 6.1, it can be inferred that the probability of factor A (0.000) falling within acceptable region is extremely low as *P*-value for factor A is much less than $\alpha=0.05$ meaning that factor A has a strong impact on tensile strength. Factors C and AC behave in the same way as factor A dose. In contrast, as *P*-value for BC (0.854) is much greater than $\alpha=0.05$, interaction between B and C is confidently rejected. In the case of factor B and ABC, the ANOVA analysis shows that the related *P*-values are approximately 10% within acceptance region which means those factors may not be considered as important factors. For factor AB, it is difficult to deny its impact on

response value as its P -value (0.115) about 5% is within acceptance region and is very close to the reject area.

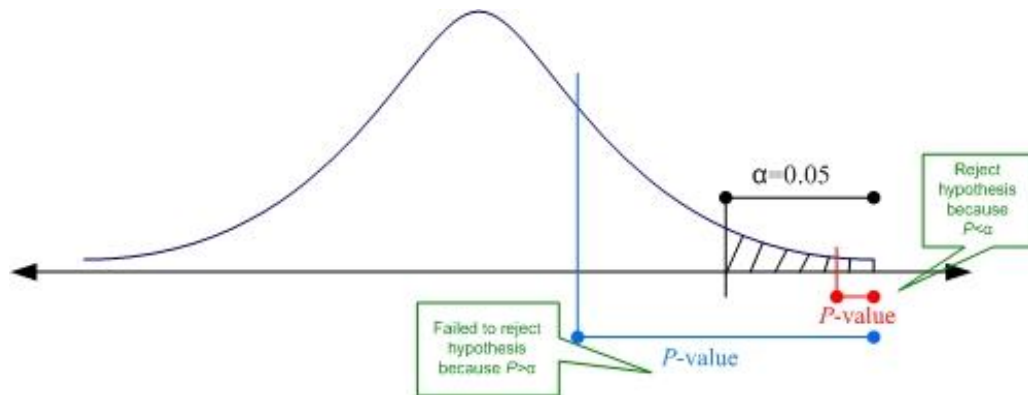


Figure 6.4. Acceptance and rejection region using P -value.

As an alternative to the P -value, we could compare the computed F -ratio to a 5% upper critical value of the F distribution. To use F -ratio, we need to compare the base $F_{0.05, V_1, V_2}$ with the gained F in ANOVA table, where V_1 is the degree of freedom for a factor and V_2 is the degree of freedom for Error. If the obtained F is less than $F_{0.05, V_1, V_2}$, then the null hypothesis is accepted. In the present ANOVA analysis, for example, F -ratio for factor A ($F_{0.05, 5, 36}$) is 2.477 and less than the value shown in the table (11.8). Thus, it can be inferred that factor A has a great impact on tensile strength. As we follow same approach for the rest of factors, the following results could be drawn:

$F_B = F_{0.05, 2, 36} = 3.259 > 2.05$, then B has no effect on response.

$F_C = F_{0.05, 1, 36} = 4.11 < 279.67$, then C has a great effect on response.

$F_{A*B} = F_{0.05, 10, 36} = 2.106 > 1.71$, then AB has no effect on response.

$F_{A*C} = F_{0.05, 5, 36} = 2.477 < 7.20$, then AC has an effect on response.

$F_{B*C} = F_{0.05, 2, 36} = 3.259 > 0.16$, then BC has no effect on response.

$F_{A*B*C} = F_{0.05, 10, 36} = 2.106 > 1.57$, then ABC has no effect on response.

Additionally, the interaction plot (Figure 6.5) provided by Minitab will also give insight into the identification of affecting factors.

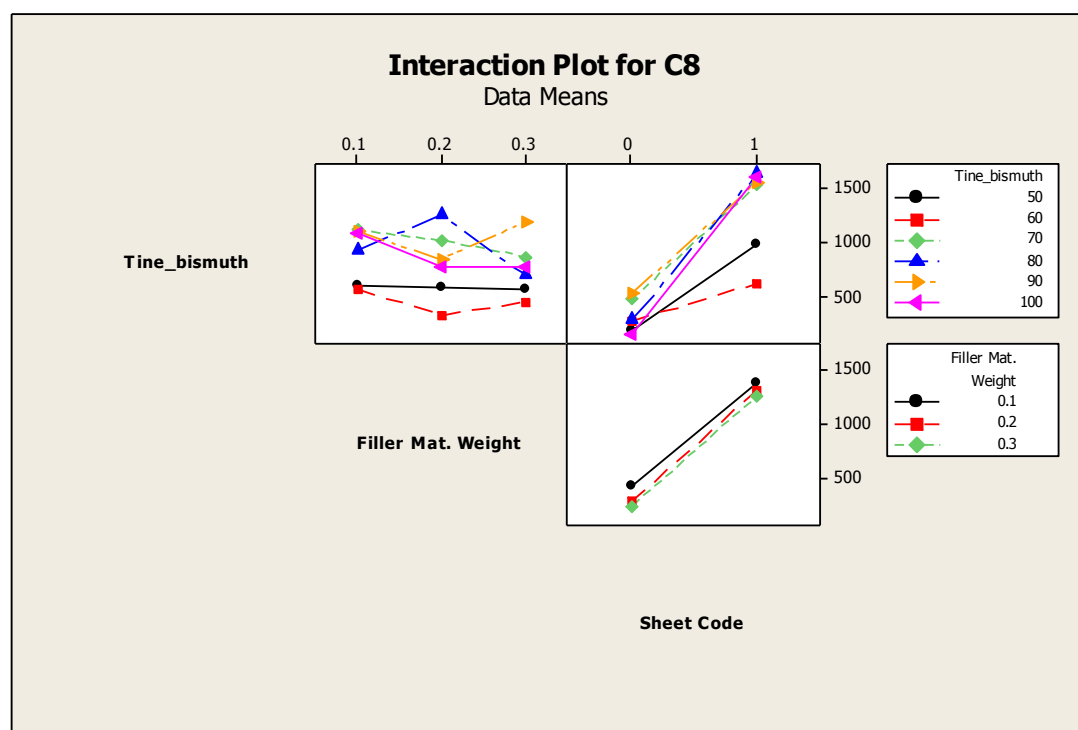


Figure 6.5. Interaction plot for tensile strength.

From the plot, it can be inferred that there is no direct correlation between factors A and B as the filler material weight increases from 0.1 to 0.3, tensile strength increases at tin percentages of 60 and 90. Conversely, tensile strength in tins of 50, 70, 80, and 100 represents inverse values. In an interaction between A and C, it is evident that for all ranges of tin the tensile strength performs much better in stainless steel sheet than galvanized one. Furthermore, as the percentage of tin goes up the tensile strength for stainless steel fairly increases. In case of BC interaction, these two factors interact the same manner as A and C do. In contrast to factor A, when the filler weight increases, tensile strength shows up good output in lower weight filler for stainless steel sheet.

To estimate the tensile strength for different values of independent factors, regression analysis would provide an appropriate formula that relates the strength of final part to independent coded variables within the acceptable range of input values. This model also provides the basis for the selection of factor settings that provide minimally desirable part strength. In the equation 6.1 attained by Minitab regression analysis, based on the most influential factors identified above, we could set the values of A, B, C as 90, 0.1, 1 and get the tensile strength of 1535psi which is close to the testing data (see Table A.2 for further information on regression).

$$\text{Strength} = - 226 + 9.21 \times A - 727 \times B + 1005 \times C \quad \text{Eq.6.1}$$

Lastly, in order to compare the optimized tensile strength obtained by the above DOE with that of brazing process, the optimal tensile strength with the target value of 5000psi within the defined low and high rate of each independent variable can be computed using optimization plot. The following plot represents the optimal tensile strength at 1957.54psi for factors tin, filler weight, and sheet code at the values of 100, 0.1, and 1, respectively (see Figure 6.6).

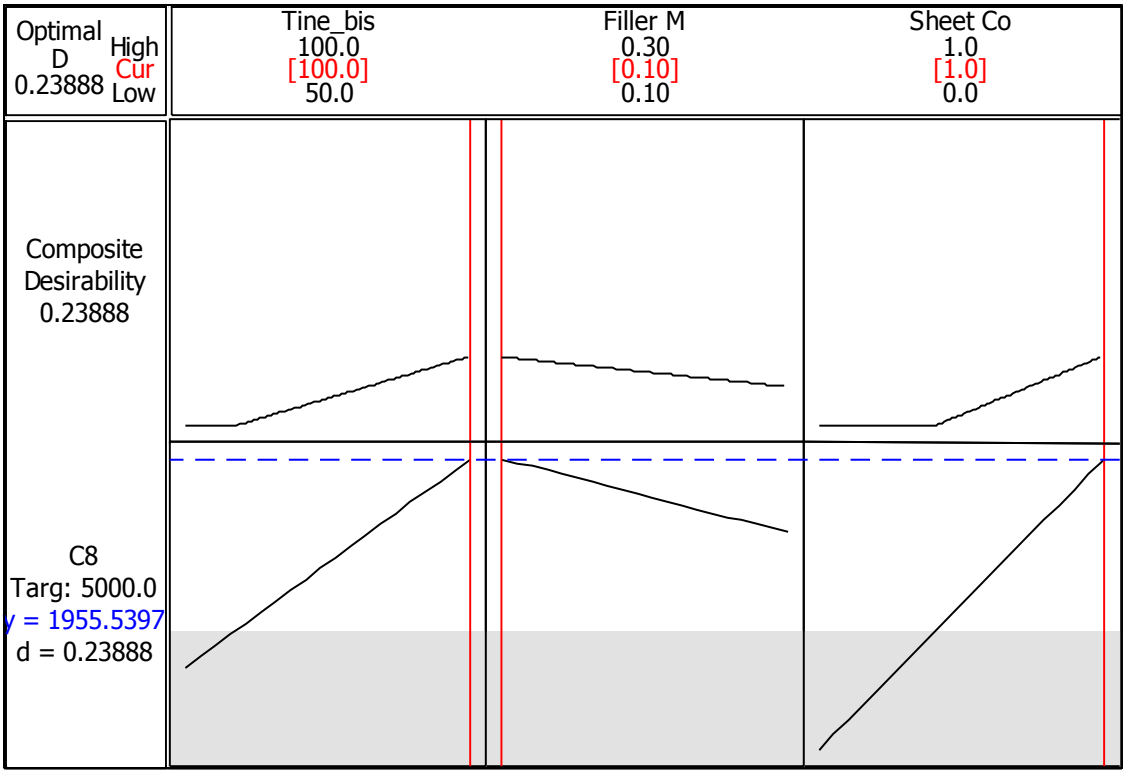


Figure 6.6. Optimization plot for tensile strength in soldering process.

To run the experiment, for each run two replicas is chosen and the total number of $3 \times 2 \times 2 \times 2$ (24) runs is needed to do for the DOE analysis purpose. To achieve proper bonding results, a proper surface preparation and use of a flux for wetting and cleaning the surfaces being bonded must be done for each sample part for total of 24 runs. This cleaning preparation can be performed by means of mechanical methods, soaking cleaning and chemical cleaning (acid etching). In doing so, contaminants, such as mineral oils, miscellaneous organic soils, polishing and buffing compounds, miscellaneous solid particles, oxides, scale, smut and rust would be removed from the part surface. To measure the magnitude of tensile strength, each sample part fabricated by the induction heating process would go through the same testing standard as soldering process did. The

randomized order of 24 runs assigned by Minitab with combination of three affecting factors plus the measured tensile strength can be found in Table A.3.

The following Table 6.4 shows ANOVA analysis for full factorial design obtained by Minitab.

Table 6.4. Analysis of Variance for tensile strength.

Source	DF	Seq SS	Adj SS	Adj MS	F	P
A	2	7914974	7914974	3957487	26.08	0.000
B	1	2208873	2208873	2208873	14.56	0.002
C	1	3002630	3002630	3002630	19.79	0.001
A*B	2	23811337	23811337	11905668	78.47	0.000
A*C	2	12484105	12484105	6242053	41.14	0.000
B*C	1	466767	466767	466767	3.08	0.105
A*B*C	2	2038969	2038969	1019485	6.72	0.011
Error	12	1820703	1820703	151725		
Total	23	53748358				

S = 389.519 R-Sq = 96.61% R-Sq(adj) = 93.51%

A, B, and C denote heating time, sheet thickness, and filler weight, respectively.

From the results shown in Table 6.1, it can be inferred that the probability of factor A (0.000) falling within acceptable region is extremely low because P -value for factor A is much less than $\alpha=0.05$ meaning that factor A has a strong impact on tensile strength. Factors B, C, AB, AC, BC, and ABC behave in the same way as factor A dose. In contrast, since P -value for BC (0.105) is greater than $\alpha=0.05$, interaction between B and C is confidently rejected.

Using F-ratio, F-ratio for factor A ($F_{0.05,2,12}$) is 3.885 and less than the value shown in the table (26.08). Thus, it can be inferred that factor A has a great impact on tensile strength. As we follow the same approach for the rest of factors, the following results could be drawn:

$$F_B = F_{0.05,1,12} = 4.743 < 14.56, \text{ then B has an impact on response.}$$

$$F_C = F_{0.05,1,12} = 4.743 < 19.79, \text{ then C has an effect on response.}$$

$$F_{A*B} = F_{0.05,2,12} = 3.885 < 78.47, \text{ then AB is the effecting factor.}$$

$F_{A*C} = F_{0.05,2,12} = 3.885 < 41.14$, then AC has an effect on response.

$F_{B*C} = F_{0.05,1,12} = 4.743 > 3.08$, then BC has no effect on response.

$F_{A*B*C} = F_{0.05,2,12} = 3.885 < 6.72$, then ABC has an effect on response.

Additionally, the interaction plot (Figure 6.7) provided by Minitab will also give insight into the identification of affecting factors.

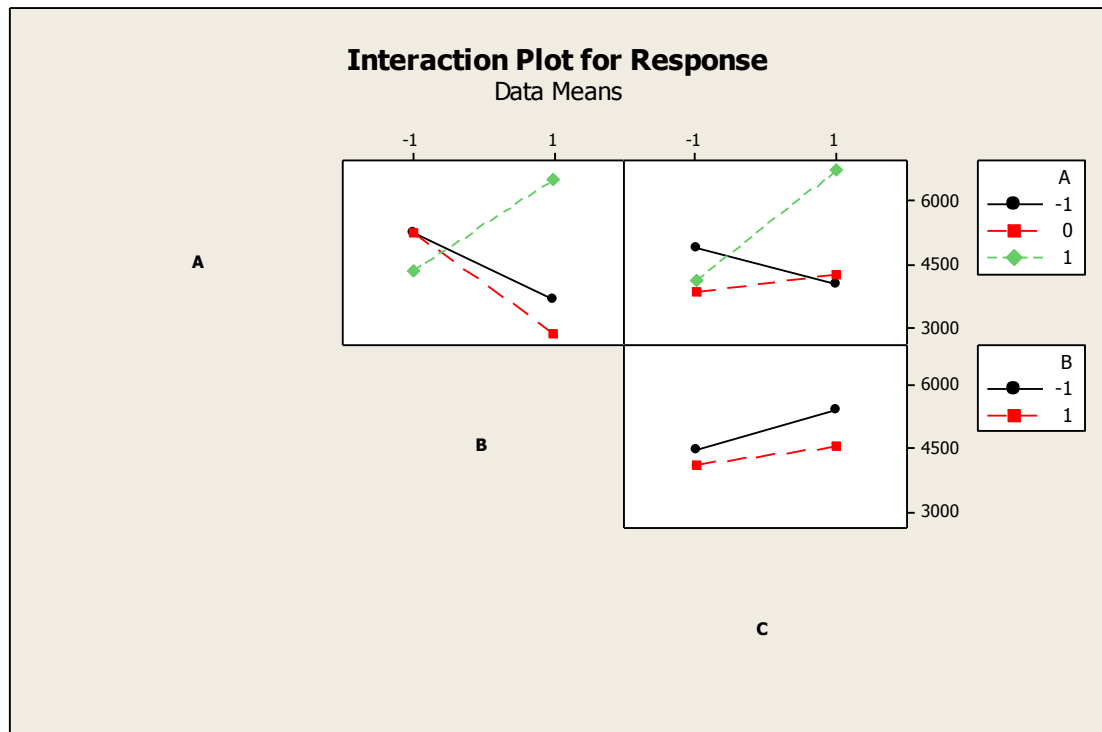


Figure 6.7. Interaction plot for tensile strength in brazing process.

From the plot, it can be inferred that the heating time dose have relatively a direct correlation with sheet thickness. The tensile strength for thick sheet at maximum heating time (40 seconds) represents the highest values compared to the two low and medium heating time. In AC interaction, sample parts with low weight filler material at the lowest heating time come up with higher tensile strength, but for high weight filler, the sample part became stronger at the maximum heating time, tensile strength reached to the highest value compared to that of low weight filler at minimum heating time. As for BC

interaction, tensile strength for thin sheet with either low or high weight filler represents the higher value than that of thick thickness. It is also interesting to see that while the weight of filler material augments, the sample part becomes stronger in terms of tensile strength in both thin and thick sheets, too.

To estimate the tensile strength for different values of independent factors, we refer to the equation 6.2 attained by Minitab regression analysis. If we, for example, plug into the formula levels 0, -1, and 1 for factors heating time, sheet thickness, and filler weight proved to be an effective combination for getting higher tensile strength, then we could get the value of 5304 psi which is relatively close to the data sample measured experimentally (See Table A.4 for further information on regression analysis).

$$\text{Response}=4647+482\times A-303\times B+354\times C+944\times A\times B+873\times A\times C+250\times A\times B\times C \quad \text{Eq.6.2}$$

Lastly, optimization plot in Minitab is utilized to obtain the optimum value of response within the defined target value. The optimum tensile strength achieved at target value of 5000 psi for soldering process was 1957.54 psi. Surprisingly, the following optimization plot represents the optimal response value of, 5000.50 psi, for brazing process which is much higher than that of soldering process at the same target value. Factor settings for heating time, sheet thickness, and filler weight at the optimized response value of 5000.50 were 30 seconds, 0.065 in., high weight, respectively (see Figure 6.8).

In another attempt to find the optimum value for the new target value (8000 psi), the optimization plot was ended up with the optimized response magnitude of 6500 psi for new factor settings which are distinct from the previous one, i.e., 40 seconds, 0.25 in., high weight. In a nutshell, the FDFP parts fabricated by the induction heating process

produce the higher quality parts in terms of strength compared to that of soldering process (see Table 6.5).

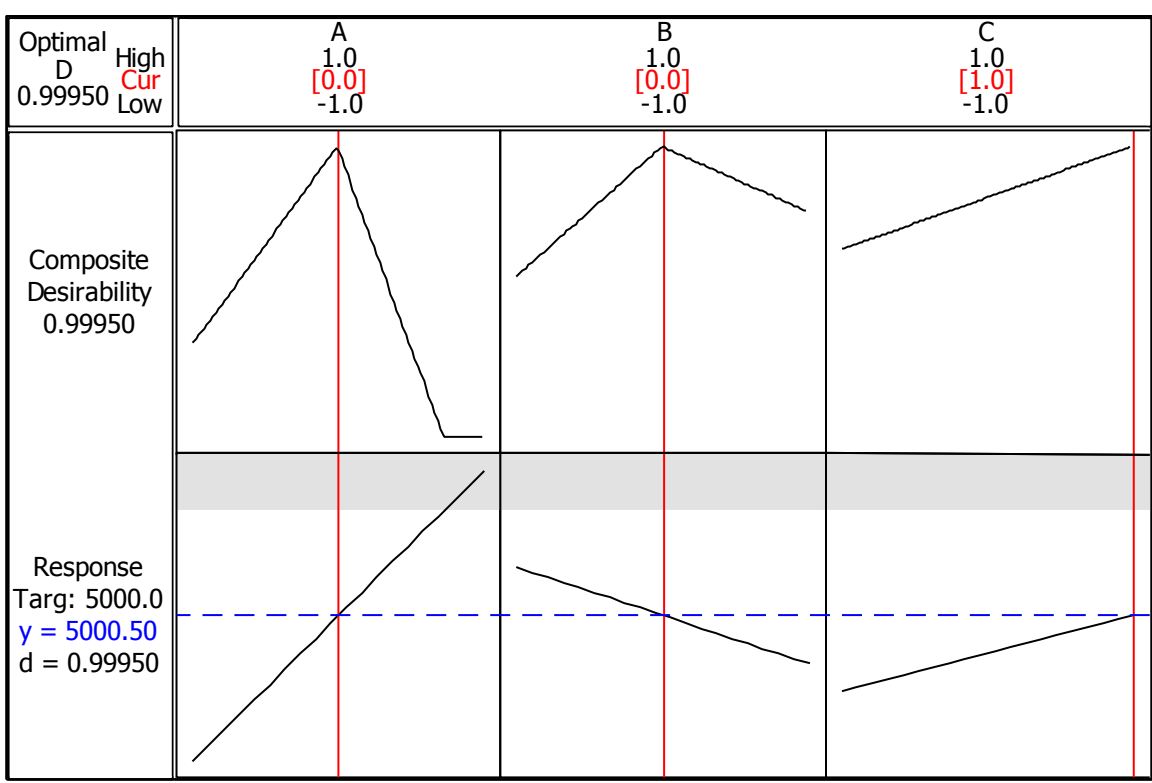


Figure 6.8. Optimization plot for tensile strength in brazing process.

Validation of optimization result

To validate the developed model, six additional sample parts were fabricated. The first set of three parts was made at the target value of 5000 psi and the second set of three parts was made at the target value of 8000 psi (Table 6.5).

Table 6.5. The optimum settings for tensile strength in brazing process.

Target value (psi)	Optimum response value (psi)	Optimum settings		
		Heating time	Sheet thickness	Filler material
5000	5000.50	35	0.065	High
8000	6500	40	0.25	High

For each response, the individual response model was used to calculate 95% prediction intervals (PI) for the average of three values taken at target values of 5000 and 8000 psi, respectively (Table 6.6).

Table 6.6. Response prediction for two best operating points setting.

Target value for response	Fit (optimum response)	95% PI for average of 3 values
5000	5000.50	(4850.33, 5349.66)
8000	6500	(5828.82, 7169.98)

Table 6.7 shows the results for the fabricated parts. The two of the actual averages fall within their respective prediction interval. The results indicate that the models are valid.

Table 6.7. Fabricated parts at optimum point setting.

Optimum Tensile Strength At two different target values	Sample 1	Sample 2	Sample 3	Average
5000.50	4677.99	4559.19	4743.83	4660.34
6500	6724.20	6574.00	6200	6499.40

CHAPTER VII

CONCLUSION AND FUTURE WORKS

Conclusion

Firstly, this research describes an adaptive slicing approach for prototypes fabricated by the FDFP process with sheets of varied thicknesses. In the proposed system, the combination of the area deviation and triangle area tolerances of the projected contours on top and side views were utilized for complex geometry detection. Since this system started cutting the CAD model from the bottom upward at the minimum thickness, any sudden changes to a part's geometry by appearing convex or concave regions were well detected in order to avoid any big geometry distortion error. Secondly in order to build FDFP parts that closely fit their original CAD model, a new curved-form adaptive slicing method is presented. This method is inspired by hand peeling of an apple in which a knife's orientation and movement is continuously changed and adjusted to cut with minimum waste in each slice. Obviously the slice thicknesses may vary from the top to the middle areas of the apple because of curvature change (Figure 7.1). In this method, multiple cuts of the edge boundary of each generated adaptive layer with variable cutting vectors angles conform well to the CAD model curved surfaces. The proposed system is compatible with 5-axis AWJ machines.

Both adaptive and curved-form slicing systems proposed were implemented by Visual Basic code inside Autodesk Inventor. The developed systems were tested for several models with complex features. The results showed that the combination of adaptive slicing with angular cutting could remarkably improve the dimensional accuracy and the surface quality of the parts through significant reduction of the part geometry distortion.

Thirdly, the quality of the FDFP parts turned out to heavily rely on the strong joining of the layers together. A bad bonding for metallic parts was addressed to be a major cause of defective FDFP parts. To realize an acceptable high quality part, it was set to investigate essential factors affecting the tensile strength of the layers bonded by either soldering or brazing processes. Two important factors (type of metal sheet, the percentage of bonding material) in the soldering process and three factors (heating time, sheet thickness, the weight of bonding material) in the brazing process were identified to be the most effective factors. Full factorial design for tensile strength of the parts built by both soldering and brazing process were conducted. The number of 64 and 24 runs were assigned for soldering and brazing process, respectively. To conclude, the tensile strength of FDFP parts fabricated by the induction heating (brazing) process in optimum point setting exhibited the stronger layers attachment than that of the soldering process. Finally through experimentation, validation was performed on the optimum parameter setting for parts built by the induction heating process. Lastly, the independent variables which influence the most the response variable outcomes were identified.

Future Works

The current slicing system is heavily dependent on Autodesk Inventor design and programming platforms. Extracting the slice information of a CAD model being represented in an exchange file (e.g., IGES, STL, and STEP) could help develop the

system independent of Autodesk Inventor. As for layer alignment, the human activity involvement in layers alignment is certainly prone to failure and would result in inferior FDFD parts. Automated layer alignment could contribute to the production of high standard parts with trivial geometry deviation from the defined CAD model geometry characteristics. In layers attachment, there is still opportunity to study on different types of materials and bonding.

Additionally, the current FDFD process lacks the integrity from sub-process of CAD model slicing through layers attachment. The integration of the entire process would be beneficial for the fabrication of cost-effective FDFD parts while maintaining the quality of the parts at an acceptable level.

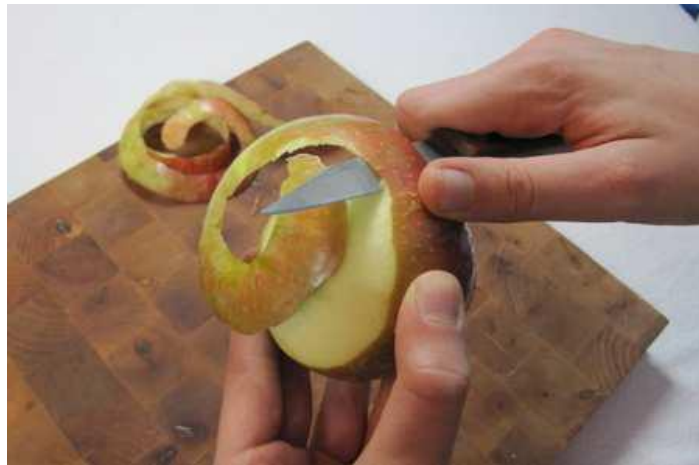


Figure 7.1. Curved-form adaptive slicing method inspired by the apple peeling function.

APPENDIX A

DATA TABLES

Table A.1. Dataset for DOE.

Dataset for both stainless steel and galvanized sheet					
Run order	Tin	Bi	Weight (gram)	Coded Sheet	Tensile strength (psi)
66	100	0	0.1	1	1694
35	100	0	0.1	0	785
19	60	40	0.3	0	60.25
4	80	20	0.3	0	227
30	60	40	0.1	0	553
22	100	0	0.2	0	87.4
7	100	0	0.1	0	104.5
18	90	10	0.1	0	577
44	100	0	0.1	0	209
67	70	30	0.2	1	1739
57	50	50	0.1	1	597
72	100	0	0.1	1	1834
10	60	40	0.1	0	210
40	70	30	0.3	0	358
26	90	10	0.3	1	1908

Table A.1-Continued

Dataset for both stainless steel and galvanized sheet					
Run order	Tin	Bi	Weight (gram)	Coded Sheet	Tensile strength (psi)
33	70	30	0.1	0	846
32	50	50	0.3	1	1535
39	70	30	0.3	0	145.6
55	50	50	0.1	1	1194
41	50	50	0.2	1	774
51	100	0	0.2	1	1442
36	90	10	0.2	1	1345
15	100	0	0.2	1	1428
60	50	50	0.3	0	71.8
8	100	0	0.3	1	1130
64	90	10	0.2	0	233
3	100	0	0.3	1	1558
52	80	20	0.1	1	1635
14	100	0	0.1	1	2240
17	90	10	0.1	1	1344
27	80	20	0.3	1	1765
53	80	20	0.1	0	232
38	80	20	0.1	1	1626
62	50	50	0.3	1	507
24	90	10	0.3	0	485.9
56	80	20	0.2	0	549
12	60	40	0.2	1	272

Dataset for both stainless steel and galvanized sheet					
Run order	Tin	Bi	Weight (gram)	Coded Sheet	Tensile strength (psi)
46	50	50	0.2	0	81.3
70	50	50	0.1	0	207
48	60	40	0.3	1	709

Table A.2. Regression analysis for soldering process.

Predictor	Coef	SE Coef	T	P
Constant	-225.5	219.9	-1.03	0.309
Tine_bismuth	9.212	2.465	3.74	0.000
Filler Mat. Weight	-726.8	515.6	-1.41	0.163
Sheet Code	1005.31	84.19	11.94	0.000

S = 357.206 R-Sq = 70.0% R-Sq(adj) = 68.7%

Analysis of Variance

Source	DF	SS	MS	F	P
Regression	3	20227555	6742518	52.84	0.000
Residual Error	68	8676551	127596		
Total	71	28904106			

Source	DF	Seq SS
Tine_bismuth	1	1782241
Filler Mat. Weight	1	253556
Sheet Code	1	18191758

Table A.3. Dataset for DOE.

Dataset for tensile strength in brazing process				
Run order	Heating Time	Sheet thickness	Filler weight	Tensile strength (psi)
13	30	0.065	Low	5302
15	30	0.065	High	5180
4	30	0.25	High	2376
7	35	0.065	High	2340
14	30	0.25	Low	5600
18	35	0.25	Low	5310
2	30	0.25	Low	5120
3	30	0.065	High	4090
11	40	0.065	High	5095
8	35	0.25	High	3040
23	40	0.065	High	5390
19	35	0.065	High	2680
9	40	0.065	Low	2760
5	35	0.065	Low	5640
21	40	0.065	Low	3230
20	35	0.25	High	3380
24	40	0.25	High	7430
16	30	0.25	High	2990
1	30	0.065	Low	5030
22	40	0.25	Low	5660
12	40	0.25	High	8130
17	35	0.065	Low	4780
10	40	0.25	Low	5700
6	35	0.25	Low	5270

Table A.4. Regression analysis for brazing process.

Predictor	Coef	SE Coef	T	P
Constant	4646.8	206.3	22.52	0.000
A	481.7	252.7	1.91	0.074
B	-303.4	206.3	-1.47	0.160
C	353.7	206.3	1.71	0.105
AB	944.4	252.7	3.74	0.002
AC	872.6	252.7	3.45	0.003
ABC	249.8	252.7	0.99	0.337

S = 1010.90 R-Sq = 67.7% R-Sq(adj) = 56.3%

Analysis of Variance

Source	DF	SS	MS	F	P
Regression	6	36375610	6062602	5.93	0.002
Residual Error	17	17372748	1021926		
Total	23	53748358			

Source	DF	Seq SS
A	1	3712366
B	1	2208873
C	1	3002630
AB	1	14271395
AC	1	12181845
ABC	1	998501

APPENDIX B

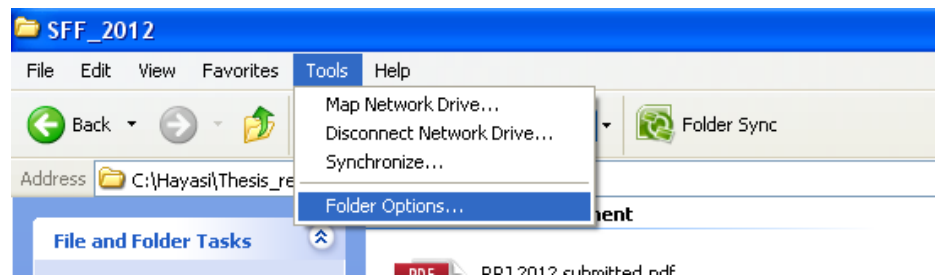
SOFTWARE MANUAL

The stages required to run the program should be in the following order.

1-As the developed system works directly with CAD model designed by Autodesk Inventor, the system needs to identify the CAD files through their extension.

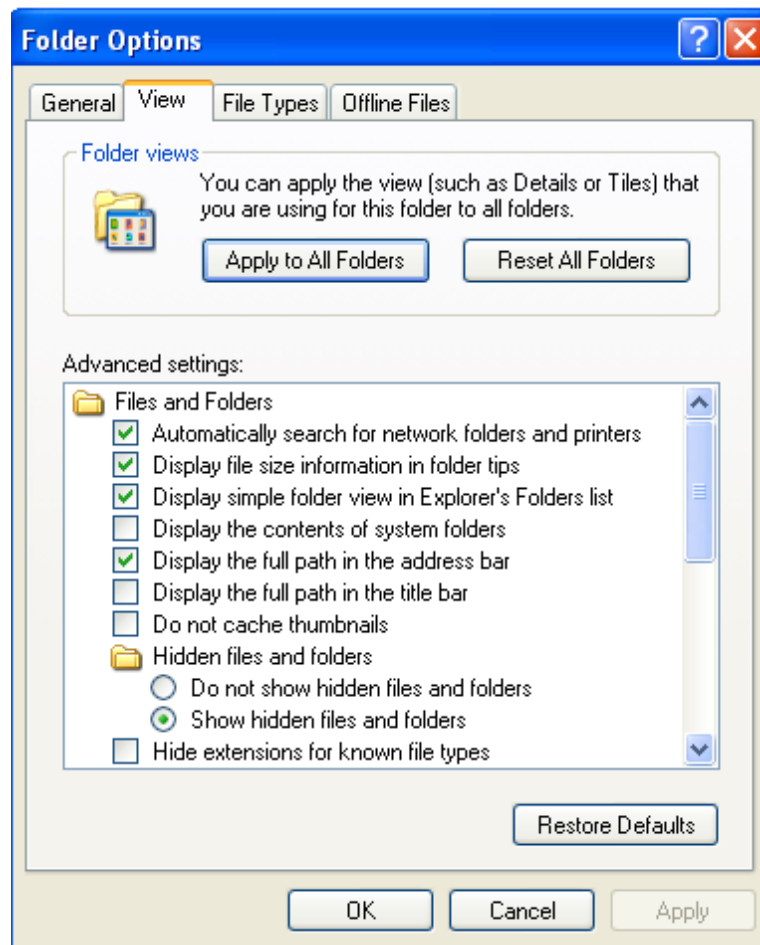
Thus, it is required to make the file extension viewable as follows:

1-1-Go to Menu “Tools” existed in Windows Explorer, and select item “Folder Options...”

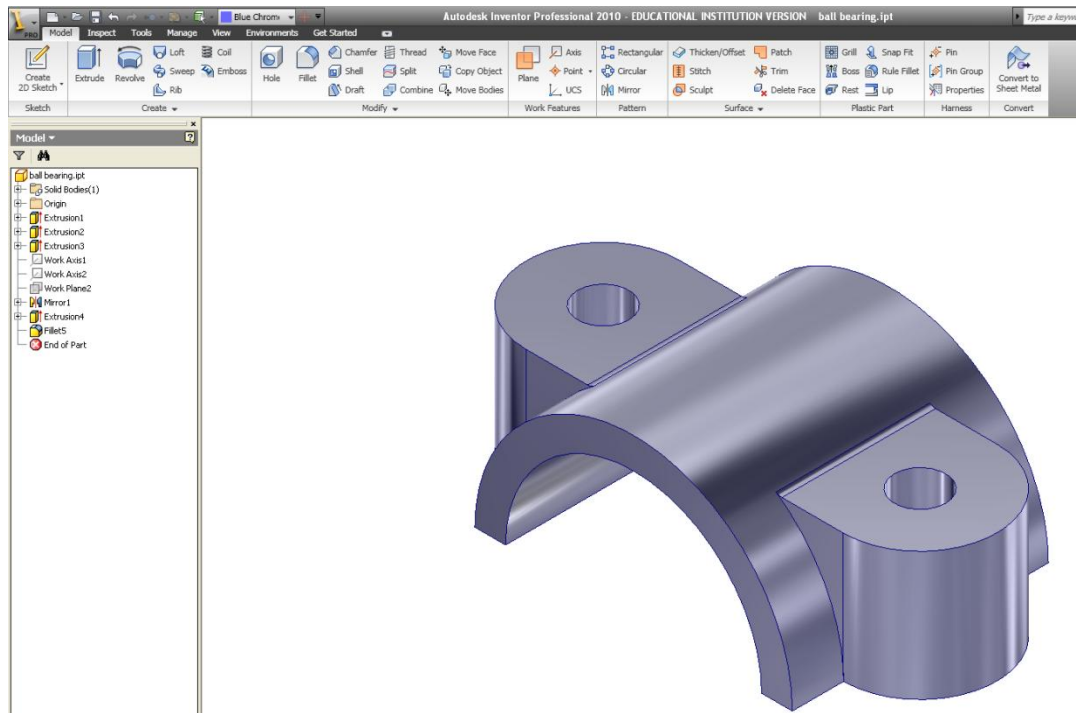


1-2-Hit tab “View”. In textbox “Advanced settings” choose option “Show hidden files and folders”. Then, uncheck “Hide extensions for known file types” .

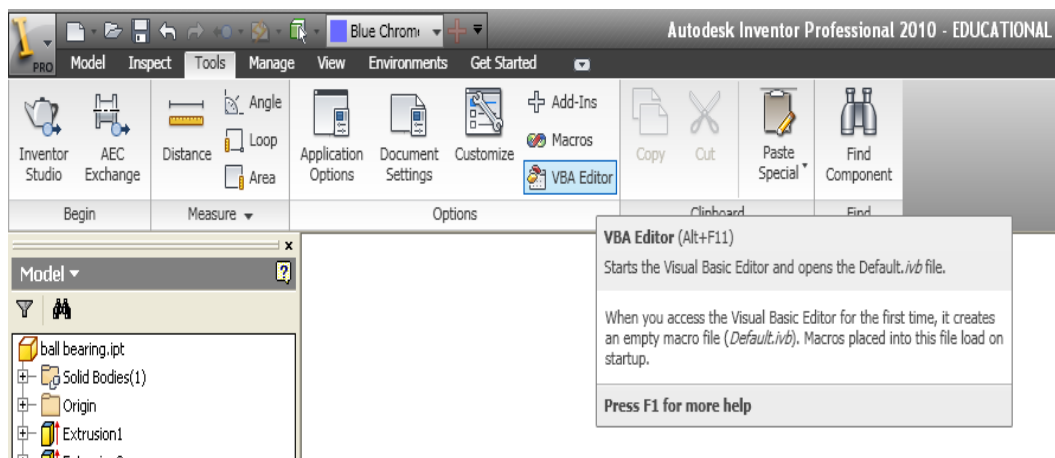
2-Furthermore, you need to have MS Access file entitled “CNC.mdb” saved into the directory “C:\Hayasi\Inventor-Project”. This file must be in its directory as the program will communicate with it for data transferring purpose.



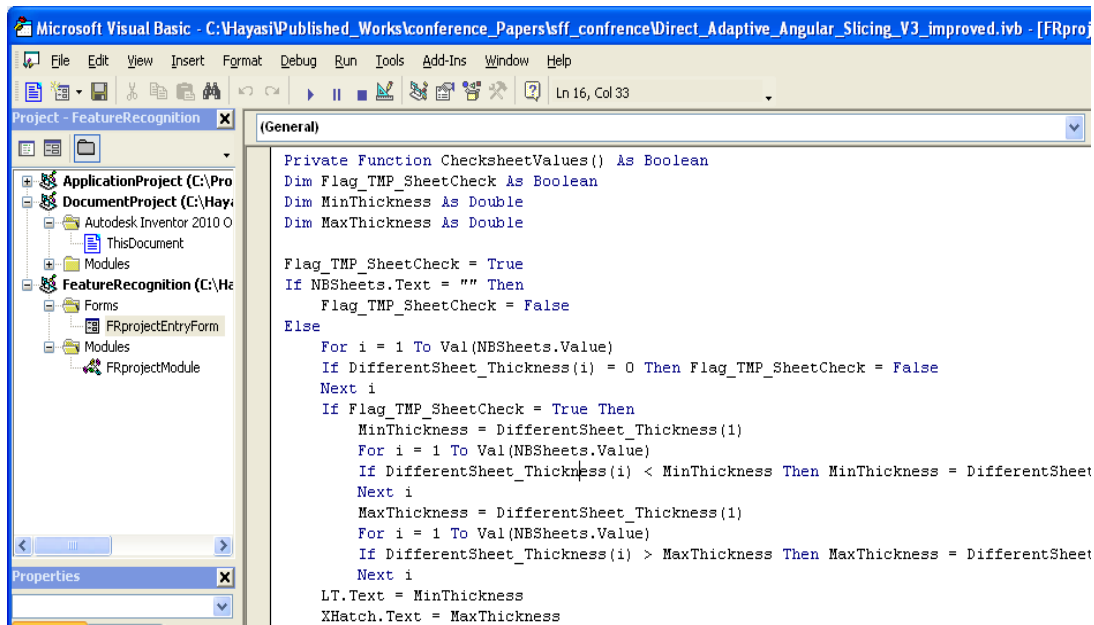
3-Run Autodesk Inventor. Start designing any CAD model and save it as IPT format. Alternatively, you may import any 3D solid model designed by other CAD package which was saved as SAT file. Once you import a SAT file, you are required to save it as IPT file in Inventor. The developed system has capability to work with both Inventor owned designed files or CAD models coming from other CAD package software. In the following, a sample CAD model designed in Inventor is depicted.



4-To run the program, go to menu “Tools” in Inventor, and then locate “VBA editor” button and hit on it.



5-Once you enter the VBA programming environment, go to menu “File” and select item “Load project”. Then, locate the file “CurvedForm_AdaptiveSlicing.ivb” on your computer. The found file will look like as follows:



```

Microsoft Visual Basic - C:\Hayasi\Published_Works\conference_Papers\lfff_conference\Direct_Adaptive_Angular_Slicing_V3_improved.ivb - [FRproj
File Edit View Insert Format Debug Run Tools Add-Ins Window Help
Ln 16, Col 33
Project - FeatureRecognition
ApplicationProject (C:\Pro
DocumentProject (C:\Hay
Autodesk Inventor 2010 O
ThisDocument
Modules
FeatureRecognition (C:\Ha
Forms
FRprojectEntryForm
Modules
FRprojectModule
Properties
(General)
Private Function ChecksheetValues() As Boolean
Dim Flag_TMP_SheetCheck As Boolean
Dim MinThickness As Double
Dim MaxThickness As Double

Flag_TMP_SheetCheck = True
If NBSheets.Text = "" Then
Flag_TMP_SheetCheck = False
Else
For i = 1 To Val(NBSheets.Value)
If DifferentSheet_Thickness(i) = 0 Then Flag_TMP_SheetCheck = False
Next i
If Flag_TMP_SheetCheck = True Then
MinThickness = DifferentSheet_Thickness(1)
For i = 1 To Val(NBSheets.Value)
If DifferentSheet_Thickness(i) < MinThickness Then MinThickness = DifferentSheet
Next i
MaxThickness = DifferentSheet_Thickness(1)
For i = 1 To Val(NBSheets.Value)
If DifferentSheet_Thickness(i) > MaxThickness Then MaxThickness = DifferentSheet
Next i
LT.Text = MinThickness
XHatch.Text = MaxThickness

```

6-Run the program. The user interface form will be appeared as follows. Before you key in the inputs, hit button “Check the Validity” to make sure no specific errors would occur. Then, key in the required inputs followed by hitting button “Run”. Finally, hit button “CNC file generation” for generating CNC codes compatible with 5-axis AWJ machine cutter.

Adaptive & Uniform Slicing-Texas State University

System Input | Additional Output Info. | System Output

Input Folder Address: c:\Hayasi\Inventor-Project\

Layer Thickness(Min): 0.025

Layer Thickness (Max): 8

Allowable "Triangle Area" Tolerance: 0.0005

Allowable "Area Deviation" Tolerance %: 1

Process Selection

Adaptive Slicing 5-Axis Angular Slicing Uniform Slicing

Elapsed Time to Slice a Sample CAD file: ??:?:??

Sheets Selection

Number of sheets: 3 **Sheet thickness:** 0.025

Sheet # 1

Sheet dimensions: L: 10 W: 20

Slicing Direction

X Y Z

Bonding Thickness: 0.001

Confirmed Run

CNC file Generation

7-Once you successfully executed the program, you may perform the simulation in AutoCAD environment. What you need is to create a new file in AutoCAD, and then run command "Script". Then, locate 2D or 3D file generated by the program in a folder you saved all files. Keep in mind that command "Script" works only if "Osnap" is off.

REFERENCES

- Abd Elghany, K. (2009). Rapid Prototyping and Manufacturing (Part 2). *Rapid Product Development*, 2, 6-29.
- Ameri, F., McArthur, C., Asiabanpour, B., & Hayasi, M. (2011). A web-based framework for semantic supplier discovery for discrete part manufacturing. *SME/NAMRC 39 Transaction*.
- Asiabanpour, B., & Khoshnevis, B. (2003). A new memory efficient tool path generation method for applying very large STL files in vector-by- vector rapid prototyping processes. *Computer and Industrial Engineering*, San Francisco, CA.
- Asiabanpour, B., & Khoshnevis, B. (2004). Machine path generation for the SIS process. *Robotics and Computer-Integrated Manufacturing*, 20, 167–175.
- ASTM International F 2792-09. (2010). *Additive Manufacturing*.
- Bryden, B.G., Wimpenny, D.I., & Pashby I.R. (2001). Manufacturing Production tooling using metal laminations. *Rapid Prototyping Journal*, 7(1), 52-59.
- Chamberlain, P.B., Van Rossendaal, M.D., & Thomas, C.L. (1998). Variable thickness ruled edge slice generation and three-dimensional graphical error visualization. *Proceedings of the Solid Free Fabrication Symposium*, August (1998), 311–318.
- Chang, C.C. (2004). Direct slicing and G-code contour. *Int J Adv Manuf Technol*, 23, 358–365.
- Chen, X., Wang, C.Y., Xiao, Y., & Huang, S. (2001). Direct slicing from PowerSHARE models for rapid prototyping. *Int J Adv Manuf Technol*, 17, 543–547.
- Choi, S.H., & Kwok, K.T. (1999). A memory efficient slicing algorithm for large STL file. *Solid Freeform Fabrication Symposium*, Austin, Texas, 155–162.
- Chua, C. K., Gan, J. G. K., & Tong, M. (1997). Interface between CAD and rapid prototyping systems. 1. A study of existing interfaces. *International Journal of Advanced Manufacturing Technology*, 13(8), 566–570.
- Chua, C. K., Gan, J. G. K., & Tong, M. (1997). Interface between CAD and Rapid Prototyping systems. 2. LMI: An improved interface. *International Journal of Advanced Manufacturing Technology*, 13(8), 571–576.

- Cormier, D., Unnanon, K., & Sanii, E. (2000). Specifying non-uniform cusp heights as a potential aid for adaptive slicing. *Rapid Prototyping Journal*, 6(3), 204–211.
- Devine, J. (1984). Joining Metals with Ultrasonic Welding. *Machine Design*, 56(21), 91–95.
- Dolenc, A., & Mäkelä, I. (1994). Slicing procedure for layered manufacturing techniques. *Comput Aided Des*, 26(2), 119–126.
- Frank, M.C., Wysk, R.A., & Joshi, S.B. (2004). Rapid planning for CNC machining – a new approach to rapid prototyping. *Journal of Manufacturing Systems*, 23(3), 242-55.
- Gao, Y., & Dourmanidis, C. (2002). Mechanical analysis of ultrasonic bonding for rapid prototyping. *Transactions of the ASME*, 124, 426-433.
- Gibbons, G.J., Hansell, R.G., Norwood, A.J., & Dickens P.M. (2003). Rapid laminated die-cast tooling. *Rapid Prototyping Journal*, 23(4), 372-381.
- Glen, T.C., Loerwald, M., Hayasi, M., & Asiabanpour, B. (2011). Layer Alignment and Lamination for the Fully Dense Freeform Fabrication (FDFF) Process. 22nd International Solid Freeform Fabrication (SFF) Symposium, Austin, TX.
- Glozer, G. R., & Brevick, J. R. (1992). Laminate tooling for injection molding. *Proceedings of the Institution of Mechanical Engineers, Part B: Journal of Engineering Manufacture*, 207, 9-15.
- Gupta, T., Chandila, P.K., Tripathi, P., & Roy Choudhury, A. (2004). Direct slicing with optimum number of contour points. *International Journal of CAD/CAM*, 4(1), 1-2.
- Hayasi, M., & Asiabanpour, B. (2011). A new adaptive slicing approach for the fully dense freeform fabrication (FDFF) process. *Journal of Intelligent Manufacturing*. Doi: 10.1007/s10845-011-0615-4.
- Hefin, R., & Jiju, A. (2003). Application of design of experiments to a spot welding process. *Assembly Automation*, 23(3), 273-279.
- Himmer, T., Techel, A., Nowotny, S., & Beyer, e. (2003). Recent developments in metal laminated tooling by multiple laser processing. *Rapid Prototyping Journal*, 9(1), 24-29.
- Hope, R. L., Jacobs, P.A., & Roth, R.N. (1997). Rapid prototyping with sloping surfaces. 1. *Rapid Prototyping Journal*, 3(1), 12-19.

- Hope, R. L., Roth, R. N., & Jacobs, P.A. (1997). Adaptive slicing with sloping layer surfaces. 2. *Rapid Prototyping Journal*, 3(3), 89-98.
- Jamieson, R., & Hacker, H. (1995). Direct slicing of CAD models for rapid prototyping. *Rapid Prototyping J*, 1(2), 4–12.
- Jung, J. Y., & Ahluwalia, R. S. (2005). NC tool path generation for 5-axis machining of free formed surfaces. *Journal of Intelligent Manufacturing*, 16(1), 115–127.
- Jurrens, K.K. (1999). Standards for the rapid prototyping industry. *Rapid Prototyping J* 5(4), 169–178.
- Kamrani, A., & Nasr, E. (2006). *Rapid prototyping: theory and practice*. Springer, New York.
- Kirzanowski, J. E. (1989). A Transmission Electron Microscopy Study of Ultrasonic Wire Bonding. *Proceeding of 39th IEEE Electronic Components Conference*, Houston, TX, 450–455.
- Koc, B., & Lee, Y.S. (2002). Adaptive Ruled Layers Approximation of STL Models and Multiaxis Machining Applications for Rapid Prototyping. *Journal of Manufacturing Systems*, 21(3), 153-166.
- Koc, B., Ma, Y., & Lee, Y. (2000). Smoothing STL files by Max-Fit biarc curves for rapid prototyping. *Rapid Prototyping J*, 6(3), 186–203.
- Kulkarni, P., Marsan, A., & Dutta, D. (2000). A review of process planning techniques in layered manufacturing. *Rapid Prototyping J*, 6(1), 18–35.
- Leong, K.F., Chua, C.K., & Ng, Y.M. (1996). A study of stereolithography file errors and repair genetic solutions. 1. *Int J Adv Manuf Technol*, 12(6), 407–414.
- Leong, K.F., Chua, C.K., & Ng, Y.M. (1996). A study of stereolithography file errors and repair special cases. 2. *Int J Adv Manuf Technol*, 12(6), 415–422.
- Limbachiya, V.J., & Patel, D.M. (2011). An Investigation of Different Material on Abrasive Water jet Machine. *International Journal of Engineering Science and Technology (IJEST)*, 3(7), 5940-5945.
- Mognol, P., Jégou, L., Rivette, M., & Furet, B. (2005). High speed milling, electro discharge machining and direct metal laser sintering: A method to optimize these processes in hybrid rapid tooling. *International Journal of Advanced Manufacturing Technology*, 29, 35-40.
- Myers, R., & Montgomery, D. (2002). *Response Surface Methodology*. 2nd ed. Wiley: New York.

- Nakagawa, T., & Kunieda, M. (1984). Manufacturing of laminated deep drawing dies by laser beam cutting. *Advanced Technology of Plasticity*, Vol. 1.
- Nee, J. G., Dufraigne, W., Evans, J., & Hill, M. (2010). *Fundamentals of tool design*, 6th ed. Dearborn, MI: Society of Manufacturing Engineers.
- Onuh, S.O., & Yusuf, Y. (1999). Rapid prototyping technology: applications and benefits for rapid product development. *J Intell Manuf*, 10, 301–311.
- Pande, S. S., & Kumar, S. (2008). A generative process planning system for parts produced by rapid prototyping. *International Journal of Production Research*, 46(22), 6431–6460.
- Pandey, P. M., Reddy, N. V., & Dhande, S. G. (2003). Real time adaptive slicing for fused deposition modelling. *International Journal of Machine Tools & Manufacture*, 43(1), 61–71.
- Pfaff, G., Forbes, J.S., & McLellan, P.J. (2006). Generating information for real-time optimization. *Asia- Pacific Journal of Chemical Engineering*, 1, 32-43.
- Prechtel, M., Otto, A., & Geiger, M. (2005). Rapid tooling by laminated object manufacturing of metal foil. *Advanced Material Research*, 6-8, 303-312.
- Schmitz, T., Davies, M., Dutterer, B., & Ziegert, J. (2001). The application of high-speed CNC machining to prototype production. *International Journal of Machine Tools & Manufacture*, 41, 1209-1228.
- Singhal, S. K., Prashant, K. J., & Pulak, M. P. (2008). Adaptive Slicing for SLS Prototyping. *Computer-Aided Design and Applications*, 5(1–4), 421–423.
- Taylor, J.B., Cormier, D.R., Joshi, s. & Venkataraman, V. (2001). Contoured edge slice generation in rapid prototyping via 5-axis machining. *Robotics and Computer Integrated Manufacturing*, 17, 13-18.
- Vouzelaud, F.A., Bagchi, A., & Sferro, P.F. (1992). Adaptive laminated machining for prototype dies and molds: part I and II. *Proceedings of the 3rd Symposium in Solid Freeform Fabrication*, Austin, TX.
- Vouzelaud, T., & Bagchi, A. (1995). An adaptive lamina generation for shape dependent process control and/or object decomposition. Patent number: 5,432,704.
- Vuyyuru, P., Kirschman, C.F., Fadel, G., Bagchi, A., & Jara, C.C. (1994). A NURBS-based approach for rapid product realization. *Proceedings of the 5th International Conference on Rapid Prototyping*, The University of Dayton, 229–239.

- Walczyk, D. Hardt. (1996). Recent developments in profiled-edge lamination dies for sheet metal forming. Proceedings of the Seventh Solid Freeform Fabrication Symposium, Austin, TX.
- Williams, R., Walczyk, D., & Dang, H. (2007). Using abrasive flow machining to seal and finish conformal channels in laminated tooling. *Rapid Prototyping Journal*, 13(2), 64–75.
- Xu, F., Wong, Y. S., Loh, H. T., Fuh, J. Y. H., & Miyazawa, T. (1997). Optimal orientation with variable slicing in stereolithography. *Rapid Prototyping Journal*, 3(3), 76–88.
- Yan, X., & Gu, P. (1996). A review of rapid prototyping technologies and systems. *Comput Aided Des*, 28(4), 307–318.
- Yoo, S., & Walczyk, D. (2005). An advanced cutting trajectory algorithm for laminated tooling. *Rapid Prototyping Journal*, 11, 199-213.
- Zhao, Z. W., & Laperriere, L. (2000). Adaptive direct slicing of the solid model for rapid prototyping. *International Journal of Production Research*, 38(1), 69–83.

VITA

Mohammad Hayasi was born in 1976. He received his B.S in Industrial Engineering from Qazvin Azad University-Iran in 1999. Upon his graduation, he joined several companies active in detergent and automotive industries as an Industrial Engineer to improve the production system and develop MRP I, II using Ms Access. His passion in the continuation of the higher degree study was a solo motivation to get abroad and complete his MSc. in Industrial and Systems Engineering from Universiti Putra Malaysia in 2008. Then, he moved to the US in 2010 to enhance his knowledge in the field of Rapid Prototyping by taking second master degree in Industrial Technology at Texas State University-San Marcos. As of 2008, he has been active in academia via the publication of more than 13 international conference papers, journal articles, and book chapter. He strongly believes in “No Pain No Gain”.

Email address: m.hayasi@gmail.com

This thesis was typed by Mohammad Hayasi.